UNIVERSITÉ DE STRASBOURG

ÉCOLE DOCTORALE SCIENCES DE LA TERRE,

DE L'UNIVERS ET DE L'ENVIRONNEMENT

LABORATOIRE IMAGE VILLE ENVIRONNEMENT

THÈSE

présentée par :

Dasaraden MAUREE

soutenue le : **19 mars 2014**

pour obtenir le grade de : **Docteur de l'Université de Strasbourg**

Discipline/ Spécialité : Sciences de la Terre et de l'Univers

Development of a multi-scale meteorological system to improve urban climate modeling

THÈSE dirigée par :

Prof. CLAPPIER Alain	Professeur, Université de Strasbourg, France

RAPPORTEURS :

Dr. HAUGLUSTAINE Didier	Directeur de recherche, CNRS, France
Dr. De RIDDER Koen	Chercheur, VITO, Belgique
Dr. MARTILLI Alberto	Chercheur, CIEMAT, Espagne

AUTRES MEMBRES DU JURY :

Dr. BLOND Nadège	Chercheur, CNRS, France
M. DESPRETZ Hubert	Ingénieur, ADEME, France

Résumé

Ce travail a consisté à developper un modèle de canopée (CIM), qui pourrait servir d'interface entre des modèles méso-échelles de calcul du climat urbain et des modèles micro-échelles de besoin énergétique du bâtiment. Le développement est présenté en conditions atmosphériques variées, avec et sans obstacles, en s'appuyant sur les théories précédemment proposées. Il a été, par exemple, montré que, pour être en cohérence avec la théorie de similitude de Monin-Obukhov, un terme correctif devait être rajouté au terme de flottabilité de la T.K.E. CIM a aussi été couplé au modèle méso-échelle WRF. Une méthodologie a été proposée pour profiter de leurs avantages respectifs (un plus résolu, l'autre intégrant des termes de transports horizontaux) et pour assurer la cohérence de leurs résultats. Ces derniers ont montré que ce système, en plus dêtre plus précis que le modèle WRF à la même résolution, permettait, par l'intermédiaire de CIM, de fournir des profils plus résolus près de la surface.

Abstract

This study consisted in the development of a canopy model (CIM), which could be use as an interface between meso-scale models used to simulate urban climate and micro-scale models used to evaluate building energy use. The development is based on previously proposed theories and is presented in different atmospheric conditions, with and without obstable. It has been shown, for example, that to be in coherence with the Monin-Obukhov Similarity Theory, that a correction term has to be added to the buoyancy term of the T.K.E. CIM has also been coupled with the meteorological meso-scale model WRF. A methodology was proposed to take advantage of both models (one being more resolved, the other one integrating horizontal transport terms) and to ensure a coherence of the results. Besides being more precise than the WRF model at the same resolution, this system allows, through CIM, to provide high resolved vertical profiles near the surface.

Remerciements

Je tiens d'abord à remercier Alain Clappier pour avoir dirigé cette thèse. Ses précieux conseils, ses explications et les innombrables tableaux remplis d'équations ont été d'une grande utilité. Je le remercie aussi pour son amitié, sa compréhension, sa patience et "la petite cellule".

Je tiens aussi à remercier, tout particulièrement, Nadège Blond, pour son encadrement, sa rigueur, son dévouement sans faille et pour les discussions que nous avons eues durant ces dernières années. Je la remercie aussi pour ses conseils et les petits repas que nous avons faits.

J'adresse mes plus sincères remerciements aux Dr. Didier Hauglustaine, Dr. Koen de Ridder et Dr. Alberto Martilli pour avoir accepté de juger et de donner leur avis sur ce travail. Je remercie aussi le Dr. Alberto Martilli pour les discussions que nous avons eues.

Merci à M. Hubert Despretz, ingénieur ADEME, qui a suivi cette thèse, pour ses conseils et pour sa confiance. Je remercie aussi Mme. Valérie Pineau de la cellule thèse de l'ADEME. Merci aussi à Mme. Aurélie Grégoire de la Région Alsace pour le suivi de cette thèse.

Je remercie aussi la direction du Laboratoire Image Ville Environnement de m'avoir permis d'effectuer ma thèse.

Un merci tout particulier à Estelle Baehrel pour sa présence, son écoute attentive et qui a toujours une solution à nos problèmes adminstratifs. Merci aussi à tous ceux qui ont contribué de près ou de loin à l'aboutissement de ce travail au laboratoire et à la Faculté de Géographie. Merci aux personnes qui ont contribué au support technique de cette thèse en particulier Romaric David et Michel Ringenbach. Je remercie, par ailleurs, Tajaneh et Ali, pour leur gentillesse.

Merci aux Jardins des Sciences de l'Université de Strasbourg, tout particulièrement Said, Christelle et Natasha, pour m'avoir permis de découvrir une autre façade de la recherche.

Je remercie aussi mes anciens collègues de bureau, Manon et Sajjad et mes nouveaux collègues Jana et Jérémy pour m'avoir encouragé pendant ces quelques mois et pour nos discussions sans fin. Merci à Richard pour son soutien au cours des derniers mois et pour les petites escapades dans une autre réalité. Merci aussi

à Claire, David, Franck, Lucie, Sophie, Yasmina et Vincent pour les pauses de midi souvent folkloriques.

Je tiens à remercier ma famille et mes amis, en France, en Suisse, en Angleterre, en Allemagne, aux Etats Unis et à Maurice pour leur soutien au cours de ces dernières années. Un merci tout particulier à mes parents, à mon frère et à ma soeur qui ont toujours été présent à mes cotés. Merci à Kreena, Kurveena et Sevahnee pour leurs supports et leurs amitiés.

Pour finir, merci à Jevita pour son soutien. Nous avons vécu la même chose aux mêmes moments. Comme tu le dis si bien: à deux c'est beaucoup mieux et plus facile!

Cette thèse a été financé par l'Agence de l'Environnement et de la Maîtrise de l'Energie, la Région Alsace et la Zone Atelier Urbaine Environnementale et a bénéficié du soutien financier du Réseau Alsace de Laboratoires en Ingénierie et Sciences pour l'Environnement (REALISE) pour l'achat de matériel informatique.

Contents

List of Figures

Chapter 1

Introduction

1.1 Climate change and building energy consumption

1.1.1 Global Climate Change

The Fifth Assessment Report (AR5) issued by the IPCC (Intergovernmental Panel on Climate Change) in 2013, stated that there is clear evidence that the current global warming is being caused by human activities. There is compelling proof this is due to the release of greenhouse gases (GHG) such as carbon dioxide (see Figure 1.1) from the combustion of fossil fuels to produce energy [IPCC, 2013].

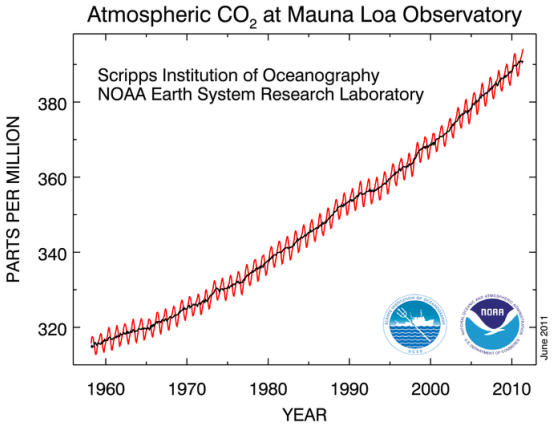

Figure 1.1: Carbon dioxide concentration at Mauna Loa Observatory from 1960 to 2011

Human induced climate change as described by the AR5, indicates that mitigation and adaptation measures have to be taken to ensure that there will be as little impact as possible on Earth and its ecosystems. Since 2007, the European Union and the French government have called for immediate actions to reduce by 4 GHG emissions by 2050.

There has been increasing concern about the world energy dependency after the first oil crisis and this has been enhanced by the ever-increasing oil prices on

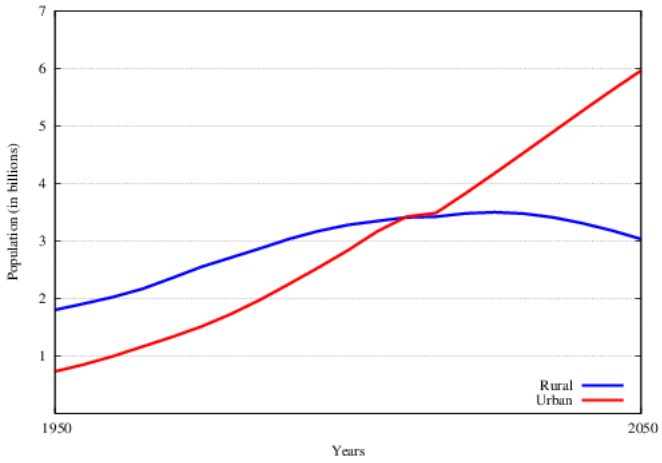

Figure 1.2: World urban and rural population (in billions) from 1950 to 2050 [UN, 2012]

the world markets (save for the 2008-2009 financial crises) and by the fact that these fuels are from non-renewable resources. This also highlighted the need for a reduction in energy consumption and increase in energy efficiency of various systems (such as fuel consumption in cars or energy use in buildings). Energy use is one of the main drivers of the world's economy and it can be expected that energy consumption will increase in the future with the rise of the world's human population.

1.1.2 Urban development

After 1970, there has been a drastic increase in urban population (see Figure 1.2) that had led to half of the world population living in urban areas in 2008 [UN, 2012]. This can be explained mainly by the fact that agriculture was not regarded anymore as the main source of revenue for a large part of the population as well as by market reforms in the 1970s [Davis, 2006].

The migration of rural dwellers to smaller cities/towns and the increasing population in these areas were met by a lack of urban planning. Buildings were constructed without careful consideration on their energy consumption and their impact on natural ecosystems. Urban development as well as the expansion of

cities, through the modification of land uses (from natural to artificial) change the local energy budget and wind patterns. This causes a phenomenon named Urban Heat Island (UHI) [Oke, 1982]. The industrialization of urban areas also brought air, noise and water pollution. Regulations have been enforced since then to protect the health and the well being of urban citizens but also that of the existing fauna and flora.

UN-Habitat [2009] projects that by 2050 the population living in urban areas will rise to 70% of the world population, with the major part of this increase taking place in developing countries. This will undeniably be accompanied by an expansion of urban areas [UN, 2012]. According to the International Energy Agency, around 70% of the final energy produced are consumed in urban areas [IEA, 2008]. An expected growth in population leading to an increase in energy consumption is thus going to accentuate the responsibility of urban areas towards climate change if more sustainable buildings and cities are not planned.

1.1.3 Adaptation and mitigation strategies

Two approaches are needed in this context: mitigation and adaptation. Mitigation solutions are required if cities and local governments want to reduce their GHG emissions. In order to achieve the target that has been set by international agreements, more efficient energy transformation systems have to be built and this should be applied to all sectors among which are the transportation, the building and the industry sectors. Adaptation strategies on the other hand means that cities have to be redesigned or adjusted to allow urban dwellers as well as the other ecosystems to live in a warming world.

In this context, it is important that cities are planned accordingly. Energy use in buildings (residential and tertiary) accounts for 40% of energy consumption in France (see Figure 1.3) and this contributes to about 25% of GHG emissions. A major part of this energy (70%) is used for heating and cooling purposes [ADEME, 2012].

Heating and cooling rates are highly dependent on the climate. In winter, at higher latitudes, more energy is used to heat the buildings while in summer energy

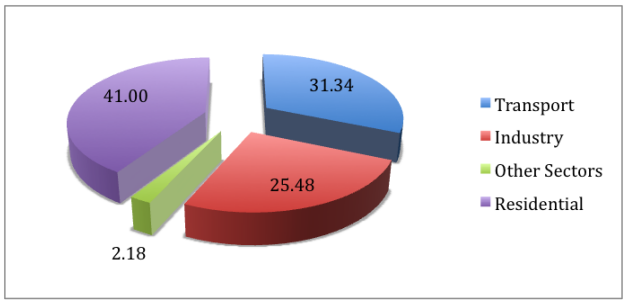

Figure 1.3: Energy consumption in urban areas by sectors [ADEME, 2012]

is used to cool these buildings. The use of energy in urban areas also modifies the local heat balance and hence can lead to an enhanced energy consumption in buildings. Architectural, designing and construction techniques (isolation of walls or roofs, double or tripled paned windows) are now used to build more efficient and less energy consuming buildings. When conceiving the latter, modeling tools are often used to provide estimates of their energy consumption.

It is thus essential to have access to tools which can evaluate, with precision, the interactions that exist between buildings, their energy use and the local climate.

1.2 Objectives

Distinct models have been used in the past to simulate the atmospheric circulations at an urban regional scale [Kondo and Liu, 1998, Masson, 2000, Martilli et al., 2002] and for building energy use [Crawley et al., 2000, Salamanca et al., 2010, Groleau et al., 2003]. There is still, however, a lack of models that can grasp the whole extent of urban processes that influence the urban heat islands intensity and which can also provide precise calculation of building energy consumption. Using high resolution meteorological mesoscale model will require extensive computational resources which is not feasible at present [Martilli, 2007].

The aim of this study was to develop a Canopy Interface Model (CIM) that could be used to couple meso-scale meteorological models to micro-scale models. The use of a canopy model is intented to improve surface representation in low

resolution meso-scale models by providing enhanced vertical profiles to micro-scale models. The history of the meteorological variables are thus taken into account with data coming from the meso-scale models. In return, the meso-scale models will get more accurate information regarding the surface layer as more precise fluxes will be calculated in the urban canopy.

This work provides the foundation to the coupling of meso-scale models and micro-scale models. It was carried out to develop a tool that will (1) improve the low-resolution meso-scale models and the computational time and (2) calculate with an enhanced precision high resolution meteorological profiles in the canopy. The intended objective is to use these profiles to evaluate more precisely building energy use and define planning and construction strategies (such as improved building isolation materials or new building thermal regulation) to reduce the impact of urban areas on the atmosphere. Adopting such strategies will not only help increase human comfort in urban areas (for example during heat waves that are expected to be more likely in a warming world) but will also help as possible mitigation solutions in view of the current climate change by reducing greenhouse gas emissions in urban areas.

1.3 Structure of the thesis

In Chapter 2 of the manuscript, an overview of the various processes at different spatio-temporal scales that influences urban climate will be provided. State of the art meso-scale and micro-scale models that are pertinent to this study are compared. It is shown that in order to further improve surface parameterization, more precise vertical meteorological profiles are required. Providing these profiles with highly resolved meso-scale model is not feasible and it is thus proposed here to develop a 1-D column model.

This development work was conducted in three parts. A Canopy Interface Model (CIM), using a diffusion process based on a 1.5 order turbulence closure, was developed in an offline mode [Mauree et al., 2014b]. The model was first tested

in a neutral environment and without obstacles. The results were compared to the surface layer theory as proposed by Prandtl [1925]. To keep the coherence between the theory and the formulation, that has been adopted, it was shown that a constant turbulent kinetic energy (T.K.E) profile is obtained above a plane surface in a neutral case. Obstacles were then integrated following the work of Krpo [2009], Kohler et al. [2012] and the model was validated with results from a C.F.D experiment from Santiago et al. [2007], Martilli and Santiago [2007].

In the second part of this study, the T.K.E equation was modified to add the buoyancy term so as to take into account the stability of the atmosphere [Mauree et al., 2014a]. The model was tested above a plane surface and the results were then compared to the Monin-Obukhov Similarity Theory [Monin and Obukhov, 1954] and the formulations proposed by Businger et al. [1971]. It was shown that in order to keep both the theory and the formulations of Businger in coherence, the buoyancy term in the T.K.E equations has to be multiplied using a correction term.

Finally in the last part of this study, the Canopy Interface Model (CIM) that has been developed is integrated in WRF v3.5 [Skamarock et al., 2008] and is coupled with the BEP-BEM model [Martilli et al., 2002, Krpo et al., 2010, Salamanca et al., 2010]. A theoretical study was designed to show the improvements that CIM has brought [Mauree et al., 2014c]. It was shown that profiles calculated from CIM are in very good agreement with a high resolution simulation from WRF.

Chapter 2

On the need for a canopy model

Abstract

The atmospheric circulation at the meso-scale is governed by various processes taking place at the global as well as at the building scale. The processes that are of interest for the present study are presented in this chapter.

Distinct models have been used in the past to simulate the atmospheric circulations at an urban scale and for building energy use. There is however still a lack of models that can grasp the whole extent of urban processes that influence the Urban Heat Islands intensity as well as precise calculation of building energy consumption. Using high resolution meteorological meso-scale model will require extensive computational resources which is not feasible at present [Martilli, 2007].

It is thus showed here that in order to represent all the different processes taking place at various spatio-temporal scales that a canopy model is needed. This canopy model is expected to be used in low resolution meso-scale model to improve surface representation as well as provide high resolution vertical profiles to either micro-scale model or urban parameterizations.

2.1 Introduction

Over 50% of the world population now lives in urban areas [UN, 2012]. This figure is expected to increase even further in the future. Understanding the processes that regulate urban climate is thus of crucial importance for several reasons including dispersion of air pollution, heat island mitigation, urban planning strategies, energy consumption and urban dwellers thermal comfort.

For the scope of this work, particular interest will be given to the influence of obstacles on urban climate and energy consumption in buildings. Urban climate and the evaluation of energy consumption inside buildings in urban areas depend on interactions between different spatio-temporal scales. To understand the processes which influence the urban climate, it is important to analyze the intricate behavior of the atmosphere. The Earth's atmosphere is composed of four layers and is illustrated in Figure 2.1.

The troposphere contains about 80% of the atmospheric mass and most of the human activities and life are concentrated in this layer. The focus will hence be given only on the troposphere. The average height of the troposphere is about 10km (16 km at the Equator and 7km at the Poles). The troposphere can be further divided in the Planetary Boundary Layer (PBL) and the Free Atmosphere (see Figure 2.2).

The PBL is directly in contact with the Earth's surface and responds to forcing from the land uses, the radiation and turbulence, as it will be explained in Section 2.2. The influence of surface friction and heating is transferred very efficiently to the PBL through turbulent mixing or transfer. These processes, which take place at different time and length scales, regulate the atmospheric circulations in the PBL. Close to the ground, a surface layer is developed. The Earth's surface exerts a frictional resistance to atmospheric motions and slow them down [Arya, 2001]. This surface layer is a region where turbulent fluxes and stress vary by less than 10% of their magnitude. This layer is also often referred to as the constant-flux layer.

However it is now generally acknowledged that this cannot be totally applied in urban areas [Roth, 2000]. The high density of vertical obstacles, the modification of the energy budget and wind patterns can lead to the formation of an additional

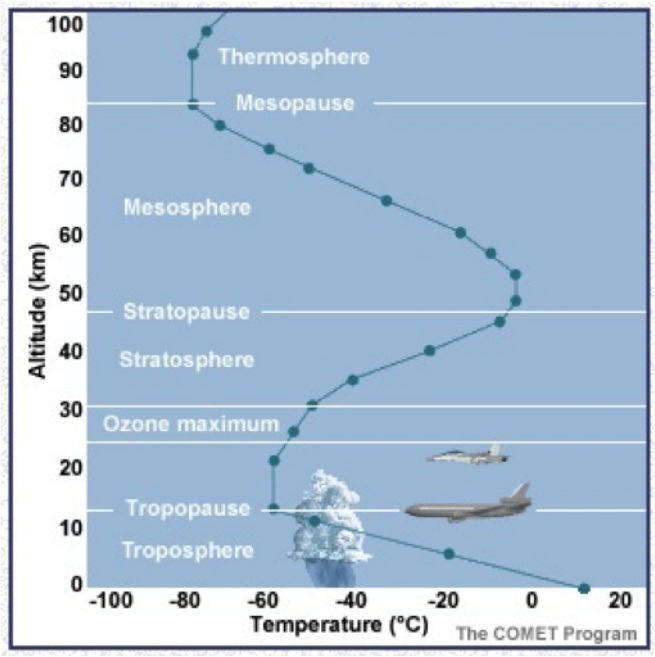

Figure 2.1: Structure of the Atmosphere (*taken from www.ncsu.edu*)

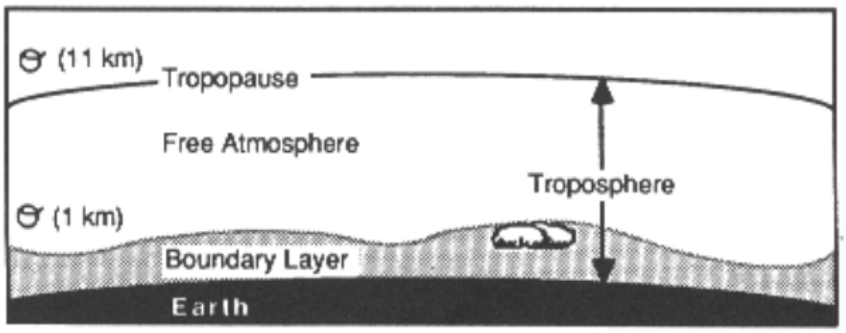

Figure 2.2: Planetary Boundary Layer

Scale	Length	Time
Global	> 500Km	Years
Meso-scale	100-200Km	Daily
Neighborhood and street	1-2Km	Hour(s)
Building	< 100m	< Hour

Table 2.1: Time and distance scale relative to the different spatial scales

phenomenon called the Urban Heat Island. Particular attention will be given in this study to the processes taking place in the urban canopy and how they have been addressed in past studies.

Section 2.2 describes of the physical phenomena driving the weather/ climate at different scales (global, meso-scale, neighborhood and building). The interactions that exist between them is given in Section 2.3. The complexity and high heterogeneity of urban areas makes modeling an excellent tool to simulate the atmospheric circulations as well as the energy use in these areas. A review of the state-of-the-art meso-scale and micro-scale models is made in Section 2.4 and the various processes that are taken into account at each of these scales are given. Finally the limitations of these models will be pointed out and it will be explained how a canopy model can be used to overcome these limitations.

2.2 From the Global to the Building scale

Atmospheric processes are governed by processes taking place at different spatial scales. Each of these spatial scales are linked to a time scale through the wind velocity [Britter and Hanna, 2003]. The relationship between the time and spatial scale can be expressed as follows:

$$x = ut \tag{2.1}$$

where x is the spatial scale, u is the velocity and t is the time scale. Table 2.1 summarizes the four spatio-temporal scales which will be discussed in this section.

Britter and Hanna [2003] had an intermediate city scale which is omitted here, but is are included here in the meso-scale. Depending on the intended application,

more or less attention have been given by previous studies for each of these scales.

2.2.1 Global

At the global scale, the weather and climate processes are dominated by three main factors:

- The main driver for Earth's climate is the Sun, more particularly the position of the Earth with respect to the Sun. The elliptic course of Earth around the sun and its rotation on itself as described by Galilei [1632, Ed. 2000], affects the global repartition of the incoming solar radiation which influences the atmospheric circulations on the entire globe.

- Earth's climate is also highly influenced by the presence of greenhouse gases in its atmosphere. Over long periods of time (more than a year), the average temperature of the Earth can be considered constant [Ramanathan et al., 1992]. The presence of carbon dioxide and other gases (water vapor for example) causes the atmosphere to warm up as they absorb some of the energy that is emitted by the planet in the infra-red wavelength. This causes Earth's average temperature to be around $15°C$ or $288K$ [IPCC, 2007].

- Other factors can also influence the Earth's climate. For example, volcanic eruptions can release large amount of gases and small particles that can influence the energy budget of the Earth. Other climate-related events, such as the El-Ñino, can also influence the atmospheric circulations for many years at various points on the globe.

Energy use inside buildings is thus mainly driven by the prevailing climate at a global scale since it will highly influence the climate at smaller scales.

2.2.2 Meso-scale

The meso-scale can be said to have a horizontal resolution of a few kilometers to several hundred of kilometers with a time scale of 1 to 24 hours.

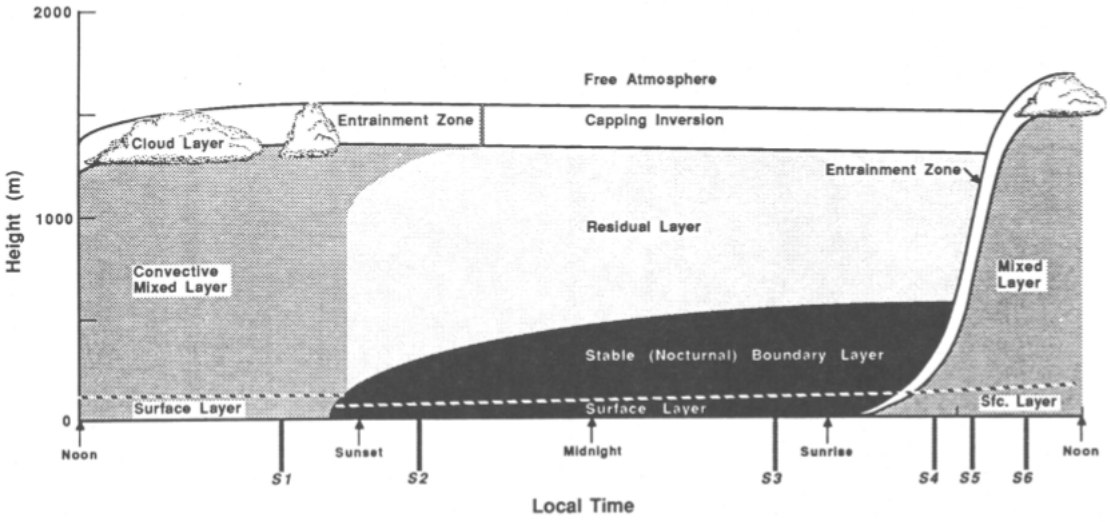

Figure 2.3: Evolution of the boundary layer during a diurnal cycle

At the meso-scale, a number of processes, along with the global variations, influences the atmospheric circulation. At this scale, complex topography, land-use characteristics, water bodies, atmospheric aerosols, snow, sea-ice and ocean interactions can have significant impact on the meso-scale atmospheric circulations.

Processes in the Planetary Boundary Layer become increasingly important for the atmospheric circulations. Figure 2.3 shows the evolution of the boundary layer during a diurnal cycle. The PBL, height and processes, evolves during the day and according to Stull [1988], the following description can be given for its evolution:

- The development of a mixed (convective) layer starts with the beginning of the day. Two situations contribute to the convection in this layer. Warm air rising from the surface creates thermals of warm air while cold air from cloud top sinks and creates thermals of cool air. The growth of this layer is entertained by the growing buoyant (heat-driven) turbulence which mixes it into the less turbulent air above the layer. The convective layer height varies in general between $1500m$ to $4000m$.

- Just before sunset, the formation of the thermals stop and turbulence starts to dissipate without any more production. This layer does not have direct

contact with the ground, but pollutant, for example, can stay trapped in this layer since it originates from "former mixed layer". This layer has thus been dubbed, the residual layer and is as such not part of the boundary layer.

- However under the influence of the ground, part of this residual layer is transformed at night in a stable boundary layer. The layer is characterized by weak turbulence. In such a layer, due to low vertical mixing, there is large horizontal dispersion, which can be seen, for example, with pollutants.

The planetary boundary layer is thus highly impacted by the land use. Large areas of vegetation, such as tropical forests, deserted areas, or urban areas can have a significant effect on the precipitation patterns [Lin et al., 2011] and the latent heat fluxes. Oke [1976] proposed that there is a distinction between the urban canopy layer and the boundary layer above it. A focus is given specially on how urban areas influence meteorological variables and circulation patterns around them.

Urban areas are made of a complex mosaic of land use and building forms. These forms are characterized by a high density of vertical surfaces and are made of artificial materials. Urban areas induce thermal and dynamic effects that are quite different from a natural environment.

The specific thermal and radiative properties of materials used in urban areas for construction purposes (roads, car parks, houses, commercial areas...) differ from natural environment and hence urban areas tend to store more energy. The presence of urban areas also modifies the surface energy budget due to change in land use and the presence of vertical surfaces as compared to the surrounding areas. This tends to cause these areas to be warmer and temperature can increase by as much as $10°C$ [Santamouris et al., 2001, Chow and Roth, 2006]. The presence of obstacles and the high density of vertical surfaces also generates a drag effect which modifies the wind patterns [Raupach, 1992, Martilli and Santiago, 2007, Hamdi and Masson, 2008, Aumond et al., 2013].

As the wind pattern and the atmospheric stability change on a daily basis, the atmospheric circulation inside urban areas is modified at the same scale (as opposed to the global scale whose time scales are quite large (years to thousands of years)). For example, at night, the atmosphere becomes very stable close to the

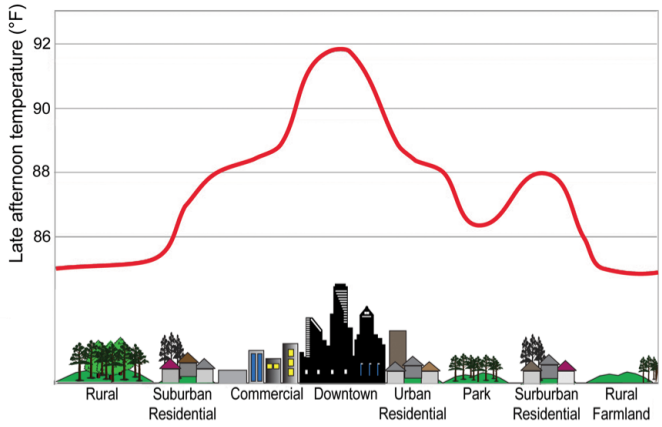

Figure 2.4: Example of an idealized Urban Heat Island - Temperature profile above an urban area (taken from *http://www.uta.edu*)

surface (see Figure 2.3) and hence a new regime is developed. Both dynamic and thermal effects modify the surface temperature and can enhance buildings' energy consumption for heating and cooling [Salamanca and Martilli, 2010, Santamouris et al., 2001].

The combination of all these effects generates a phenomenon which is referred to as an Urban Heat Island, which was first described by Luke Howard for a case study on London [Mills, 2008].

Below are a few of the physical reasons explaining the occurrence of this phenomenon:

1. *Thermal Properties.* Urban areas are built using man-made materials such as concrete and asphalt. These materials often have different thermal properties when compared to natural environment such as trees/forests. They have a distinctive specific heat capacity, thermal conductivity, albedo and emissivity [Oke, 1982]. They thus modify the surface energy budget of a particular area, since they will absorb and re-emit differently. Urban materials usually tend to have a larger specific heat capacity which means that there will be a change in the sensible heat fluxes coming from the Earth's surface as compared to vegetated environments. The heat released by the artificial materials at night is however trapped inside the urban areas due to the high density of vertical

surface (see next paragraph). This thus creates a distortion in the energy budget of the urban canopy layer and hence a temperature profile that is unlike that of the surrounding natural areas (see Figure 2.4).

2. *Building structures.* The geometry of the buildings in urban areas has a great influence on the energy balance of cities and creates a particular temperature distribution over these areas. This is due to the fact that buildings can provide shade to the incoming solar radiation and also block the release of radiation back into the atmosphere depending on the sky view factor (a measure of the degree to which the sky is observed by the surrounding for a given point [Grimmond et al., 2001])[Arnfield, 2003, Oke, 1982]. Reflection of energy between surfaces is enhanced as well as energy absorption. The great density of high vertical surfaces further increases these effects in comparison to rural areas that are relatively flat. Longwave radiations emissions into the atmosphere are thus reduced while more short wave radiations are absorbed [Oke, 1982], hence leading to a disruption in the energy balance leading to higher temperature than surrounding areas [Arnfield, 2003, Chow and Roth, 2006, Oke, 1982, Santamouris et al., 2001].

3. *Available humidity.* Construction of buildings and roads requires the cutting down of trees and natural vegetation. The lack or absence of vegetation and water bodies in urban areas leads to the reduction of available humidity and of evapo-(transpi)ration [Oke, 1982]. A change in the latent heat fluxes inevitably contributes to the formation and enhancement of the Urban Heat Island, since the surface energy budget is modified. Evapo-(transpi)ration would normally act as a cooling agent whenever trees or vegetation are present and could help mitigate the effect of sudden heating [Taha, 1997].

4. *Heat Generation.* The presence of human population in metropolitan areas implies presence of buildings, cars, industries and so on. This leads to the use of energy for a variety of purposes such as cooling, heating and transportation. This is dubbed Anthropogenic Heat Generation. According to the IEA [2008], around 50% of the energy used in buildings (world energy use) were directly related to space heating/cooling. At mid and higher latitudes,

during winter, this also account for a significant part of the occurrence of the Urban Heat Island [Offerle et al., 2006]. In summer, the use of air conditioning system will contribute to the enhancement of Urban Heat Islands [Ohashi et al., 2007, Salamanca et al., 2011] which can in turn decrease the efficiency of air conditioning devices [Ashie et al., 1999].

5. *Greenhouse gas emissions.* Transportation, buildings and industries emit greenhouse gases from their energy consumption. Most of this energy produced are used in urban areas. In France, for example, buildings only account for about 23% of the emission of greenhouse gases, for 40% energy consumption. Local emissions of greenhouse gases and other air pollutants can enhance local warming [Oke et al., 1991, Oke, 1982] but more importantly they affect the global climate. According to the IPCC, the global mean temperature would increase by as much as $6°C$ by 2100 and this could lead to an increase in the occurence of heat waves in urban areas, hence causing further distress to local population in these areas [IPCC, 2007].

6. *Other factors.* An increase in wind speed and cloud cover will tend to have a negative effect on the presence of Urban Heat Island [Arnfield, 2003]. However, anti-cyclonic conditions, city size and population will tend to have a positive feedback on the Urban Heat Island intensity. This intensity is also increased at night and during summers. The presence of topographical features such as mountains can also impact the intensity of Urban Heat Island.

All these different factors contribute to make the temperature in cities around $3 - 10K$ higher than in rural areas [Oke, 1987]. One of the most dangerous and negative effects of the presence of an Urban Heat Island is the thermal comfort inside the city. Heat waves are enhanced and can lead to increased mortality like it was the case in France during the summer of 2003 [Poumadre et al., 2005, Fouillet et al., 2006]. However, it should be noted that the presence of an Urban Heat Island would lead to lower energy consumption during winter, particularly for high and mid-latitude countries, since cities tend to be warmer.

Since the population and activities inside cities are projected to increased in the future, an expansion of the urban areas and hence of the Urban Heat Islands can

be expected. This will thus lead to a rise in temperature during both summer and winter. While in winter this will cause the energy consumption linked to heating to drop (for high and mid-latitudes countries), in summer the energy consumption will escalate with the use of air conditioning. This will further be enhanced by the likelihood of more heat waves as mentioned by the Fourth Assessment Report of the IPCC on the impacts of global warming [IPCC, 2007].

To summarize, the meso-scale is affected by a number of factors (land cover, topography, global climate, ...). Flow above the urban canopy is disturbed and deflected, and is even sometimes visible with a capping cloud [Britter and Hanna, 2003]. Due to the variations of land uses in urban areas, there is an increase in the complexity of the weather processes in the planetary boundary layer. The time scale for processes driving the weather at this scale is relatively small ($\sim$ day) as compared to the global scale ($\sim$ year(s)) while the spatial scale here is of the order of a couple of hundred of kilometers. It can thus be seen here that the macro-scale structure of the city can significantly influence the atmospheric circulations at the meso-scale in particular with regards to the the Urban Heat Island occurence.

2.2.3 Neighborhood and Street scale

At the neighborhood scale, the urban canopy interacts directly with the atmosphere and thus impacts directly the atmospheric circulations in the canopy. The spatial scale here varies from 1-2km. The flow can be assumed to be at quasi-equilibrium, and is a result of change from other scales [Britter and Hanna, 2003].

Even though above the canopy the wind can correspond to a classical logarithmic profile, the same thing is not necessarily true inside the urban canopy [Britter and Hanna, 2003, Kastner-Klein and Rotach, 2004] as the flow structure in the roughness sublayer is highly impacted by the morphological characteristics (height and size of buildings,...) of urban areas.

In this transition zone, the impact of urban areas on turbulence production is also enhanced [Rotach, 1993a,b, Kastner-Klein and Rotach, 2004].

Excess heat produced inside buildings is rejected in street canyons in urban areas. The flux exchanges between the urban canopy and the atmosphere are hence modified and can bring changes in the circulation patterns at a larger scale.

The presence of building or green areas at the neighborhood scale can also modify the wind and the temperature profiles [Park et al., 2012]. At the neighborhood level these changes occur at the time scale of an hour and thus can influence very rapidly the heat island and the atmospheric circulations.

2.2.4 Building scale

The horizontal spatial scale for this category is from a few meters to about one hundred meters and concern the lowest 5-10% of the PBL [Foken, 2008]. The time scale for processes at this scale is of the order of the hour. People inside cities live at this particular scale and most of their activities (including emissions of pollutants) takes place here. One of the reason why processes at this scale drew attention, was to evaluate the dispersion of pollutants inside street canyons.

This scale is highly influenced by the roughness elements that are present such as buildings or plants. In the case of urban areas, the variation of building heights and density will impact this roughness length [Foken, 2008].

For the scope of this study, exchange with the street canyon will be the main interest. The surface layer is the layer where the main energy exchange takes place (see Section 2.1). Processes involved at this scale include solar energy transformed into other forms of energy and also the modification of wind patterns due to friction [Foken, 2008].

The heat coming from the surface will influence the production of turbulence since it will influence the atmospheric stability in the surface layer. The occupants of a building will use more or less energy inside buildings depending on the time of the day but this usage will also be influenced by the local heat exchanges. Buildings which are better equipped (e.g. better insulation) will tend to less disrupt less the atmospheric circulations at this scale.

Moreover, at this scale, mechanical turbulence is generated and enhanced by the presence of obstacles. The presence of obstacles generates a drag effect which modifies the wind patterns [Raupach, 1992, Martilli and Santiago, 2007, Hamdi and Masson, 2008, Aumond et al., 2013] and hence have an effect on the wind flow.

Both of these effects will contribute as sources or sinks of heat and momentum within the street canyons. Thermal turbulence at this scale is small as compared

to the production of mechanical turbulence. This then induces changes that will impact the meteorological variables profiles in the urban canopy. *In fine* the intensity of the Urban Heat Island can be modified (e.g. on a calm day or stable night), simply with modifications taking place at this scale.

Besides, the surface layer turbulence is responsible for exchanges between the atmosphere and the Earth's surface. The flow in the street canyon will also depend on the characteristics of the flow above [Britter and Hanna, 2003]. This is for example the case at night when there is a stable boundary layer.

2.3 Interactions and feedbacks

In Section 2.2, the different scales were presented and it has been made clear that a number of processes influences each of these scales but, that there are strong interactions between each one of them. Figure 2.5 shows the chain of interactions that creates a feedback loop up from the building scale (micro-scale) to the scale of the city (meso-scale) to influence the intensity of a heat island above an urban area. The fact that building energy consumption depends on all the different scales highlights the importance of determining the impacts of buildings on the climate at the meso-scale level and vice-versa.

The global climate is driven essentially by the position of the Earth with respect to the Sun. The time scales at which these changes occur are larger than the time scales that are involved at the other three scales (meso-scale, neighborhood and building). Since the global scale has such a different time scale than the other ones, one can assume that there is no direct feedback on the global scale (although it is known that urban areas are responsible for an important part of greenhouse gases emissions - which in turn contribute to global climate change).

Previous studies have also suggested that Urban Heat Islands (or the presence of urban areas themselves) do not have a direct significant influence on the global climate or global temperature [IPCC, 2007, Parker, 2006]. However a few recent studies have shown that it is not to be totally neglected at the global scale [Mahmood et al., 2013]. A recent study also suggested that energy consumption at meso-scale can influence, on a relatively short time scale, the global climate and there can be disruption or changes in global wind circulations [Zhang et al., 2013].

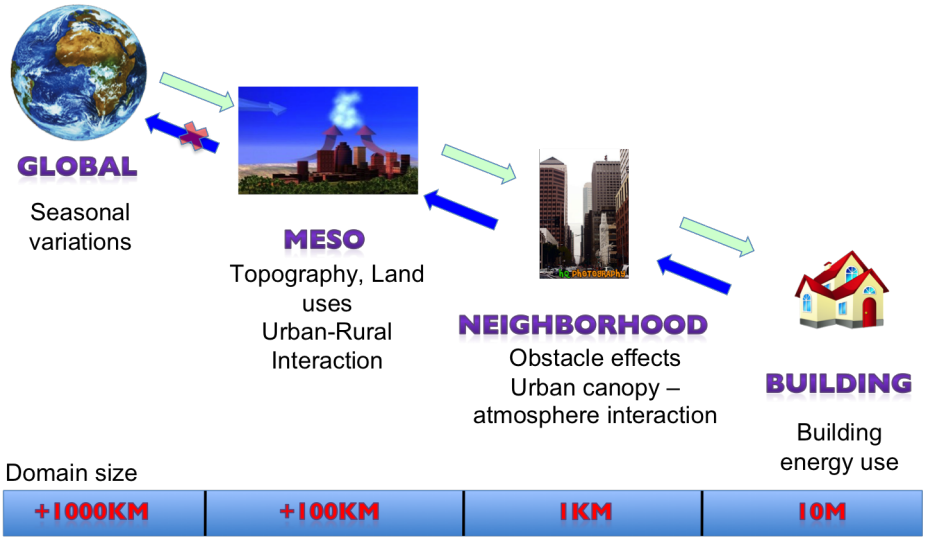

Figure 2.5: Multi-scale climate interactions (Global scale to micro-scale)

Assuming that this is not the case, the following chain of action and interactions can be proposed. Changes in the global climate are essentially driven by the Sun and hence are seasonal or yearly. It thus influences the meso-scale atmospheric circulations. At this scale, the land use becomes increasingly important and the presence of urban areas, the modification of the energy budget and wind circulation, cause the development of an Urban Heat Island. This, in turn, will impact the weather processes in the urban canopy which then interacts with the buildings. The energy consumption inside buildings within urban areas is regulated by all these processes. The buildings themselves will release heat inside the urban canopy and will also have an impact on the circulation pattern at the neighborhood scale. In this transition zone, the buildings' top will also be responsible for an increase in turbulence at this scale. The modifications brought at the urban canopy scale will then impact the weather processes at the meso-scale level, influencing again the intensity of the Urban Heat Island. As atmospheric circulations, and not climate processes, are the main goal of this study, it can be assumed on small time scales that there is no feedback to the global scale. Figure 2.6 show the different processes and interactions between the meso- and micro-scales.

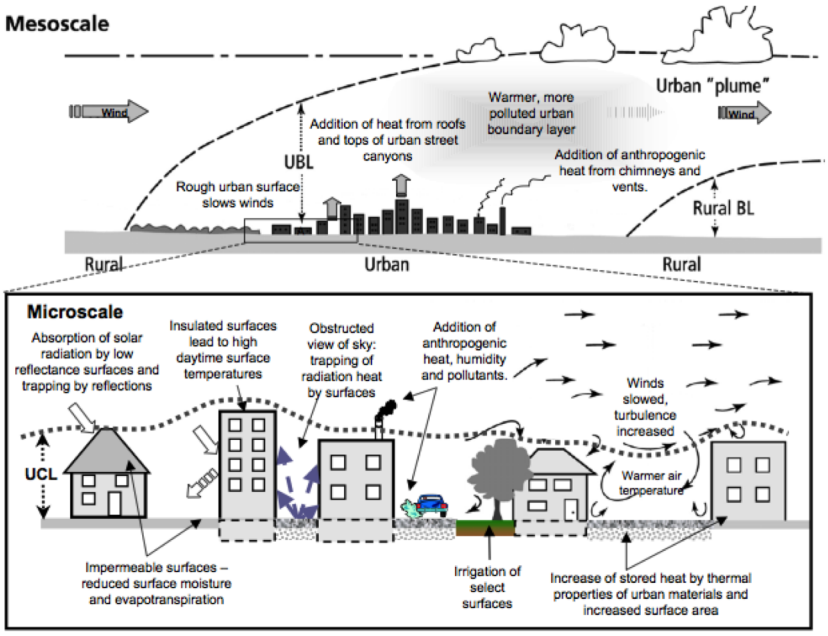

Figure 2.6: Interactions between the meso-scale and building (micro-scale) (*Voogt, 2007*)

2.4 Models

As it was seen in Section 2.3, urban meteorology and the occurrence of Urban Heat Islands are the result of very complex non-linear physical processes and can cause a number of environmental disturbances. A lot of progress has been made during the last decades in this particular field particularly regarding weather forecast at the urban scale [Baklanov et al., 2002, 2005]. But there is still a lack of models that can grasp the whole extent of urban processes that influence the intensity of Urban Heat Islands.

It would be unrealistic to try to represent the complete heterogeneous nature of urban areas due to the limited CPU power and data availability [Martilli, 2007]. However, there have been several attempts, using various techniques, to understand the processes that regulate the climate around a metropolitan area. At first, observations of the surface energy budget were used to build empirical models [Grimmond and Oke, 1999]. These models were just as realistic as the data that

were obtained through intensive measurement campaigns. Results were obtained using statistical tools to reproduce the existing conditions. Nevertheless, these models could only be used under the same conditions in which the measurements were made and could not be applied in cities with different situations.

This hence highlighted the importance of more physically-based numerical modeling. Since it was not possible to reproduce an urban area to the finer details, it was proposed that only the basic structures of cities were considered. Below, a description of models at the meso-scale as well as models at the building scale are given. Most models at the meso-scale that have been developed were used to evaluate the impact of urban areas and land use changes on the weather at this scale and on pollutant dispersion. Models at the building scale that are given here were used to calculate and represent the impacts of buildings on the energy use inside these buildings. These descriptions will show how the processes described in Section 2.2 are taken into account in these models, and hence how realistic they are. The differences between the models will also be shown.

2.4.1 Meso-scale models

As mentioned in Section 2.2, the horizontal scale of the meso-scale varies from a few to hundred of kilometers with a time range varying from hours to a day. The smallest scale matches with atmospheric features for weather forecasting whose characteristics can be represented statistically, while the longer limits correspond to the smallest features which can be seen at a synoptic scale [Pielke, 2002].

The horizontal domain size is sufficiently big to make the hydrostatic approximation, but is too small for geostrophic wind to be an appropriate approximation in the Planetary Boundary Layer. The resolution that is used at this scale also depends on the computer performance [Martilli, 2007].

Meso-scale models working at this scale have been designed to take a number of processes, specially in urban areas, into account. Several models have been developed in the recent years including NIRE-MM [Kondo, 1989], MM5 [Grell et al., 1994], FVM [Clappier et al., 1996], MESO-NH [Lafore et al., 1997] or WRF [Skamarock et al., 2008]. Each model was developed for several functions: (1) operational forecast models or (2) for dispersion or (3) to evaluate the thermal energy

budget of urban areas or (4) for other research purposes.

For the current study, focus is given on the impact of urban areas on meso-scale meteorology. In this context, the following processes are known to be taken into account in these models:

Vertical Processes Each of the model reproduces the generation of the surface layer (see Figure 2.2). This means that they include a calculation of the solar radiation and are able to calculate the production of mechanical and thermal (buoyant) turbulence. Some of them, such as WRF, include cloud formation which can also influence the occurrence or the intensity of Urban Heat Islands.

Horizontal Processes The formation of an Urban Heat Island is also represented in these meso-scale models. This would mean that they have been able to take into account the interactions that can exist between the rural and urban areas at these scales. To do so, these models should be able to modify the energy budget in urban areas as compared to a natural environment, and also modify the wind profile, which show that the model should be capable of accounting for more complex land use. Modification of wind pattern at this scale also arises due to the interaction between rural and urban areas, highlighting the need for large domains where advection processes can take place.

According to Baklanov et al. [2005], two types of approaches have been adopted in the past to calculate the influence of urban areas in meso-scale meteorological models:

- *Monin-Obhukov Similarity Theory (MOST)* The MOST developed by Monin and Obukhov [1954] and adapted by Businger et al. [1971] and Zilitinkevich and Esau [2007], was mainly applied for non-urban surfaces. It is modified by using new values for the roughness length, displacement height and heat fluxes. The first model level is generally displaced at the top of the canopy (displacement height). The main disadvantage of such models is that they cannot take into account the high heterogeneity of urban areas. Roth [2000] argued that the MOST does not hold in urban areas, and according to Arya

[2005] the similarity theories can only be applied over homogeneous surfaces. New diagnostic analytical models have thus been developed for the urban roughness layer to modify the calculation of the meteorological variables [Baklanov et al., 2005].

- *Urban parameterization* In these types of models, new sources and sinks terms, for each of the variables (momentum, heat and turbulent kinetic energy), representing building effects are calculated [Masson, 2000, Kusaka et al., 2001, Martilli et al., 2002]. These parameterizations calculate the mean thermal and dynamic effect of urban areas on the atmosphere [Salamanca et al., 2011].

A focus is given here on urban parameterizations as they are more pertinent to this study. With increasing computer performance, simplified parameterizations of cities were introduced in urban models coupled with atmospheric models to understand its impact on the boundary layer as well as the meteorological variables. In these models, the buildings and urban areas were simply represented as porosities.

The first generation of models, that included urban parameterization did not take into account the vertical surfaces present in urban areas. Their primary goal was essentially to modelize the modification of the energy budget of urban areas [Grimmond and Oke, 1999].

In a second attempt, the buildings were represented as uniform cubes that were regularly spaced [Kikegawa et al., 2003], so as to take into account the high density of vertical surfaces, which influence the energy budget of the city.

Furthermore two other types of models were developed and gave rise to more complete parameterization schemes. Both schemes solved the energy budget in a 3-dimensional urban canopy where buildings are represented with a basic geometry. Urban areas have a variety of surfaces that are exposed to radiation (roof, wall and streets) and those surfaces radiate part of the energy they receive back into the canopy layer. In addition, these models also take into account the influence of buildings or obstacles on the wind circulation pattern via a drag-force approach.

The main difference between these two schemes is that in one the urban canopy layer can be immersed in several vertical layers of the meteorological model (hence multi-layer)[Kondo and Liu, 1998, Kondo et al., 1999, Ca et al., 1999, Martilli

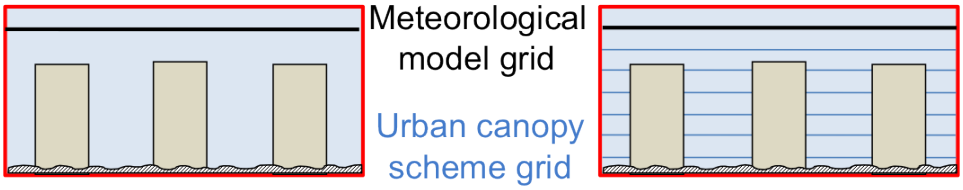

Figure 2.7: Representation of the urban canopy: left: single layer and right: multi-layer

et al., 2002] while for the other the canopy layer is forced from data coming from the first meteorological layer[Kusaka and M., 1999, Kusaka et al., 2001, Masson, 2000]. This is illustrated in the Figure 2.7.

Another difference between some of the models is that some do not take into account the orientation of the canyon and hence there can be discrepancies in the energy budget that is calculated at this scale and that is received by the buildings [Kusaka et al., 2001].

Previous works were carried out to improve the calculations of the fluxes that feedback on the meteorological model. A Finite Volume Method model (FVM), developed by Clappier et al. [1996], has been used to make such developments. Martilli et al. [2002] worked on the source terms from the surface while Rasheed [2009] worked on the diffusion processes in the urban canopy. Krpo [2009] developed a Building Energy Model (BEM), which was coupled with FVM, and Salamanca et al. [2010], Salamanca and Martilli [2010] showed that BEM is highly influenced by the weather processes at this scale.

Table 2.2 shows a selection of urban canopy parameterizations that have been implemented in meso-scale models as well as some of the characteristics of these models. Salamanca et al. [2011] compared the different schemes (Bulk, UCM, Building Effect Parameterization (BEP) and BEP-Building Energy Model) and showed that depending on the use for the meso-scale model, the appropriate scheme should be then chosen.

As it was mentioned in Section 2.2, a number of different factors affects the intensity of Urban Heat Islands. Depending on the use of the model, several schemes have been adopted and validated. For numerical weather prediction at this scale,

Model	Authors	Resolution of canopy	Vegetation	Primary use	Anthropogenic heat
MM5 MRF BL	Liu et al. [2006]	No canopy, roughness length modification	No	Weather Forecast	No
ARPS	Sarkar and De Ridder [2011]		Yes	UHI formation	Yes
Meso-NH-TEB	Masson [2000]	Single layer	Yes	Urban meteorology	from fixed temporal files
	Kusaka et al. [2001]		Yes		Yes
SUMM	Kanda et al. [2005]		Yes		No
FVM-BEP	Martilli et al. [2002]	Multi-layer	Yes	Air pollution modeling	No
WRF-BEP			Yes		No
NIRE-M	Kondo et al. [2005]		Yes		No
MM-CM-BEM	Kikegawa et al. [2003]	Multi-layer	Yes	Building energy use, air pollution modeling and urban planning	Yes
WRF-BEP-BEM	Salamanca et al. [2010]		Yes		Yes

Table 2.2: Urban canopy parameterization implemented in meso-scale models (adapted from Salamanca et al. [2011])

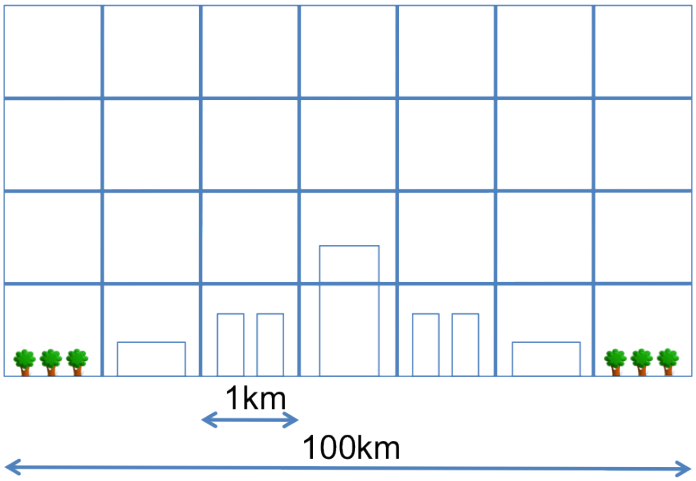

Figure 2.8: Grid in a meso-scale model

simple urban parameterization can grasp Urban Heat Island generation and be used to forecast at this scale. For other needs, such as pollutant dispersion or energy budget of urban areas, more complex parameterizations have been developed [Salamanca et al., 2011]. These parameterizations have shown that they are able to reproduce the effect of urban areas on the planetary boundary layer. Even though these parameterizations are really powerful now and have been able to represent the interactions between the urban areas and the atmosphere, buildings and streets are still not 'seen' in the grid cells of the meso-scale models due to the low vertical and horizontal resolution (see Figure 2.8). To be able to achieve this, an increase in the vertical and horizontal resolution would be needed and this would require tremendous amount of computational time and data collection.

2.4.2 Micro-scale models

A series of micro-scale models have been developed in the recent decades. Each has been used in different configurations and thus have different capabilities (air pollution problem, vegetation, building energy use, ...). In the present work, the focus will be given mainly to models used in the evaluation of energy use in buildings.

The processes driving the meteorology at the micro-scale is limited by phenomena which originate from the surface layer of the Planeteray Boundary Layer

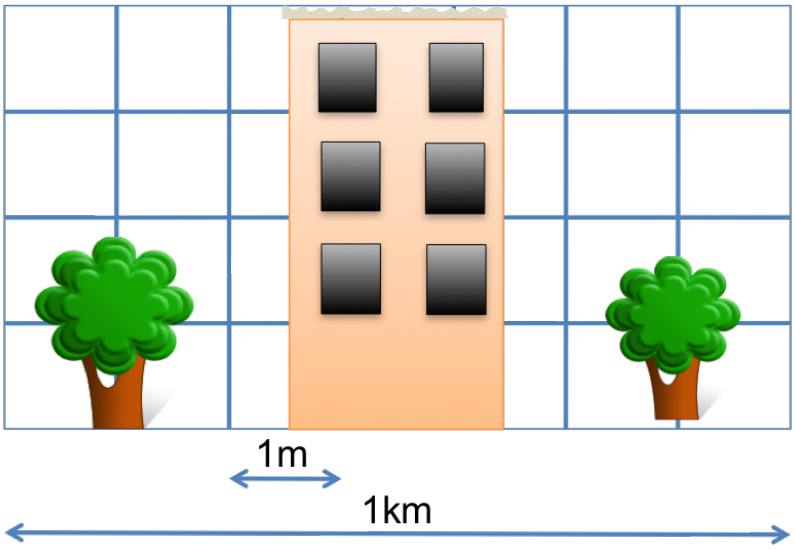

Figure 2.9: Grid in a micro-scale model

[Arya, 2001] and which are essentially influenced by the frictional forces,.

In micro-scale models obstacles are not represented like porosities. Buildings, roads and other obstacles can be explicitly described(see Figure 2.9) in these models which allow for precise calculations of the variables (momentum, energy and turbulent fluxes and energy consumption).

Standard E-ϵ (turbulent kinetic energy - dissipation) closure models and Navier-Stokes equation are usually used to resolve the turbulence and variables respectively [Yang et al., 2013]. Sources or sinks, for the momemtum, energy (heat) or humidity, are calculated and impact each of these variables. These models take into account the following processes:

Mechanical Effect At these scales, as it was shown in Section 2.2, mechanical effect of the buildings or obstacles are an important source of perturbation of the atmospheric circulations. These obstacles will modify the wind and temperature profiles and will generate turbulence. Micro-scale models can thus calculate the impact of the obstacles, often parameterized using a drag-force approach, on the wind flow.

Thermal Effect Some of the micro-scale models have been developed to account for the thermal effect (change in radiation). In these models, the height to

which an air parcel can travel, can be as high as the PBL, due to the convection processes that can be initiated. Such models can also differentiate between humid and dry convection which can influence the latent heat fluxes, crucial for the dissipation of heat.

Some micro-scale models such as Envimet [Bruse and Fleer, 1998] use a prognostic equation to calculate the evolution of the variables. These models can reproduce a more typical climate at this scale than steady-state simulations which can only simulate for small period of time [Bruse and Fleer, 1998]. Micro-scale model can receive their hourly data either from other meso-scale model or from a database where they can extract an average dataset for a particular location.

Table 2.3 shows a selection of micro-scale models used to simulate energy balance and used in urban areas. A more complete description of building energy use models can be found in Crawley et al. [2008].

2.5 Limits of existing models

The simulations using meso- and micro-scale models remain however incomplete and lack precision if the primary goal is to evaluate building energy consumption or urban planning scenarios, since the effect of the surrounding environment, which impacts the local energy balance and the dynamical flow around the obstacles, is not fully taken into account.

Meso-scale models have a coarse horizontal resolution (around $1Km$) which does not allow for complete description of the landuses and hence of the interactions that can exist between the atmosphere and the Earth's surface. Until now, computer power and capacity have limited the resolution of these models [Martilli, 2007], but with increasing performances, the resolution of meso-scale models have been enhanced over the past decades.

From a physical point of view, meso-scale models, must able to take a number of processes, such as the development of the Planetary Boundary Layer, and interactions, such as rural-urban areas interactions, which demand the domain to be sufficiently large. Their time-scale is mainly governed by the wind advection and the change in solar radiation. Urban canopy parameterizations have been developed and used in meso-scale models during the past decades. Even though these

Model	Authors	Coupling with MM	Vegetation	Anthropogenic heat
BEM	Kikegawa et al. [2003]	Yes	Yes	Yes
Building Energy Model	Krpo et al. [2010] Salamanca et al. [2010] Salamanca et al. [2011]	Yes	Yes	Yes
Energy Plus	Crawley et al. [2000]	No	No	Yes
EnviMET	Bruse and Fleer [1998] Yang et al. [2013]	No	Yes	No
Solene	Groleau et al. [2003] Idczak et al. [2010]	No	Yes	Yes
CitySim	Robinson et al. [2009] Kämpf and Robinson [2007]	Yes	No	Yes

Table 2.3: Micro-scale models used to evaluate building energy use

parameterizations have improved the representation of the impact of urban areas on atmospheric circulations, they still do not simulate correctly the near-surface temperature and wind speed [Salamanca et al., 2011].

As opposed to meso-scale models, micro-scale models have a high enough resolution which means that obstacles, such as buildings or plants, can be explicitely described. Increasing the size of the domain to capture large scale processes would require high amount of computing power and time and is not feasible for the time being.

Due to these restrictions, their boundary conditions are often specified using either averaged climatic data or they come from a database. They hence have a significant flaw in the data used for their boundary conditions due to the limitation of their horizontal domain. The meteorological variables, that have been calculated by the micro-scale model or are coming from averaged data from a database, do not take into account the advection processes that could bring wind, heat or turbulence from a different area/region upstream. This means that the data used as input for these models do not have a history of the thermal or mechanical effects which can travel large distances.

2.6 Conclusion

In the urban canopy, the atmospheric circulations are mostly impacted by mechanical effects. There are also thermal effects which can influence more or less turbulence generation. According to Santiago and Martilli [2010] the size of turbulent eddies inside the canopy is limited by the presence of buildings and they showed that these eddies can be considered to have a constant height inside the canopy. Inside the urban canopy, mechanical production of turbulence (proportional to the size of the eddies) are pre-dominant. In the Monin-Obhukov Similarity Theory, it is assumed that after a height, L (often above the height of the urban canopy), the buoyancy effects becomes much greater than the mechanical effect. It can thus be seen that there is a transition zone, which happens to be between two different scales, which is not often easy to grasp and take into account in models.

Moreover, an enhancement of the boundary conditions in models (both meso-scale for the surface layer and in micro-scale for actual boundary condition) is

needed to improve simulations and also to include the spatial and chronological history of the weather variables.

Britter and Hanna [2003] pointed out that there is still a gap into how the neighborhood scale should be addressed and how it should be connected to the city and street scale. We proposed here to develop a canopy model, that will be at the interface between these two scales, and can thus be used to connect meso-scale models and micro-scale models. The aim of this canopy model is to use data from meso-scale models as input so as to calculate new profiles for the various variables which can then be used as input for urban parameterization schemes or micro-scale models. The model also aims at addressing the limits mentionned in Section 2.5. The canopy model will be able to provide an improved profile for the micro-scale models where the history of these variables are taken into account with data coming from the meso-scale models. In return, the meso-scale models will get more precise information concerning the surface layer as more precise fluxes will be calculated in urban areas and hence the impact of obstacles and buildings will be properly described.

Besides the fact that meso-scale models can now interact directly with micro-scale models, it will not be necessary to increase the vertical resolution of the meso-scale models to improve simulations. With the use of a canopy model the first level of the meso-scale model can thus be increased as the use of the canopy model is expected to improve the calculation of more precise and accurate vertical meteorological profile for the meso-scale grid. It is hence expected that computer processing time will be reduced with the use of a canopy model as compared to highly resolved meso-scale model simulations.

Chapter 3

Development of a 1D-CANOPY model. Part I: Neutral case and comparison with a C.F.D

This chapter corresponds to "Mauree, D. et al. 2014b, Development of a 1D Canopy Interface Model. Part I: Neutral case and comparison with a C.F.D, in preparation, 2014"

Abstract

A new Canopy Interface Model (CIM) is developed to evaluate the influence of obstacles on the atmosphere in the boundary layer. The objective is to analyze urban parameterizations and guarantee the coherence between these propositions to simulate their influence on spatially averaged variables (wind speed, temperature, humidity and turbulent kinetic energy).

CIM development is presented through the main governing equations, with a specific focus on the coherence with past propositions and the modification brought to these equations. Compared to previous studies, obstacles characteristics are computed using surface and volume porosities in each cell of the model domain. These porosities are used to weight several terms in the Navier-Stokes equations and have been introduced to prepare a coupling of the model with micro-scale model including the modeling of different kind of obstacles. A 1.5 order turbulence closure using the Turbulent Kinetic Energy (T.K.E) is used in the model. The mixing length is computed to take into account the obstacle density in the canopy layer as proposed by Santiago and Martilli [2010].

Results are compared with analytical solutions obtained in neutral atmospheric conditions, and also with data collected from a C.F.D experiment. When no obstacles are present, the comparison of results from CIM with the analytical solutions shows that CIM is able to reproduce the surface layer processes over a plane surface. We show that over such a surface, a constant turbulent kinetic energy profile is obtained. With the presence of obstacles, few scenarios are performed in order to analyze the effect of obstacles on wind and turbulent kinetic energy profiles. The results show that fluxes from vertical surfaces have the most important effect. CIM is also able to reproduce an Inertial Sub-layer as described by the Prandlt or constant-flux layer theory above a displacement height over a homogeneous canopy. The comparison of CIM with the C.F.D results show good agreements.

Keywords: atmospheric boundary layer, turbulence parameterization, turbulent kinetic energy, surface layer theory, urban canopy.

3.1 Introduction

The study of the effects of urban areas on the boundary layer structure and on the wind fields were first motivated by the will to understand the dynamics of the planetary boundary layer with respect to pollutant dispersion [Delage and Taylor, 1970, Bornstein, 1975]. The enhancement of computer performance in the last decades has also allowed more precise meso-scale models to be developed with several new propositions to parameterize the surface fluxes and their diffusion [Masson, 2000, Kusaka et al., 2001, Martilli et al., 2002]. However in view of the current state of the art models and growth of computer performance, it is still not possible to use very high resolution (for ex. 1m) that would be able to integrate obstacles (such as buildings or trees) in meso-scale models [Martilli, 2007] while at the same time simulating large enough domains so as to capture large scale interactions.

Indeed the complexity and high heterogeneity of urban surfaces (buildings, roads, green spaces) make it very difficult to simulate the urban boundary layer. The surfaces and obstacles present in such areas modify the fluxes as well as the profiles of various meteorological variables inside the canopy itself [Oke, 1987, Foken, 2008]. They also influence the boundary layer above the urban canopy impacting meso-scale weather processes [Craig Jr, 2002]. The use of traditional theories (such as the similarity theory), to simulate the boundary layer in an urban context, is thus not expected to work [Rotach, 1993a, Roth, 2000]. The turbulent flux of momentum, for example, is not constant with height anymore but instead decreases to zero up to the zero-displacement height.

Masson [2000] developed a single layer canopy model where an urban canopy parameterization is used to calculate the effects of urban areas on various meteorological variables. The first level of the meteorological model is displaced above the urban areas and a mean value of the variables in the canopy is used to calculate the source and sink terms due to urban areas. Martilli et al. [2002] proposed another parameterization scheme. The multi-layer scheme they developed was fully integrated in the meso-scale model. Using the same methodology as Martilli et al. [2002], Muller [2007] designed experiments to show that a canopy module can be used to enhance the computational time while decreasing the vertical resolution.

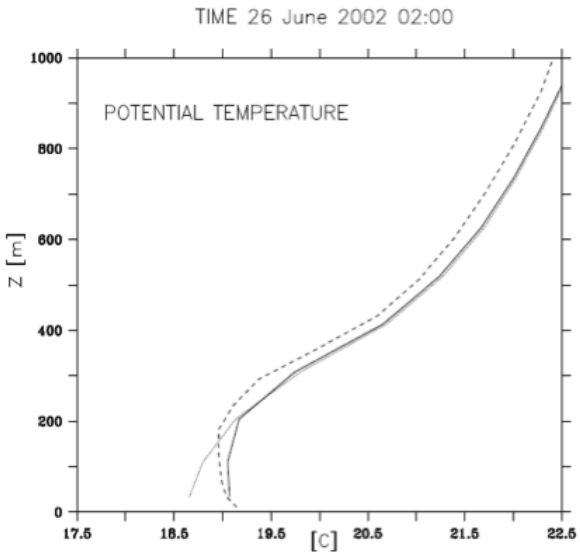

Figure 3.1: Use of a canopy module allows low vertical resolution (results from Muller, C., 2007) Bold black line (-) high resolution (20m) in meso-scale model; dotted line (- -) canopy model in meso-scale with low resolution (60m); pale black line (-) meso-scale model with low resolution (60m)

Figure 3.1 shows that the use of a canopy module with a low resolution (60m) in a meso-scale model gives the same trend as using a very high resolution (20m) in such models [Muller, 2007]. Using a canopy model is hence expected to reduce computational time while allowing at the same time a more precise integration of obstacles and calculation of the fluxes generated by the presence of these obstacles. However in this work, the canopy model developed by Muller [2007] was not independent of the meso-scale model.

Based on this statement, a new Canopy Interface Model (CIM) has been developed. The objective was to develop a 1D model that could be used independently of a meso-scale model, but could also be coupled with a meso-scale model. The coupling with meso-scale model could be done to improve urban boundary layer description or to give the possibility to the user to couple the meso-scale model with a micro-scale model that may provide a detailed representation of the geometry of the surface obstacles (real building or urban vegetation shapes) or even computation of surface fluxes.

This work is based on developments, proposed by Martilli et al. [2002], as well as on the work of Muller [2007], to improve the effect of urban parameterization on meteorological variables. The multi-layer scheme, that was previously developed, was modified to include a diffusion process based on a 1.5 order turbulence closure using the turbulent kinetic energy in order to calculate a more precise profile for the variables. A diagnostic mixing length is used in the model based on the formulation proposed by Santiago and Martilli [2010]. To be able to take into account any obstacle, an interface has been developed to represent the obstacle's effects in terms of porosities inside the Navier-Stokes equations.

When developing the model, a specific attention was brought to test several urban parametrizations and control their relative coherence. For that purpose, the model is here first tested offline in neutral atmospheric conditions over a plane surface and results are compared to classical theories such as the Prandtl surface layer theory. Obstacles are then integrated in CIM and the results are compared with data issued from a C.F.D experiment [Santiago et al., 2007, Martilli and Santiago, 2007].

In Sect. 3.2, the main assumptions and theories proposed to describe the surface layer are given. In Sect. 3.3, a complete description of CIM and the set of equations on which the model is based are presented. Section 3.5 shows the comparison of CIM, without obstacles and in neutral conditions, with an analytical solution obtained using the Prandtl's surface layer theory. The results are also compared in the presence of obstacles with results from a C.F.D experiment. The results that are obtained and their limits are finally discussed in Sect. 3.6 as well as the different perspectives for CIM.

3.2 The Surface Layer

A number of processes have been parameterized in the past to describe the flow in the surface layer. Important characteristics of the surface layer were first described by Prandtl [1925] and has been afterwards recognized as the Prandtl or constant flux layer theories. Consequently, several studies were conducted to improve the mathematical representation of the different processes taking place in this surface layer and under different atmospheric stability conditions [Monin and Obukhov,

1954, Foken, 2006, Zilitinkevich and Esau, 2007].

The surface layer theory is commonly described using a series of theory and assumptions:

1. **Homogeneity assumption**
   When considering large enough horizontal distances, it is assumed that the horizontal properties of a flow is homogeneous and hence that the vertical fluxes are relatively more important as compared to the horizontal fluxes.

   Following this assumption, the averaged characteristics of the flow are considered to be a function of the z(vertical)-coordinate only.

2. **The K-Theory**
   The vertical kinematic turbulent fluxes can then be approximated to:

$$\overline{u'w'} = -\mu_t \frac{\partial U}{\partial z} \tag{3.1}$$

   where u' and w' are the fluctuations of the horizontal and vertical wind velocity components respectively, where U is $\overline{U}$ and is the horizontally averaged wind velocity (ms^{-1}) and μ_t is the eddy diffusion coefficient (m^2s^{-1}).

3. **Boundary layer theory**
   The boundary layer theory states that in the surface layer, above a plane surface, the vertical fluxes can be assumed constant (variation of less than 10% and while neglecting the effect of the Coriolis forces). This surface layer is called the Prandtl or constant-flux layer. This gives rise to the boundary layer assumption where

$$\mid \overline{u'w'} \mid = u_*^2 = constant \tag{3.2}$$

   where u_* is the friction velocity.

4. **First order turbulence closure in neutral conditions**
   To compute the turbulent diffusion coefficient, an analogy with the molecular diffusion process is made. The diffusion coefficient can be described as the

product of a velocity scale, V', times a length scale, l, like when describing the molecular diffusion and is given by Eq. (3.3).

$$\mu_t = V'l \tag{3.3}$$

Over a plane surface, the length l is the mixing length. It is usually assumed to be equal to the height z or kz. If we follow the analogy to the molecular diffusion, we will consider that the mixing length is equal to z, as it could represent the maximum distance that an air parcel will travel before it touches the surface; it could also, in this way, represent the maximum size of the turbulent eddies. The velocity scale can be replaced by the friction velocity u_* and a constant k, yielding the following equation:

$$\mu_t = ku_*z \tag{3.4}$$

where k is the von Kármán constant (0.41) according to Högström [1996]. Recent studies showed however that k was closer to 0.39 and suggest that this value can change with stability [Zhang et al., 2008].

These theories and assumptions, all build together, produce the so-called **Prandtl surface layer theory**. The wind profile can then be calculated using Eqs. (3.1), (3.2) and (3.4):

$$\frac{\partial U}{\partial z} = \frac{u_*}{kz} \tag{3.5}$$

Integrating between z_0 (which is also commonly known as the roughness height and represents the height of obstacles that can be placed randomly on the ground and around which the mean horizontal velocity is equal to zero) and z, the following logarithmic profile is obtained:

$$U(z) = \frac{u_*}{k}\ln\left(\frac{z}{z_0}\right) \tag{3.6}$$

When the roughness elements are closely packed together, such as in a city or in a forest, the top of the elements act as a displaced surface [Stull, 1988].

The wind speed can then be assumed to be equal to zero at that displaced height. Equation (3.6) can be written as follows to take this into account:

$$U(z) = \frac{u_*}{k} \ln\left(\frac{z-d}{z_0}\right) \tag{3.7}$$

where d is the displacement height (m) and U is defined as being equal to zero when z is $d + z_0$.

3.3 Canopy Interface Model

The Canopy Interface Model is developed with the objective of testing the coherence between parameterizations proposed to represent the effects of built surfaces on the atmosphere, and to prepare a 1D-column model that could be used offline or online in a meso-scale model. One of the goals of CIM, is to prepare the coupling of meteorological meso-scale models with micro-scale models in such a way that the user of the micro-scale model may provide coherent information of the geometry of the obstacle (such as volume or surface porosities) and eventually exchange surface fluxes. The coupling of the models is not presented here. This article aims at showing how CIM was developed, testing step by step the coherence with past propositions.

As it has been stated before, the high complexity of surfaces in urban areas is a major problem for their integration inside models. The presence of urban surfaces inside the canopy has a major influence on the air-flow:

1. Radiation trapping and heat conduction by building
2. Drag force induced by vertical and horizontal surfaces
3. New ways of transformation of Mean Kinetic Energy into Turbulent Kinetic Energy.

Each of these effects needs to be taken into account as they impact the different meteorological variables (temperature, wind speed and turbulent kinetic energy).

In this specific study, we will not describe the effect of building on the radiation and heat exchanges, but we will focus on mechanical effects only. For this purpose, we will consider the atmosphere in a neutral stability condition.

3.3.1 Governing Equation: Momentum Equation

The transport of a quantity, can be written in a conservative form [Clappier et al., 1996]. The resulting equation for the momentum calculates the time evolution of the mean momentum in the following way.

$$\frac{\partial U_i}{\partial t} + U_j \frac{\partial U_i}{\partial x_j} = -\delta_{i3} g + f_c \varepsilon_{ij3} U_j - \frac{1}{\overline{\rho}} \frac{\partial \overline{P}}{\partial x_i} + \nu \frac{\partial^2 U_i}{\partial x_j^2} - \frac{\partial (\overline{u_i' u_j'})}{\partial x_j} + f_u^s \tag{3.8}$$

where U_i or U_j are the mean wind (ms^{-1}) with three components depending on i and j which are indices for each direction, x_i or x_j are the distance in each direction (m), t is the time (s), δ_{i3} is the Kronecker delta (a scalar quantity), g is the acceleration due to gravity(ms^{-2}), f_c is the Coriolis force (s^{-1}), ε_{ij3} is a unit tensor (also a scalar quantity), ρ is the density (kgm^{-3}), P is the pressure ($kgm^{-1}s^{-2}$), ν is the kinematic viscosity (m^2s^{-1}) and u_i' and u_j' are the turbulent component of the wind (ms^{-1}).

The first term on the left hand side is the mean momentum while the second term is the advection of the mean momentum by the mean wind. The terms on the right hand side represents respectively the effect of gravity, the influence of the Earth's rotation (Coriolis force), the mean pressure-gradient forces, the influence of the viscous stress on mean motions, the influence of Reynolds' stresses on the mean motions due to air parcels friction and the specific sources of momentum f_u^s due to the friction of air with surfaces (bare soil, vegetation, buildings...). Additional information about these specific sources can be found in Martilli et al. [2002] and Krpo [2009].

CIM is a 1-D column model. It was developed taking into account that:

1. when working at the canopy (neighborhood) scale, it is possible to assume horizontal homogeneity, that is, it is assumed that the $\frac{\partial}{\partial x}$ and $\frac{\partial}{\partial y}$ terms are equal to zero

2. the subsidence can also be considered to be small (with W, the vertical wind component being of the order of mm/s compared to the horizontal wind component, U and V which are of the order of m/s) [Stull, 1988]

3. at this scale the Coriolis effect is also neglected

4. viscous stress is very small compared to the other terms in Eq. (3.8)

5. the Reynolds stress can be approximated, under certain conditions, to a be proportional to the wind gradient (see Sect. 3.2)

6. advection processes as well as the mean pressure gradient are also neglected.

Using such approximations, Eq. (3.8) gives:

$$\frac{\partial U_i}{\partial t} = \frac{\partial}{\partial z}\left(\mu_t \frac{\partial U_i}{\partial z}\right) + f_u^s \tag{3.9}$$

where μ_t is the turbulent diffusion coefficient and U_i is the wind speed. In CIM the turbulent diffusion coefficient is computed using a 1.5 order turbulence closure.

3.3.2 1.5 order turbulence closure

When obstacles are present, it is however no longer possible to make the same assumption on the mixing length which was made in the first order turbulence closure [Coceal and Belcher, 2004, Santiago and Martilli, 2010]. Furthermore u_* cannot be considered constant anymore in the presence of obstacles [Högström, 1996, Roth, 2000, Foken, 2008]. In such cases, Eq. (3.4) is thus not applicable and it was proposed to use a different calculation for the diffusion coefficient.

Besides the one derived from the K-Theory (Eq. 3.1), the turbulent diffusion coefficient can be computed using a 1.5 order turbulence closure using the Turbulent Kinetic Energy (T.K.E) as given in the following equation:

$$\mu_t = C_k \sqrt{E} l \tag{3.10}$$

where C_k is a constant. A value of 0.4 has been used by different authors [Therry and Lacarrère, 1983, Bougeault and Lacarrère, 1989, Abart, 1999]. In

Sect. 3.3.4, to further guarantee the coherence of the formulations that have been proposed, a different methodology to compute this value will be presented.

3.3.3 Coherence between formulations of the turbulent diffusion coefficient

Equation (3.4) may be applied only over a plane surface in neutral conditions where no obstacles are present. However, Eq. (3.10) may be applied on any kind of surfaces and stability conditions. A statement to build CIM was that these two formulations should be coherent over plane surfaces and neutral conditions. In such cases, if the two different propositions for the turbulent coefficients are equal, then it can be shown that a constant turbulent kinetic energy profile will be obtained :

$$E = \left(\frac{ku_*}{C_k}\right)^2 \tag{3.11}$$

This coherence statement will be used to simplify the turbulent kinetic energy governing equations which will be presented in Sect. 3.3.4.

3.3.4 Governing Equation: Turbulent Kinetic Energy Equation

As for the momentum, the same equation could be obtained for computing the Turbulent Kinetic Energy (T.K.E). For the purpose of this paper a focus is given only to the neutral conditions and the equation will be given for accordingly. Assuming horizontal homogeneity, a prognostic equation can be used to calculate the Turbulent Kinetic Energy (T.K.E):

$$\frac{\partial E}{\partial t} = \frac{\partial}{\partial z}\left(\lambda_t \frac{\partial E}{\partial z}\right) + P - \varepsilon + f_e^s \tag{3.12}$$

where λ_t can be assumed to be equal to μ_t.

Equation(3.12) gives the time-evolution of the T.K.E in neutral conditions and the buoyancy term is hence neglected here. The terms on right hand side represent respectively the diffusion term, the mechanical production term, the dissipation

term and the fluxes due to the presence of obstacles.

The production term represents the wind shear caused by wind gradient and friction over surfaces and is given by the following equation:

$$P = -\overline{u'w'}\frac{\partial U}{\partial z} \tag{3.13}$$

where $\overline{u'w'}$ is the momentum flux. Note here that a negative sign is present so that the production term actually contributes positively to the generation of turbulence since the term $\overline{u'w'}$ is negative.

Based on the surface layer theory, $\overline{u'w'}$ can be replaced using Eq. (3.1). This then yields a production term equal to:

$$P = \mu_t \left(\frac{\partial U}{\partial z}\right)^2 \tag{3.14}$$

The dissipation term represents the breaking down of the larger turbulent eddies into smaller ones and can be expressed as:

$$\varepsilon = C_\varepsilon^* \frac{E^{\frac{3}{2}}}{l} \tag{3.15}$$

where l is still the parameterized mixing length representing the maximum size of the turbulent eddies and C_ε^* a constant. One can note that the dissipation term is not written as usual: in other studies another a specific dissipation length is defined [Chen and Kim, 1987] with various formulations [Louis et al., 1983, Delage, 1974]. This dissipation length is sometimes assumed to be different from the mixing length scales [Christen et al., 2009, Santiago and Martilli, 2010]. It is argued in this article that the geometry of the canyon is the most important parameter and there is no reason to use a different mixing length in the dissipation term. However, it is important to take into account a constant to scale the dissipation compared to the production. One can say that the mixing length, defined here as the maximum distance that could reach an air parcel (analogy with the molecular diffusion) is weighted in the dissipation term using only a constant. Thus the C_ε^* value is chosen to be different from the traditional C_ε.

Replacing Eqs. (3.14) and (3.15) in Eq. (3.12) yields:

$$\frac{\partial E}{\partial t} = \frac{\partial}{\partial z}\left(\lambda_t \frac{\partial E}{\partial z}\right) + \mu_t \left(\frac{\partial U}{\partial z}\right)^2 - C_\varepsilon^* \frac{E^{\frac{3}{2}}}{l} + f_e^s \tag{3.16}$$

Using Eq. (3.10) to replace the diffusion coefficient in Eq. (3.16), the following equation is obtained:

$$\frac{\partial E}{\partial t} = \frac{\partial}{\partial z}\left(\lambda_t \frac{\partial E}{\partial z}\right) + C_k \sqrt{E} l \left(\frac{\partial U}{\partial z}\right)^2 - C_\varepsilon^* \frac{E^{\frac{3}{2}}}{l} + f_e^s \tag{3.17}$$

Re-arranging Eq. (3.16):

$$\frac{\partial E}{\partial t} = \frac{\partial}{\partial z}\left(\lambda_t \frac{\partial E}{\partial z}\right) + C_\varepsilon^* \frac{\sqrt{E}}{l}\left(E_{stat} - E\right) + f_e^s \tag{3.18}$$

The simplicity of Eq. (3.18) makes it easy to resolve when discretizing it with an implicit and explicit term. E_{stat} represents the stationary value of the T.K.E that can be obtained over a plane surface under neutral conditions (i.e. when the local production of T.K.E is equal to the dissipation). It is written as follows:

$$E_{stat} = \frac{C_k}{C_\varepsilon^*} l^2 \left(\frac{\partial U}{\partial z}\right)^2 \tag{3.19}$$

From this, the value of C_k can be calculated. As mentioned in Sect. 3.3.3 both formulations of the turbulent diffusion coefficient (Eqs. 3.4 and 3.10) have to be equal. If it is assumed here again that the mixing length is equal to the height and that the wind gradient is proportional to the friction velocity (as in Eq. 3.5), then it can be calculated that:

$$\frac{C_k^3}{C_\varepsilon^*} = k^4 \tag{3.20}$$

Thus, if we consider that the most important result is that the production term should be scaled compared to the dissipation term (or the countrary), it can be seen here that if a value of 1 is chosen for C_ε^*, C_k is equal to $k^{\frac{4}{3}}$.

To sum up this section, it has been shown that CIM solves 1-D transport equations. If CIM is coupled with a meso-scale model, the top boundary conditions,

for the different variables, are expected to come from the meso-scale model.

3.3.5 Discretization

CIM uses a Finite Volume Method to find a solution for the partial differential equation given in Eq. (3.21). The discretization of the equations is only done here for the momentum equation but the same methodology is applied for both the U and the V wind component as well as for the discretization of the T.K.E equation.

$$\frac{\partial U}{\partial t} = \frac{\partial}{\partial z}\left(\mu_t \frac{\partial U}{\partial z}\right) + f_u^s \tag{3.21}$$

where the term f_u^s is the source term representing the fluxes that will impact the flow.

$$\int_{\delta V} \frac{\partial U}{\partial t} dV = \int_{\delta V} \frac{\partial}{\partial z}\left(\mu_t \frac{\partial U}{\partial z}\right) dV + F_u \tag{3.22}$$

where F_u is the integral over a volume dV of f_u^s (for additional information refer to [Martilli et al., 2002]).

Using Gauss-divergence theorem to change the volume integrals of the diffusion term into surface integrals:

$$\int_{\delta V} \frac{\partial U}{\partial t} dV = \int_{\delta S} \left(\mu_t \frac{\partial U}{\partial z}\right) dS + F_u \tag{3.23}$$

Discretizing Eq. (3.23) to determine the solution:

$$U_I^{t+1} = U_I^t + \triangle t \frac{S_i}{V_I} \mu_t \frac{U_{I-1} - U_I}{\triangle z} + \triangle t \frac{S_{i+1}}{V_I} \mu_t \frac{U_I - U_{I+1}}{\triangle z} + \triangle t F_u \tag{3.24}$$

where S and V are the surface and the volume of the obstacles respectively and i and I are indices representing the cell face or centre respectively. These surfaces and volumes could be replaced by surface and volume porosities. These values can be obtained from a different model where the porosities will be represented more precisely. These porosities could represent any obstacles (such as buildings or trees) present in the canopy.

3.3.6 Obstacles integration

CIM calculates the fluxes generated by horizontal and vertical surfaces mainly based on the formulation proposed by Martilli et al. [2002] but reformulated here using porosities. The objective is to be able in the future to include any kind of obstacles.

Geometrical obstacles characteristics

Obstacles sizes are specified here *at each of the levels* inside the urban canopy module for the x- and y-directions (until now obstacles, and specially buildings, were only considered as regular cubes). These dimensions are then used to calculate the volume and surface porosities which will be used in the calculation of the fluxes and the diffusion coefficient.

Obstacles 3-D geometry are described according to Krpo et al. [2010], Kohler et al. [2012] and are shown in Fig. 3.2. The obstacles (buildings and street canyons) are repeated to fill the space inside a grid cell. Surface and volume porosities are then defined as in Fig. 3.3 where I represents variables assigned to the cell centre and i to the cell face.

The geometrical characteristics of the obstacles are calculated as follows and their values vary from 0 to 1.

- The free volume porosity is then given by:

$$\phi(I) = 1 - \hat{\phi}(I) \tag{3.25}$$

  where the occupied volume $\hat{\phi}$ is given by:

$$\hat{\phi}(I) = \frac{B_x(I)}{(B_x(I) + W_x(I))} \frac{B_y(I)}{(B_y(I) + W_y(I))} \tag{3.26}$$

- Based on volume porosity, the free surface porosity can be calculated as follows:

$$\varphi(i) = min(\phi(I), \phi(I-1)) \tag{3.27}$$

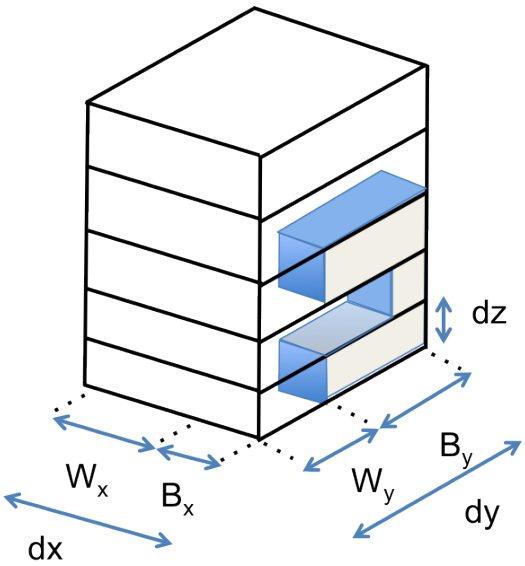

Figure 3.2: Integration of obstacles inside CIM (B_x and B_y are the building length and W_x and W_y are the street width in the x and y-directions respectively. dx and dy are the horizontal grid resolution while dz is the vertical resolution)

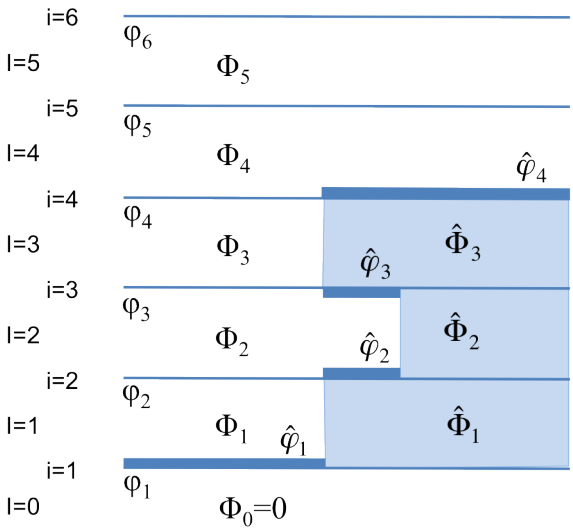

Figure 3.3: Side view of a section of the 1-D column showing the interpretation of porosity by CIM

- The obstacles horizontal ($\hat{\varphi}_h$) and vertical ($\hat{\varphi}_{vx}$ and $\hat{\varphi}_{vy}$) surfaces (not shown on Fig. 3.3) are computed as follows:

$$\hat{\varphi}_h(i) = \phi(I) - \phi(I-1) \tag{3.28}$$

$$\hat{\varphi}_{vx}(I) = \frac{B_y(I)}{(B_y(I)+W_y(I))}\frac{B_x(I)}{(B_x(I)+W_x(I))}\frac{1}{(B_x(I))} \tag{3.29}$$

$$\hat{\varphi}_{vy}(I) = \frac{B_y(I)}{(B_y(I)+W_y(I))}\frac{B_x(I)}{(B_x(I)+W_x(I))}\frac{1}{(B_y(I))} \tag{3.30}$$

Modification of the governing equations

The surface and volume porosity, as calculated with Eqs. (3.27) and (3.26) respectively, can be used to replace the S and V terms from Eq. (3.24).

$$U_I^{t+1} = U_I^t + \triangle t\frac{\varphi_i}{\phi_I}\mu_t\frac{U_{I-1}-U_I}{\triangle z} + \triangle t\frac{\varphi_{i+1}}{\phi_I}\mu_t\frac{U_I-U_{I+1}}{\triangle z} + \triangle t F_u \tag{3.31}$$

where F_u in Eq. (3.8) represents the additional forces that will impact the momentum.

As stated before, the presence of obstacles inside the canopy alters the flow pattern, the surface fluxes and the generation of turbulence. The influence of obstacles has been parameterized and has been used in previous models [Masson, 2000, Martilli et al., 2002]. The parameterization of these fluxes are adapted from Martilli et al. [2002]. The geometrical variables given in Sect. 3.3.6 will influence the diffusion coefficient as shown in Eq. (3.31) and the calculations of the different fluxes as shown in Sects. 3.3.6 and 3.3.6.

Modification of the momentum flux terms

Horizontal surfaces in the canopy (roofs, streets...) induce a frictional force on the movement of air masses and lead to a loss of momentum. Above such surface, the surface layer theory can be used to express the fluxes that are induced [Louis,

1979, Martilli et al., 2002].

$$\vec{F}u_I^H = -\rho \left[\frac{k}{\ln\left(\frac{\Delta z/2}{z_0}\right)} \right]^2 \mid U^{hor} \mid \vec{U_I} \frac{\hat{\varphi}_h}{\phi} \tag{3.32}$$

where k is the von Kármán constant (0.41), Δz is the size of the vertical levels, z_0 is the roughness length ($0.05m$), U^{hor} is the horizontal wind speed and $\hat{\varphi}_h$ is the total horizontal obstacle surfaces at each level.

Vertical surfaces of the obstacles create a pressure gradient which is parameterized as a drag-force [Raupach, 1992, Otte et al., 2004, Martilli, 2007, Hamdi and Masson, 2008, Aumond et al., 2013] in the momentum conservation equation.

$$\vec{F}u_I^V = -\rho C_d \mid U^{ort} \mid \vec{U_I} \frac{\hat{\varphi}_v}{\phi} \tag{3.33}$$

where I is the x or y-direction, C_d is the drag coefficient as parameterized by Santiago and Martilli [2010], U^{ort} is the orthogonal wind component and $\hat{\varphi}_v$ is the total vertical obstacle surfaces in each direction at each level.

Modification of the Turbulent Kinetic Energy

To evaluate the production of T.K.E by horizontal surfaces of obstacles, it is possible to use the E_{stat} value given by Eq. (3.19) which has been obtained over a plane horizontal surface. Using Equation (3.5) from the surface layer theory, $\partial U/\partial z$ can be replaced to obtain the following equation:

$$E_{surf} = \frac{C_k}{C_\varepsilon^*} \left(\frac{u_*}{k}\right)^2 \tag{3.34}$$

It can clearly be seen, that when no obstacles are present and under stationary conditions, this value is constant with height as it is proportional to u_*.

To take into account these additional sources in the T.K.E equation in each grid cell, E_{surf}, is weighted by the obstacles horizontal surfaces as this term is due to the production of T.K.E due to the movement of fluids layers on horizontal

surfaces while E_{stat} is weighted by the 'free surface' porosity as this is due to fluid-fluid interactions.

$$E_{surf} = \frac{C_k}{C_\varepsilon^*} \left(\frac{u_*}{k}\right)^2 \frac{\hat{\varphi}_h}{\phi} \tag{3.35}$$

$$E_{stat} = \frac{C_k}{C_\varepsilon^*} l^2 \left(\frac{\partial U}{\partial z}\right)^2 \frac{\varphi}{\phi} \tag{3.36}$$

Since both terms (from Eqs. 3.35 and 3.36) have been weighted proportional to the surface from which they have been generated they can simply be summed up.

For the vertical surfaces that are present, there is additional transformation of Mean Kinetic Energy into T.K.E. The production of T.K.E by vertical surfaces is parameterized using Eq. (3.37):

$$Fe_I^V = \rho C_d \mid U_I^{ort} \mid^3 \frac{\hat{\varphi}_v}{\phi} \tag{3.37}$$

where C_d is the drag coefficient and $\hat{\varphi}_v$ is the total vertical obstacles surfaces in each direction at each level.

3.4 Experiments with CIM

After a detailed presentation of CIM development strategies, three sets of experiments are proposed. Each of these simulations are done in a domain with a vertical height of 50m which corresponds to twice the height of the obstacles that would be included in the domain. This is based on the fact that the bottom of the inertial sub-layer is twice that of the surface layer [Roth, 2000].

When developing these tests, the meteorological boundary conditions for CIM are fixed at the top of the domain. The surface temperature inside the model is kept at 293K such that a neutral atmospheric condition prevails. CIM is initialized with values given in Table 3.1.

Wind speed	$9.68ms^{-1}$
Potential Temperature	$293K$
Canyon width	$25\ m$
Building width	$25m$
Building height	$25m$

Table 3.1: Boundary conditions and obstaclees characteristics used for CIM in neutral conditions

3.4.1 Comparison of CIM with an analytical solution over a plane surface

CIM is first tested in the absence of obstacles under neutral conditions and its results are compared to the analytical solutions. Using Eq. (3.6), a logarithmic profile of the horizontal wind can be computed and the same is expected from CIM. From Eqs. (3.4) and (3.10) the T.K.E should give a constant value.

3.4.2 Scenarios to evaluate the impact of obstacles

The objective is to analyze how the presence of cubic obstacles (see Table 3.1) inside the canopy model impacts the wind and T.K.E profiles. For that purpose, the mechanical effect of the obstacles will be introduced progressively. Firstly, only the porosity terms will be added in Eq. (3.31) while keeping the same ground surface fluxes as when there were no obstacles. Secondly, the horizontal roof surfaces are added. Finally, the effect of vertical surfaces are analyzed.

3.4.3 Comparison of CIM with a C.F.D model over an array of buildings

One of the shortcomings of this study is the lack of experimental measurements in urban areas and the fact that known theories such as the surface layer theory or the Monin-Obhukov Similarity Theory cannot be applied when there are obstacles [Högström, 1996, Roth, 2000], especially in urban areas.

Therefore, it is not a simple task to validate the results that are obtained with

these types of models. In view of these constraints, it was chosen to compare results from CIM with a C.F.D experiment in the neutral case. The results that are used here to validate CIM are from a C.F.D experiment from Santiago et al. [2007], Martilli and Santiago [2007], Santiago and Martilli [2010].

Cubic obstacles with a height of 25 m are integrated in CIM. The width of the obstacles also correspond to the street width such that the occupied volume porosity, ϕ, is equal to 0.25, which is the value that was used in the C.F.D experiment from Santiago et al. [2007], Martilli and Santiago [2007]. As opposed to CIM, the C.F.D experiment used a higher (2.5) order turbulent closure to calculate the diffusion coefficient.

A pressure gradient has been imposed in the C.F.D to create an entrainment movement in the canopy, which is not present in CIM as we expect the fluxes coming from the surfaces to be sufficient to cause these movements. As CIM is not expected to work over very long vertical distances, there is no need for such a gradient to be included in the model. However, for comparison purposes with the C.F.D, a pressure gradient is added as an explicit term in the momentum equation.

Two parameterizations for mixing length were tested.

Mixing length proportional to the height

As a first approach, the mixing length was chosen to be equal to the height. The first parameterization for the mixing length was first developed by Prandtl [1925] and have been the object of several studies [Therry and Lacarrère, 1983, Watanabe and Kondo, 1990, Coceal and Belcher, 2004].

Mixing length as proposed by Santiago and Martilli [2010]

One of the disadvantages of using a linearly increasing mixing length is that the presence of obstacles as well as the density of obstacles (which can vary in the case of urban areas) is not taken into account. This can largely contribute to the reduction of the mixing length as the geometry will limit the maximum distance that an air parcel can travel. Hence, eddy sizes can be very far from the assumption, made above, that the mixing length increases linearly with height. Santiago and Martilli [2010] proposed a new formulation that modifies the calculation of the mixing length. Inside the canopy, they argued that the mixing length is close

to a constant which corresponds to results from Raupach et al. [1996] but are however in contradiction with other results from Coceal and Belcher [2004]. They proposed to calculate a displacement height (see Eq. 3.7) that takes into account the obstacles density using the following equation:

$$d = h(1 - \phi)^{\lambda} \tag{3.38}$$

where h is the obstacle's height, ϕ is the volume porosity and λ is equal to 0.13 and is taken from Santiago and Martilli [2010].

A specific mixing length is then calculated and constrained inside the canopy while increasing linearly with height above the canopy.

$$l = max(h - d, z - d) \tag{3.39}$$

3.5 Results in neutral atmospheric conditions

All following results were obtained in neutral atmospheric conditions. For this reason, it is chosen, in this particular context, not to show the potential temperature profiles, but to present only the wind and T.K.E profiles.

3.5.1 Without obstacles

The first two set of calculations were performed considering a surface without any obstacle : one profile is based on the Prandtl surface layer theory, giving an analytical solution for the wind profile (Eq. 3.6) and a constant value for the T.K.E (Eq. 3.11); the other is issued from CIM.

Figure 3.4 shows the set of profiles obtained from these calculations for the wind and the T.K.E.

It can be seen that the wind profile and a constant profile for the T.K.E are obtained and that they correspond to what is expected from the theory. This shows that the mechanical production of turbulence and the diffusion processes are well represented in the formulations that have been adopted.

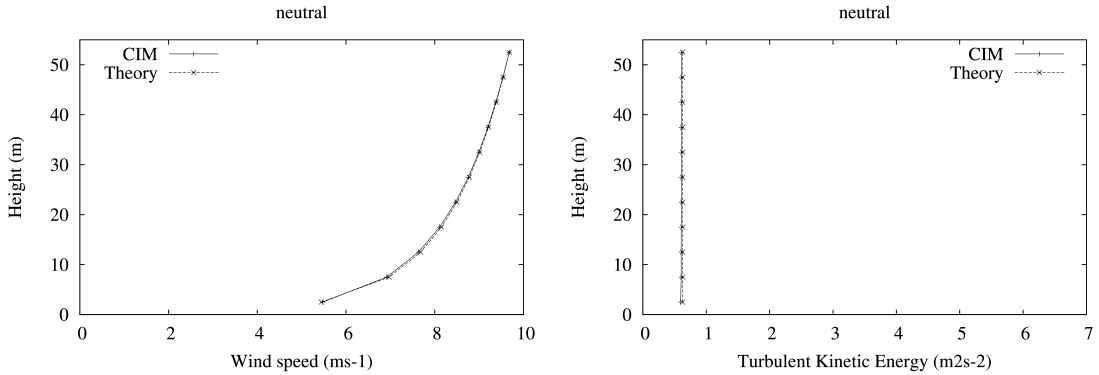

Figure 3.4: Comparison of the wind (in ms^{-1}) and T.K.E (in m^2s^{-2}) profiles computed using the analytical solution from the Prandtl surface layer theory and CIM. Altitude is in meter.

3.5.2 With obstacles

As mentionned earlier, obstacles have a mechanical effect on the atmosphere through the friction of the air on horizontal (ground and building roofs) and vertical surfaces, and a drag force also due to the vertical surfaces. The global effect and the effect of each type of surfaces are analyzed in this section.

Impact of the sources

In this section, three different tests are carried out to evaluate how the presence of obstacle may impact and modify the wind and the T.K.E as computed in Sect. 3.5.1.

Evaluation of the impact of the obstacle porosities

The difference between the case without obstacles and this scenario, is that the integration of obstacles is impacting only the free volume available in the domain with the porosity terms in the governing equation (see Eq. 3.31). This test aims to demonstrate how the presence of obstacles inside the grid cell can impact the wind and T.K.E profiles, previously computed, via the diffusion terms in Eq. (3.31).

For this test, in addition to the base case where the occupied volume for each grid cell was 25%, another simulation was done with an occupied volume of 75%. Fig 3.5 shows that the sole presence of obstacles inside the canopy impacts only

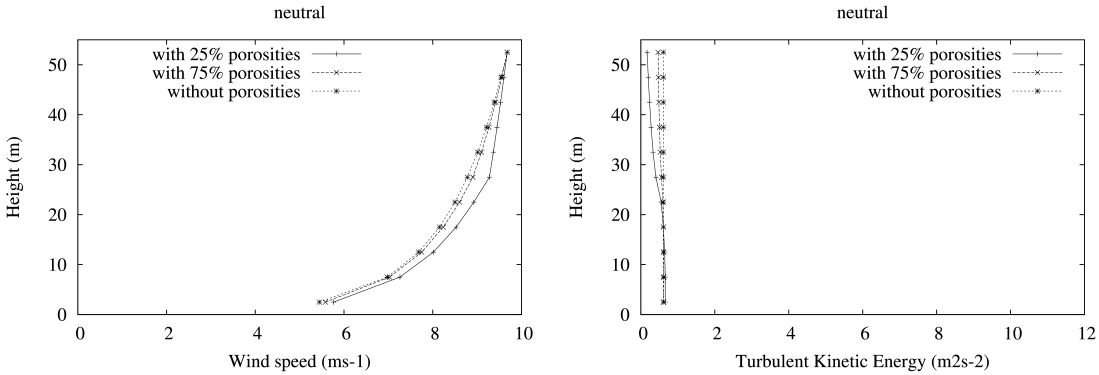

Figure 3.5: Comparison of the wind (in ms^{-1}) and T.K.E (in m^2s^{-2}) profiles computed to evaluate the impact of the obstacle porosities (with 25% and 75% of empty space in a grid cell). Altitude is in meter.

slightly the diffusion process. The wind profile changed on average by only 0.3% in the case where the obstacles filled 25% of the volume. The main difference between these two scenarios are noted on the T.K.E profiles above the canopy (average of 20% difference above the obstacles top). There is a decrease in the T.K.E above the canopy when the obstacles are integrated, while inside the canopy there is a slight increase. One can assume that the production of T.K.E is increased in the lowest layers but it is also more dissipated just above the obstacles where strong turbulent eddies may be observed.

Evaluation of the impact of obstacles roof surfaces

In this test, an evaluation of the impact of the momentum sources from horizontal surfaces inside the canopy (such as the ground or roof) is undertaken. All vertical sources are also not considered in this test.

Figure 3.6 shows that the momentum and T.K.E sources from the surface and 'roof' of the obstacles also have very little impact on the wind speed profile. The T.K.E is slightly more sensitive to this test and there is an increase in the T.K.E. This is due to the additional source of T.K.E at the top of the obstacles which thus modifies the profile.

Evaluation of the impact of vertical surfaces

For this last test, only the vertical sources are taken into account. It can be seen in Fig. 3.7 that the wind and T.K.E profiles are considerably modified. There is a

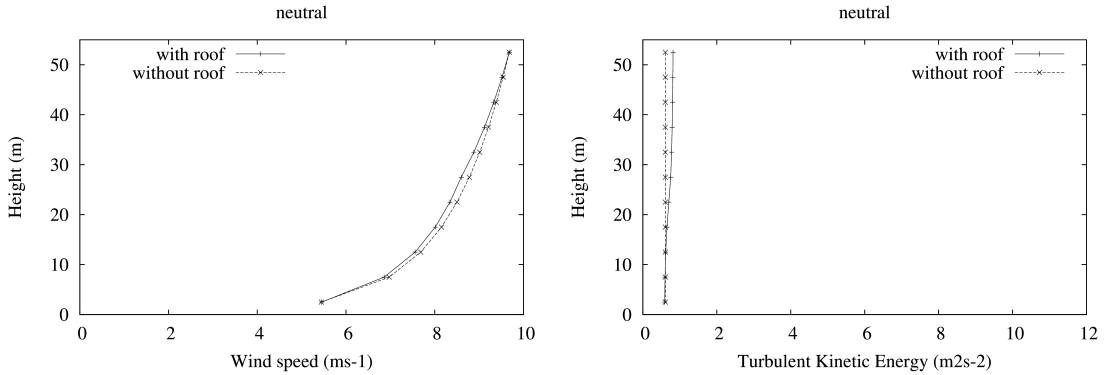

Figure 3.6: Comparison of the wind (in ms^{-1}) and T.K.E (in m^2s^{-2}) profiles computed to evaluate the impact of obstacles roof surfaces. Altitude is in meter.

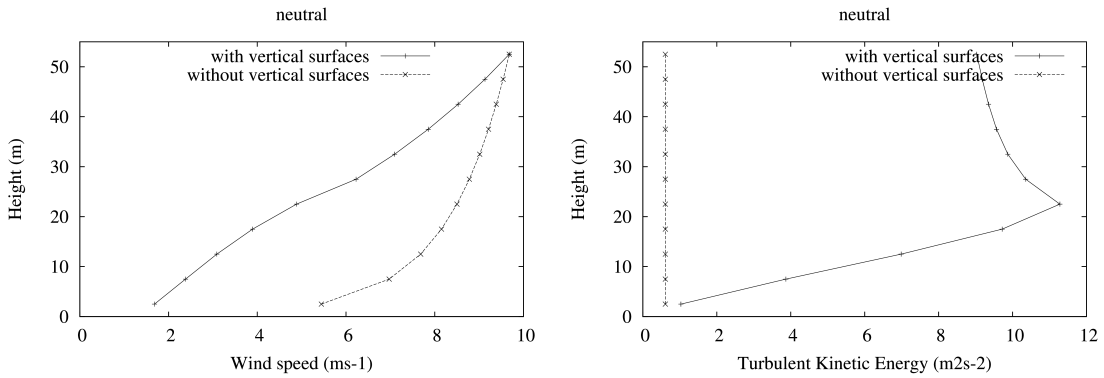

Figure 3.7: Comparison of the wind (in ms^{-1}) and T.K.E (in m^2s^{-2}) profiles computed to evaluate the impact of obstacles vertical surfaces. Altitude is in meter.

decrease in the wind speed in the canopy and an increase in the T.K.E. up to the top of the obstacles.

These separate tests have shown that the main momentum sources inside the canyon are from the vertical surfaces. This can be explained from Eq. (3.32) and (3.33) which represents the horizontal and vertical forces respectively. This is in agreement with various studies which stressed on the importance of the drag parameterization in urban canopy models but without showing the quantitative evaluation [Martilli et al., 2002, Raupach, 1992, Martilli et al., 2002, Martilli and Santiago, 2007, Hamdi and Masson, 2008, Aumond et al., 2013]. One unexpected result from this series of test, is the relatively low impact of the porosities on the

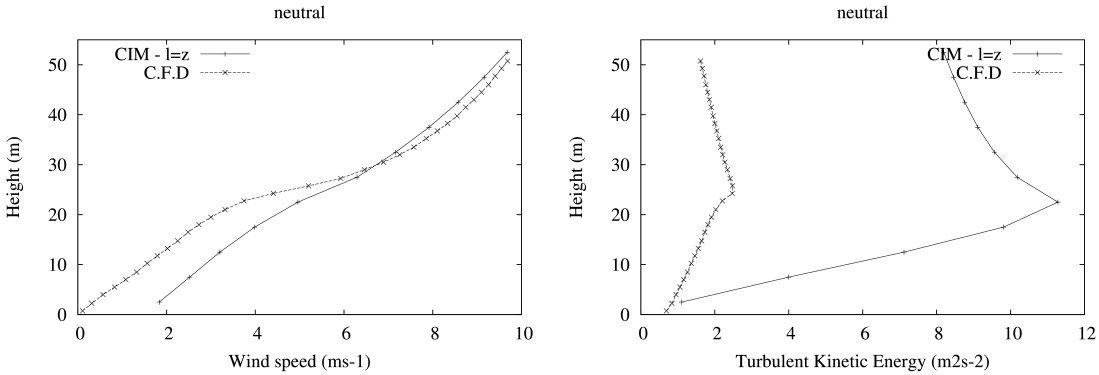

Figure 3.8: Comparison of the wind (in ms^{-1}) and T.K.E (in m^2s^{-2}) profiles obtained with obstacles from CIM and the C.F.D experiment with the mixing length equal to the height. Altitude is in meter.

diffusion process.

Comparison with C.F.D

CIM is here again tested in a neutral boundary layer.

Results with a mixing length equal to the height, z

The mixing length is first taken as increasing linearly with height (equal to z). Figure 3.8 gives the wind and turbulent kinetic energy profiles in the canopy in the presence of obstacles as well as the profiles obtained from the C.F.D experiment.

Note that the C.F.D height was normalized and hence had to be multiplied by the height of our obstacles for a more appropriate comparison. It can be seen that CIM overestimates the wind speed inside the canopy while above it there is a better correspondence. The higher wind speed is very likely to be due to the higher T.K.E. Furthermore, as obstacles are present in the canopy, a drag force term is added to the T.K.E. This drag force term is proportional to the cube of the wind speed and hence further accentuates the errors in the T.K.E.

Results with a modified mixing length [Santiago and Martilli, 2010]

Based on the poor results obtained when using a mixing length proportional to the height, a formulation adopted from Santiago and Martilli [2010] was used.

Figure 3.9 shows that wind profile differences are less than 5%. It can be seen that in the presence of obstacles, when the mixing length is modified to take into

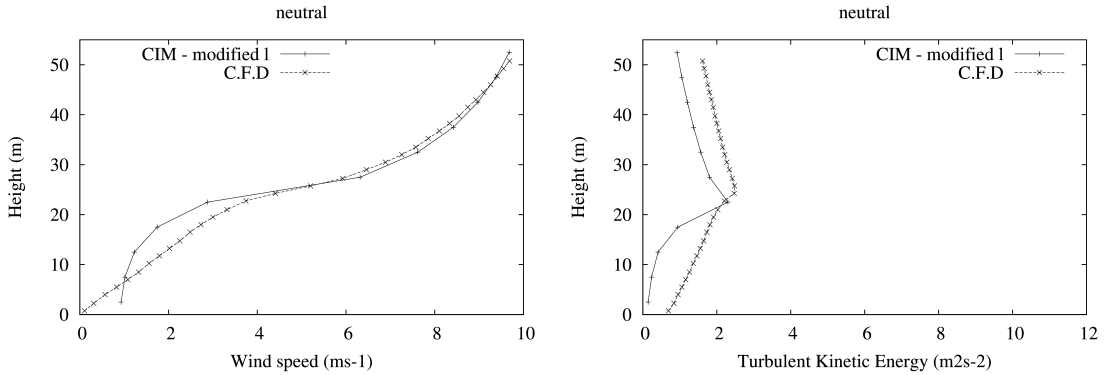

Figure 3.9: Comparison of the wind (in ms^{-1}) and T.K.E (in m^2s^{-2}) profiles obtained with obstacles from CIM and the C.F.D using the mixing length as given by Eq. (3.39) from Santiago and Martilli [2010]. Altitude is in meter.

account the density and presence of obstacles, the profiles and the diffusion of the fluxes are modified. There are still some differences in the T.K.E profile and more particularly in the height at which the maximum T.K.E occurs. Santiago and Martilli [2010] showed that there were already differences between the C.F.D experiment and data from a wind tunnel experiment. The negative gradient for the T.K.E above the buildings top which appears in the C.F.D can also be reproduced in CIM by fixing a pressure gradient. The presence of this pressure gradient hence modifies the expected constant T.K.E value which was expected above a plane surface.

3.6 Discussions and Conclusion

A Canopy Interface Model was described with a specific attention on the need to put theories in coherence and prepare a 1-D column model to be used as a coupling tool between meso-scale and micro-scale model. A new methodology was proposed for the calculation of the Turbulent Kinetic Energy. We proposed here to calculate a stationary value of T.K.E which simplified the numerical resolution of the T.K.E in the model.

CIM was first run in neutral conditions over a plane surface and results were compared to the analytical solutions obtained using the Prandtl surface layer the-

ory. The results were coherent with what was expected. It was shown that over a plane surface a constant profile of the Turbulent Kinetic Energy is obtained.

Scenarios were built with CIM in order to analyze the effects of obstacles on the wind and T.K.E profiles. It was shown that vertical surfaces, due to the parameterization of the fluxes they generate, have more influence, on the wind speed profile and on the production of T.K.E than the horizontal surfaces or even the porosities of the obstacles.

Results from CIM in a neutral case were then compared to results from a CFD experiment. Very good agreement was obtained for the wind speed. Although the general trend for the turbulent kinetic energy corresponds to what is obtained from the C.F.D (increase in the canopy to a maximum at the top of the obstacle and a decreasing trend above), there are still discrepancies in the profile however. The T.K.E is under-estimated at the bottom of the domain (and more particularly at the ground) as well as above the obstacles. One of the reason for this difference can also be due to wake production of T.K.E, for which no parameterization is included in CIM [Christen et al., 2009]. Additionally, a new formulation for the T.K.E has been developed. It has been argued that in the canopy the most important parameter is the mixing length and that there is no need to use a coefficient to weigh the dissipation term. It has been shown that there is a strong coherence between the formulation that has been developed and what can be expected from the theory over a plane surface and in neutral conditions.

It was seen, in the present study, that the formulation of the mixing length is a very important parameter, if not the most, in the determination of the wind profile. The T.K.E profile still has some discrepancies but the formulation we have adopted are in coherence with past propositions. Even though there are still differences in the T.K.E profile, CIM computation of the wind profile is in very good agreement with the C.F.D experiment.

The use of CIM to resolve high resolution profile inside a canopy, using meso-scale data as boundary condition, has been shown to be possible. This first part of the study was meant to demonstrate the capacity of CIM to compute and give appropriate result over a plane surface as well as when obstacles are present in neutral conditions. As Rotach [1995] stated, generally the roughness sub-layer is in near-neutral condition, we feel confident that CIM can be used very effectively

to act as an interface between meso-scale and micro-scale model based on the results from this study. However, a modified version of CIM that takes into account atmospheric stratification has to be developed.

Chapter 4

Development of a 1D-CANOPY model. Part II: Stable and Unstable case - modification brought to the T.K.E equation

This chapter corresponds to "Mauree, D. et al. 2014a, Development of a 1D Canopy Interface Model. Part II: Stable and Unstable case - modification brought to the T.K.E equation, in preparation, 2014"

Abstract

The development of a Canopy Interface Model (CIM) was presented in a neutral case by Mauree et al. [2014b]. In the present study, the implementation of new terms into the governing equations of the model is discussed to take into account the effects of the stability of the atmosphere on the vertical profiles of the main atmospheric variables. Two different atmospheric stability (stable and convective) conditions are tested, with or without the presence of obstacles. These results are compared with what is expected from the Monin-Obukhov Similarity Theory (MOST).

In order to keep the coherence with the MOST over plane surfaces, it is proposed to add a correction to the buoyancy term of the turbulent kinetic energy balance equation. Results from CIM showed good correspondence with the MOST when this adjustment is brought. Simulations are also run in the presence of obstacles and the profiles are compared to profiles obtained in a neutral environment.

Keywords: urban canopy, atmospheric boundary layer, urban meteorology, urban climate, turbulence parameterization, turbulent kinetic energy, similarity theory

4.1 Introduction

Several studies have been conducted to investigate the impact of the atmospheric stability on the evolution of the meteorological variables and the surface fluxes: using experimental data, Monin and Obukhov [1954] first proposed a set of universal functions that were based on the Obukhov length described by Obukhov [1971] to modify the turbulent diffusion coefficients; Businger et al. [1971] also analyzed measurement data to provide other formulations of those empirical functions. All these studies have been conducted over plane surfaces to improve weather forecast, and are not adapted to built areas [Roth, 2000, Foken, 2008].

On the other hand, urban parameterizations were developed to be included in mesoscale meteorological models in order to improve the representation of urban heat island as well as the calculation surface fluxes [Masson, 2000, Martilli et al., 2002]. These parameterizations take into account different atmospheric stability conditions through the buoyancy term of the T.K.E equation (used to compute the turbulent diffusion coefficient) and with the use of Louis functions [Louis, 1979] to modify the surface fluxes.

Recently, a Canopy Interface Model was developed to improve the representation of the surface in meteorological mesocale models [Mauree et al., 2014b] and proposed a calculation that brought coherence between past propositions. The first development of the Canopy Interface Model (CIM) integrating the influence of obstacles on the first layer of the atmosphere under neutral conditions was presented by Mauree et al. [2014b]. Under neutral conditions, the results from CIM were compared with the Prandtl surface layer theories when there were no obstacles. In the case where obstacles are present, the results were compared with a C.F.D experiment based on a study from Santiago et al. [2007] and Martilli and Santiago [2007].

The aim of the present study is to show how the effect of the atmospheric stability is taken into account in CIM. A prognostic equation for the T.K.E is solved to compute the turbulent diffusion coefficient. Buoyancy effects are also taken into account by using Louis functions [Louis, 1979] to modify surface fluxes. As compared to Masson [2000] and Martilli et al. [2002], new formulations are proposed in order to keep CIM in coherence with the Monin-Obukhov Similarity

Theory (MOST) when applied over a plane surface. To do so, it is shown that the buoyancy term in the T.K.E equation has to be multiplied by a coefficient. Obstacles are then integrated in the canopy and the impact of the fluxes on the variables is evaluated.

In Sect. 4.2, the Monin-Obhukov Similarity Theory, is presented as applicable to the unstable and stable conditions. In Sect. 4.3, modifications brought to CIM, more specifically to the set of equations used, are given. Section 4.4 describes the experiments that have been done to determine whether CIM can work in different stability conditions. Section 4.5 shows the results that are obtained under stable and unstable conditions without obstacles and how these compare to what is expected from the MOST. An overview of the results that are obtained with obstacles and how these compare to the results that were presented in [Mauree et al., 2014b] are also given in Sect. 4.6. The results that are obtained and their limits are finally discussed in Sect. 4.7 as well as the different perspectives for CIM.

4.2 Monin-Obukhov Similarity Theory

The similarity theory developed by Monin and Obukhov [1954] has been applied and validated over plane surfaces in several studies under different types of conditions [Monin and Obukhov, 1954, Foken, 2006, Zilitinkevich and Esau, 2007]. It is now called the Monin-Obhukov Similarity Theory (MOST).

The MOST considers that the turbulent diffusion of the momentum and the heat are dependent of the stability of the atmosphere. In this way, it proposes to add functions in the computation of turbulent diffusion coefficients as proposed by the Prandtl Theory [Prandtl, 1925]:

$$\mu_t = \frac{k u_* z}{\phi_m} \tag{4.1}$$

$$\kappa_t = \frac{k u_* z}{\phi_h} \tag{4.2}$$

where ϕ_m is a universal stability function for the momentum and ϕ_h is a universal stability function for the heat.

Monin and Obukhov [1954] studied the wind and temperature profiles under different atmospheric stability to fit these functions. Businger et al. [1971] proposed reformulations for these functions (more details can be found in Dyer [1974] who proposed an extensive review of the topic):

$$\text{For } 0 < \frac{z}{L} < 1 \begin{cases} \phi_m = 1 + \beta_m \frac{z}{L} \\ \phi_h = Pr. \left(1 + \beta_h \frac{z}{L}\right) \end{cases} \tag{4.3}$$

$$\text{For } -2 < \frac{z}{L} < 0 \begin{cases} \phi_m = \left(1 - \gamma_m \frac{z}{L}\right)^{-1/4} \\ \phi_h = Pr. \left(1 - \gamma_h \frac{z}{L}\right)^{-1/2} \end{cases} \tag{4.4}$$

where L is the Obukhov Length [Obukhov, 1971] written as:

$$L = \frac{u_*^2 \theta}{kg\theta_*} \tag{4.5}$$

where u_* if the friction velocity, θ is $\overline{\theta_v}$ and is the mean virtual potential temperature, k is the von Kármán constant (and is taken to be 0.41), g is the acceleration due to gravity and $u_*\theta_*$ is the heat flux. These functions were then re-evaluated by Högström [1988] who proposed that β_m is 6, β_h is 7.8, γ_m is 19.3, γ_h is 11.6. Pr is the Prandtl number that represents the ratio between the momentum (Eq. 4.1) and heat turbulent diffusion coefficients (Eq.4.2) showing clearly that Pr depends on the stability of the atmosphere, [Priestley and Swinbank, 1947]:

$$\frac{1}{Pr} = \frac{\phi_h}{\phi_m} > 1 \tag{4.6}$$

Pr is however often considered as a constant: Monin and Obukhov [1954] chose this number to be 1. Other studies [Högström, 1996, Foken, 2006] considered it as having a constant value of 0.95.

Using these formulations, a partial differential equation for the wind can be written as follows:

$$\frac{\partial U}{\partial z} = \frac{u_*}{kz}\phi_m \tag{4.7}$$

A similar reasoning can be used to determine the temperature profile:

$$\frac{\partial \theta}{\partial z} = \frac{\theta_*}{kz}\phi_h \tag{4.8}$$

Integrating Eqs. (4.7) and (4.8) between z_0 and z the following equation giving the vertical profiles are obtained:

$$U(z) = \frac{u_*}{k}\left[\ln\left(\frac{z}{z_0}\right) - \psi_m\right] \tag{4.9}$$

$$\theta(z) - \theta_{surf} = \frac{\theta_*}{k}\left[\ln\left(\frac{z}{z_0}\right) - \psi_h\right] \tag{4.10}$$

where

$$\psi_m = \int_{z_0}^{z}(1-\phi_m)\frac{dz}{z} \tag{4.11}$$

and

$$\psi_h = \int_{z_0}^{z}(1-\phi_h)\frac{dz}{z} \tag{4.12}$$

The complete set of equations relating to the ψ values can be found in Jacobson [1999].

There are two main constraints with these equations. First, the Obukhov Length is determined by using fluxes (u_*^2 and $u_*\theta_*$) that have to be computed simultaneously so as to calculate the variables themselves. This is done using an iterative process which can thus use extensive computer resources. Second, this theory is not applicable when obstacles are present as the fluxes are not constant anymore in the surface layer. This theory is used in this study to build reference simulations when CIM is applied and tested over plane surfaces.

4.3 CIM developments considering atmospheric stability

A description of the governing equations was given for the momentum and turbulent kinetic energy under neutral conditions in Mauree et al. [2014b]. It was shown how the horizontal and vertical surfaces of obstacles impact these variables. In this

study, a modified version of these equations taking into account the atmospheric stability is given.

Only the momentum, heat and turbulent kinetic energy equations are described here. CIM also resolves a humidity equation, but is not presented here as it is very similar to the heat equation.

4.3.1 Turbulent diffusion coefficient and condition of a coherence

To overcome the limitations of the MOST when obstacles are present on the surface, the diffusion coefficient used in CIM to resolve the momentum equation is calculated using Eq. (4.13) while the diffusion coefficient for the heat equation has to be weighted by the Prandtl number (Pr), chosen to be equal to 0.95.

$$\mu_t = C_k \sqrt{E} l \tag{4.13}$$

$$\kappa_t = \frac{C_k \sqrt{E} l}{Pr} \tag{4.14}$$

where C_k can be calculated to be equal to $k^{\frac{4}{3}}$ according to Mauree et al. [2014b].

The first task of CIM's development was to write the condition for this formulation to be in coherence with the MOST in stable and unstable conditions over a plane surface. Thus based on the turbulent diffusion coefficient calculated from the MOST (Eq. 4.1) and the turbulent diffusion coefficient calculated from CIM (Eq. 4.13), the T.K.E can be calculated using the following equation:

$$E = \left(\frac{u_*}{k^{\frac{1}{3}} \phi_m} \right)^2 \tag{4.15}$$

Equation (4.15) shows that the T.K.E is constant with height only under neutral conditions (when ϕ_m is equal to 1).

4.3.2 Momentum

The momentum equation is solved using the following equation.

$$\frac{\partial U}{\partial t} = \frac{\partial}{\partial z}\left(\mu_t \frac{\partial U}{\partial z}\right) + f_u^s \tag{4.16}$$

where f_u^s in Eq. (4.16) represents the forces (stress) that will impact the momentum.

The influence of the atmospheric stability is only applied to fluxes coming from horizontal surfaces (the fluxes from the vertical surfaces remain unchanged from the description given by Mauree et al. [2014b]). Horizontal surfaces in the canopy (roofs, streets...) induce a frictional force on the movement of air masses and leads to a loss of momentum. Above such surfaces the Monin-Obhukov Similarity Theory (MOST) can be used to express the fluxes that are induced [Louis, 1979, Martilli et al., 2002].

$$\vec{F} u_I^H = -\rho \left[\frac{k}{\ln\left(\frac{\Delta z/2}{z_0}\right)}\right]^2 * g_m\left(\frac{\Delta z/2}{z_0}, Ri_B\right) |U^{hor}| \vec{U_I} \frac{\hat{\varphi}_h}{\phi} \tag{4.17}$$

where k is the von Kármán constant (0.41), Δz is the size of the vertical levels, z_0 is the roughness length ($0.05m$) and U^{hor} is the horizontal wind speed. $\hat{\varphi}_h$ is the total horizontal obstacle surface at each level and ϕ is the volume porosity as described by Mauree et al. [2014b]. g_m is the Louis function for momentum that will be given in Sect. 4.3.6.

4.3.3 Energy

The energy equation is solved using the following equation:

$$\frac{\partial \theta}{\partial t} = \frac{\partial}{\partial z}\left(\kappa_t \frac{\partial \theta}{\partial z}\right) + f_\theta^s \tag{4.18}$$

where θ is the mean virtual potential temperature, f_θ^s represent the additional flux sources coming from the obstacles.

Based on the MOST, the same type of equation as Eq. (4.17) can be used for

the energy transfer from horizontal surfaces to the atmosphere.

$$F\theta_I^H = \rho \left[\frac{k}{\ln\left(\frac{\Delta z/2}{z_0}\right)} \right]^2 * g_h \left(\frac{\Delta z/2}{z_0}, Ri_B \right) |U^{hor}| \Delta\Theta_H \frac{\hat{\varphi}_h}{\phi} \tag{4.19}$$

where g_h is the Louis function for energy that will also be given in Sect. 4.3.6 and $\Delta\Theta_H$ is the difference between the air potential temperature and potential temperature of the horizontal surface.

For the energy equation, the classical drag-force parameterization cannot be used as the heat fluxes from the vertical surface are a function of the difference between the air temperature and the wall temperature [Martilli et al., 2002]. A different formulation which has been used by Martilli et al. [2002] and was first formulated by Arnfield and Grimmond [1998] is hence adopted.

$$F\theta_I^V = -\frac{\eta}{C_p} \Delta\Theta_V \frac{\hat{\varphi}_v}{\phi} \tag{4.20}$$

where $\Delta\Theta_V$ is the difference between the air potential temperature and potential temperature of the vertical surface, $\hat{\varphi}_v$ is the vertical surface in each direction at each level, C_p is the air heat capacity and is taken as $1004 J/kg.K$ and η is given by Eq. (4.21),

$$\eta = c_c \left(a_c + b_c \left(\frac{\mid U_I^{hor} \mid}{d_c} \right) \right) \tag{4.21}$$

where a_c, b_c, c_c, d_c are 1.09, 0.23, 5.678 and 0.3048 respectively taken from Martilli et al. [2002].

4.3.4 Turbulent Kinetic Energy

A prognostic equation is used to calculate the Turbulent Kinetic Energy (T.K.E) and consecutively to compute the turbulent diffusion coefficients as used in the 1.5 turbulence closure.

A complete description of the resolution of the T.K.E was given in Mauree

et al. [2014b]. In the present article, a buoyancy term is added to the equation.

$$\frac{\partial E}{\partial t} = \frac{\partial}{\partial z}\left(\lambda_t \frac{\partial E}{\partial z}\right) + P + G - \varepsilon + f_e^s \tag{4.22}$$

Equation (4.23) gives the time-evolution of the T.K.E. It is assumed here that λ_t is equal to μ_t. The terms on the right hand side represent respectively the diffusion term, the mechanical production term, the buoyancy term, the dissipation term and the surface fluxes due to the presence of obstacles. One can note that Eq. (4.23) could be written as follows:

$$\frac{\partial E}{\partial t} = \frac{\partial}{\partial z}\left(\lambda_t \frac{\partial E}{\partial z}\right) + P(1 - Ri_f) - \varepsilon + f_e^s \tag{4.23}$$

where Ri_f is the flux Richardson number and is $\frac{G}{P}$.

This equation could also be written as proposed by Mauree et al. [2014b]:

$$\frac{\partial E}{\partial t} = \frac{\partial}{\partial z}\left(\lambda_t \frac{\partial E}{\partial z}\right) + C_\varepsilon^* \frac{\sqrt{E}}{l}\left(E_{stat} - E\right) + f_e^s \tag{4.24}$$

where

$$E_{stat} = \frac{C_k}{C_\varepsilon^*} l^2 \left(\frac{\partial U}{\partial z}\right)^2 (1 - Ri_f) \tag{4.25}$$

where C_ε^* is a constant chosen to be equal to 1 [Mauree et al., 2014b]. It should be reminded that the turbulent kinetic energy is constant with height only in neutral stability conditions. This means that the diffusion term is not always equal to zero and E_{stat} is not necessarily the stationary value. However in order to simplify the study we keep the same denomination for this term as in Mauree et al. [2014b]. E_{stat} will represent here the stationary value that is obtained over a plane surface in neutral stability conditions and without obstacles.

Taking into account that the mechanical production is equal to:

$$P = \overline{u'w'}\frac{\partial U}{\partial z} \tag{4.26}$$

and that the buoyancy term is:

$$G = \overline{w'\theta'}\frac{g}{\theta} \tag{4.27}$$

Ri_f can be written as in Eq. (4.28) based on Stull [1988]:

$$Ri_f = \frac{\frac{g}{Pr\theta}\frac{\partial\theta}{\partial z}}{\left(\frac{\partial U}{\partial z}\right)^2} \tag{4.28}$$

Over plane surfaces, when momentum and heat diffusion coeffcients may be computed using Eqs. (4.1) and (4.2), a relation between $\frac{z}{L}$ and Ri_f, can be used [Businger et al., 1971]:

$$Ri_f\phi_m = \frac{z}{L} \tag{4.29}$$

4.3.5 Coherence over a plane surface

The formulation of E_{stat} should be in coherence with other propositions in the case of a plane surface as discussed in Mauree et al. [2014b]. Indeed it was shown that in stationary flow, over a plane surface and in a neutral environment, the T.K.E has a constant value that has to be equal to the E_{stat} value written in this study. It is actually the case when ϕ_m is equal to 1 and Ri_f is equal to 0. Since the local production still equilibrates the local dissipation, as in the neutral case and as it was demonstrated by Brouwers [2007], Charuchittipan and Wilson [2009], Eqs. (4.15) and (4.25) should yield the same result over a plane surface in any stability case:

$$E_{stat} = \frac{C_k}{C_\varepsilon^*}l^2\left(\frac{\partial U}{\partial z}\right)^2(1 - Ri_f) = \left(\frac{u_*}{k^{1/3}\phi_m}\right)^2 \tag{4.30}$$

Since above a plane surface Eq. (4.7) can be used to replace $\frac{\partial\overline{U}}{\partial z}$ in Eq. (4.30), a relation appears between ϕ_m and Ri_f:

$$\phi_m = (1 - Ri_f)^{-1/4} \tag{4.31}$$

This equation has to be compared to the Businger et al. [1971] functions, as presented in Eqs. (4.3) and (4.4), which show very close formulation.

In order to propose a coherent methodology that could be used in any stability case with and without the presence of obstacles on the surface these statements were listed:

1. *the Ri_f should be computed using the gradient of the wind and the mean virtual potential temperature, and not the fluxes;*

2. *the function as presented in Eq. (4.31) should be kept but it should be slightly adapted to satisfy the Businger et al. [1971] propositions for any stability cases. The new proposition is:*

$$\phi_m = (1 - C_G \cdot Ri_f)^{-1/4} \tag{4.32}$$

where C_G can be determined for different stability cases.

Thus C_G could be linked to Businger's functions at least over plane surfaces. Indeed in an unstable atmosphere, using Eqs. (4.4) and (4.31) a coefficient can be calculated to lead to:

$$(1 - C_G \cdot Ri_f)^{-1/4} = \left(1 - \gamma_m \frac{z}{L}\right)^{-1/4} \tag{4.33}$$

$$(1 - C_G \cdot Ri_f) = \left(1 - \gamma_m \frac{z}{L}\right) \tag{4.34}$$

Considering that:

$$\frac{z}{L} = Ri_f \phi_m \tag{4.35}$$

It is then possible to write:

$$(1 - C_G \cdot Ri_f) = (1 - \gamma_m (Ri_f \phi_m)) \tag{4.36}$$

$$C_G = \gamma_m \phi_m \tag{4.37}$$

In the same way, for the stable case, the same can be done using Eqs. (4.31) and

(4.3) and using Taylor series to eliminate the power functions (if $\mid C_G \cdot Ri_f \mid << 1$).

$$(1 - C_G \cdot Ri_f)^{-1/4} = \left(1 + \beta_m \frac{z}{L}\right) \tag{4.38}$$

$$\left(1 + \frac{C_G}{4} Ri_f\right) = \left(1 + \beta_m \frac{z}{L}\right) \tag{4.39}$$

$$C_G = 4\beta_m \phi_m \tag{4.40}$$

Equations (4.32), (4.37) and (4.40) could be also interpreted in this way: in order to ensure the maximum coherence between previous theories, the Richardson number, from the T.K.E. governing equation of CIM's, should be multiplied by a new term in order to take into account the atmospheric stability.

To conclude CIM solves this equation:

$$\frac{\partial E}{\partial t} = \frac{\partial}{\partial z}\left(\lambda_t \frac{\partial E}{\partial z}\right) + \frac{\sqrt{E}}{l}\left(E_{stat} - E\right) + f_e^s \tag{4.41}$$

where E_{stat} can now be expressed as:

$$E_{stat} = \frac{C_k}{C_\varepsilon^*} l^2 \left(\frac{\partial U}{\partial z}\right)^2 (1 - C_G \cdot Ri_f) \tag{4.42}$$

with C_G values computed as proposed by Eq. (4.37) when the atmosphere is unstable and Eq. (4.40) when the atmosphere is stable. Ri_f is computed using Eq. (4.28).

This new proposition could also be seen as an adjustment that can be made to the buoyancy term in the T.K.E equation in order to obtain an expression equivalent to that which was first proposed by Monin and Obukhov [1954] and modified by Businger et al. [1971]. This adjusment is further justified by the fact that Mauree et al. [2014b] already showed that the mechanical production term of the T.K.E was coherent with the theory. It will be called the C_G correction in the following sections.

In order to avoid having a vanishingly small $\frac{\partial U}{\partial z}$ term at the denominator in the Ri_f, which is very likely in stable atmosphere when the frictional stress can

be small, it is proposed to calculate E_{stat} as follows:

$$E_{stat} = \frac{C_k}{C_\varepsilon^*} l^2 \left(\left(\frac{\partial U}{\partial z} \right)^2 - C_G \frac{g}{Pr\theta} \frac{\partial \theta}{\partial z} \right) \tag{4.43}$$

4.3.6 Atmospheric stability

To avoid the iteration process involved in the calculation of the Obukhov length and of the Richardson number, an approximation can be made by calculating a bulk Richardson number.

$$Ri_b = \frac{g \Delta\theta_H (z - z_0)}{\theta [U^{hor}]^2} \tag{4.44}$$

where $\Delta\theta_H$ is the difference between the potential temperature θ at this level and the surface potential temperature θ_{surf}.

Louis [1979] used this number to calculate different functions that will influence the fluxes depending on the atmospheric stability:

When $Ri_b \leq 0$

$$g_m = 1 - \frac{9.4 Ri_b}{1 + \frac{70 k^2 (|Ri_b| z/z_0)^{0.5}}{ln^2(z/z0)}} \tag{4.45}$$

$$g_h = 1 - \frac{9.4 Ri_b}{1 + \frac{50 k^2 (|Ri_b| z/z_0)^{0.5}}{ln^2(z/z0)}} \tag{4.46}$$

When $Ri_b > 0$

$$g_m = g_h = \frac{1}{(1 + 4.7 Ri_b)^2} \tag{4.47}$$

4.4 Experiments with CIM

A series of experiments are proposed to illustrate CIM's development and its results:

1. CIM is run over a plane surface with the different stability conditions and the simulated profiles are compared to the profiles calculated using the Monin-Obukhov Similarity theory as presented in Sect. 4.2. First we compare the

Wind speed	$9.68ms^{-1}$
Potential Temperature	$293K$
Stable surface Temperature	$286K$
Convective surface Temperature	$300K$

Table 4.1: Boundary conditions used for CIM

results with the traditional formulation of the T.K.E (without the C_G correction). The results from CIM with the MOST using the modification we brought to the T.K.E equation (with the C_G correction) is then presented.

2. Secondly, we evaluate the influence of an array of cubic obstacles on the meteorological variables in different atmospheric conditions. The results for these simulations are only presented to give an insight on the capacity of CIM to perform in various atmospheric conditions. Data with such resolution are difficult to obtain and the purpose here is only to show how CIM handles the diffusion process in various atmospheric conditions. Cubic obstacles with a width 25m are integrated in CIM and the size of the street canyons are also given as 25m.

For all experiments, the meteorological boundary conditions for CIM, fixed at the top of the domain, are given in Table 4.1. The same configurations as Mauree et al. [2014b] are used here. However the comparison of CIM with the C.F.D experiments are not possible as the C.F.D can only be used for the moment in neutral stability conditions. The surface temperature is taken such that it corresponds to an unstable and stable atmosphere.

4.5 Comparison of CIM with the MOST over a plane surface

4.5.1 Results from the MOST

Figures 4.1 and 4.2 shows the profiles that can be calculated using the MOST in stable and unstable conditions and how they compare with the Prandtl surface

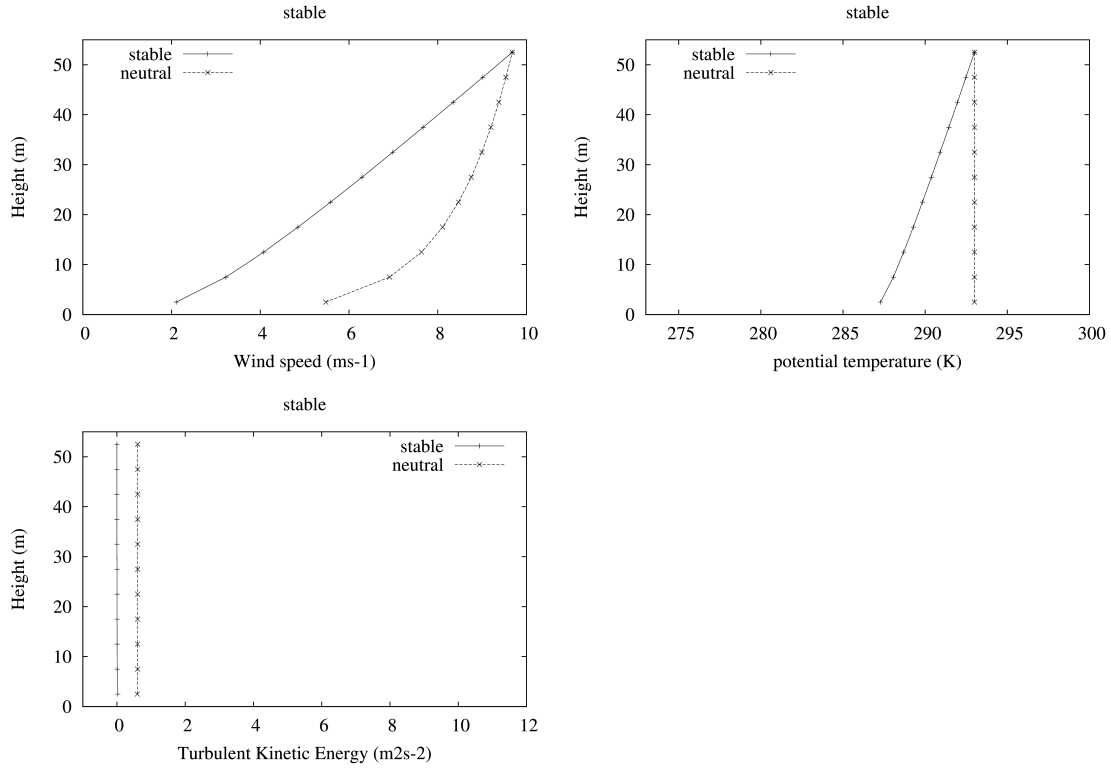

Figure 4.1: Comparison of wind (in ms^{-1}), potential temperature (in K) and T.K.E (in m^2s^{-2}) vertical profiles obtained with the MOST over a plane surface in neutral and stable cases. Altitude is in meter.

layer theory in neutral condition over a plane surface. It is shown here that in a stable condition, when compared to a neutral environment, both the wind speed and the T.K.E decrease. The opposite situation occurs in an unstable environment where the wind speed increases as does the T.K.E.

4.5.2 CIM with a traditional formulation of the T.K.E

This section is dedicated to the presentation of the CIM's results without considering the C_G correction as proposed in Sect. 4.3.5. In this case, the production and the buoyancy terms are computed as commonly done in other studies. The wind, temperature and T.K.E profiles calculated with CIM in a stable atmospheric condition are shown in Fig. 4.3. It can be seen that the wind speed for the stable case in the first levels is much higher than what is obtained from the MOST (over

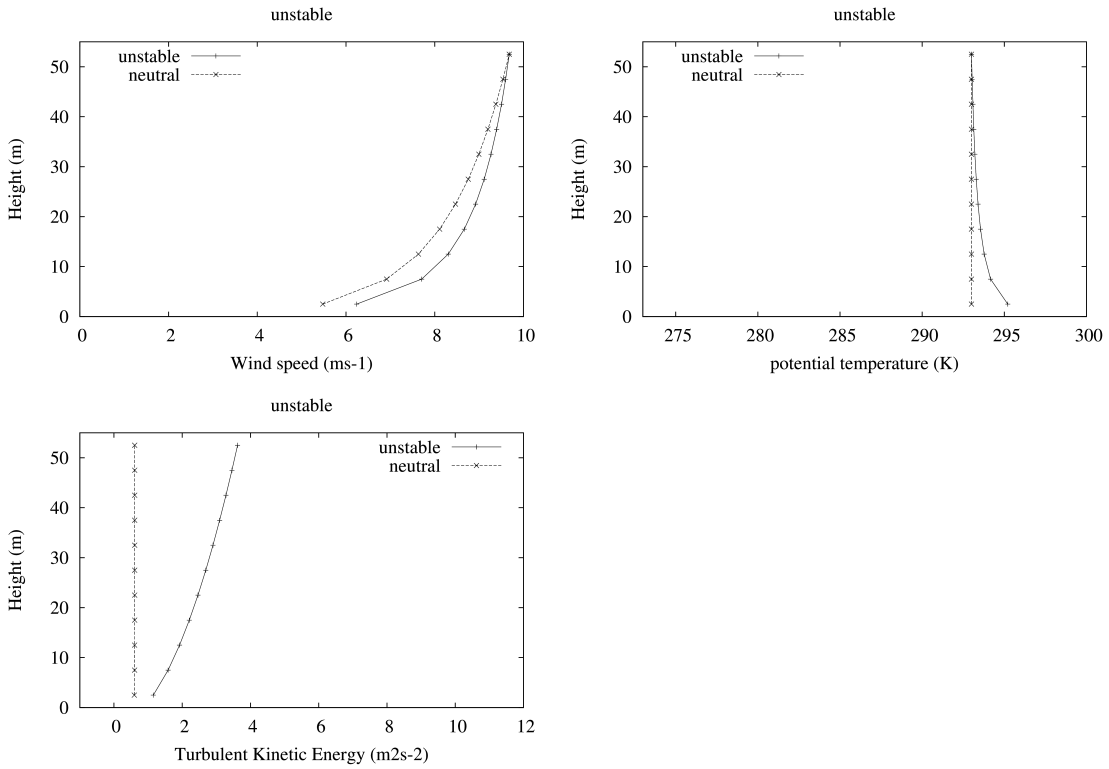

Figure 4.2: Comparison of wind (in ms^{-1}), potential temperature (in K) and T.K.E (in m^2s^{-2}) vertical profiles obtained with the MOST over a plane surface in neutral and unstable cases. Altitude is in meter.

50% difference on average with a maximum of 150% near the surface). The T.K.E profile obtained from the MOST is close to zero as is expected in a stable atmosphere while with CIM a higher value of the T.K.E is calculated and this is very likely to be due an over-estimation of the buoyancy term of the T.K.E. Figure 4.4 shows the wind, temperature and T.K.E profiles calculated with CIM and with the MOST for an unstable case. In the unstable case, the wind speed is lower than the wind speed obtained with the MOST formulations over the whole domain (less than 5% difference on average with a maximum of 10% at the surface). The potential temperature profiles are in good agreement here with less than 1% error. It can be noted here that the T.K.E profile calculated from CIM is quite different (an average of 60% over the domain with more than 70% difference at the top of the domain), in the unstable case, from the MOST profile. Even though the differences for the potential temperature profiles are small, the profiles showed some differences particularly near the surface.

4.5.3 CIM using the C_G correction of the T.K.E equation

In order to improve previous results, an adjustment was proposed to this buoyancy term (see Sect. 4.3.5).

Figures 4.3 and 4.4 highlight the fact that when these corrections are brought, the wind and turbulent kinetic energy profiles calculated from CIM correspond better to the profiles computed using the MOST.

In both the stable and unstable cases, the wind speed and the potential temperature were in very good agreement with the MOST (less than 0.5% difference). There were no significant differences in the profile calculated for the T.K.E. In the stable case however the magnitude of the T.K.E still differed and since the values are very close to zero the percentage differences were around 60%.

4.6 Results with obstacles

CIM is run in this section with obstacles with the same characteristics as those described in Part I of this study. The simulations done under stable and unstable atmospheric conditions are compared to the results obtained for neutral condi-

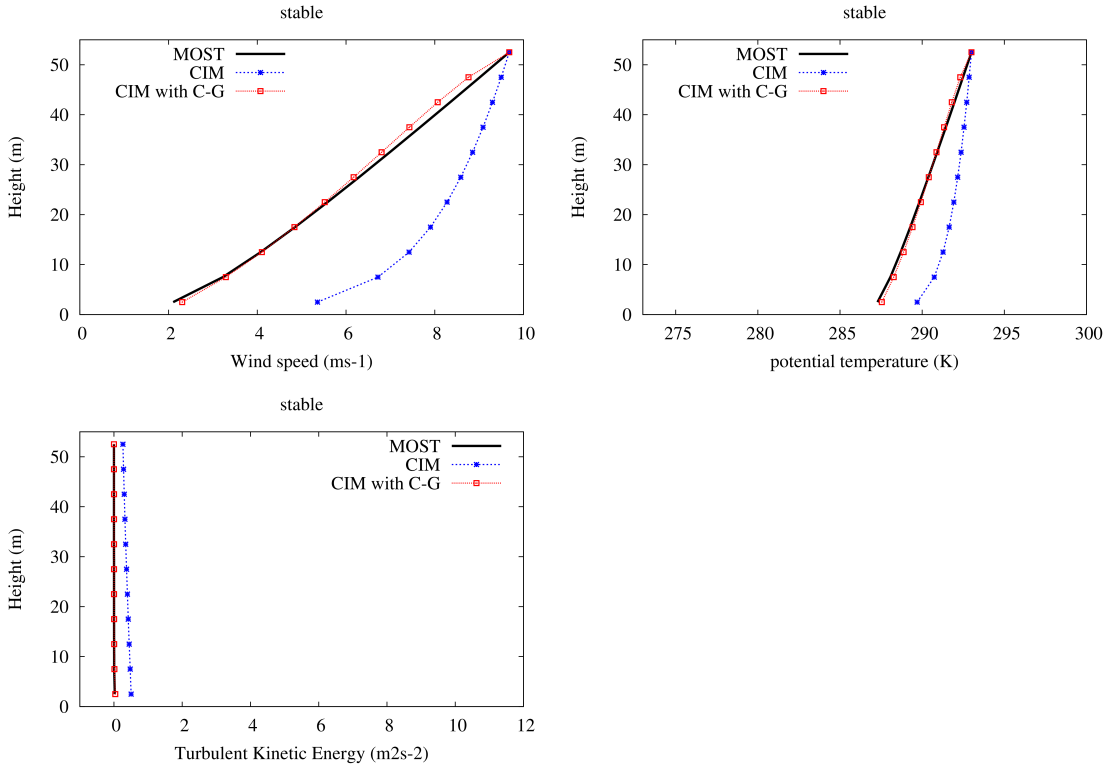

Figure 4.3: Comparison of wind (in ms^{-1}), potential temperature (in K) and T.K.E (in m^2s^{-2}) vertical profiles obtained with the MOST over a plane surface and with CIM (without and with the C_G correction in the T.K.E.) under stable conditions. Altitude is in meter.

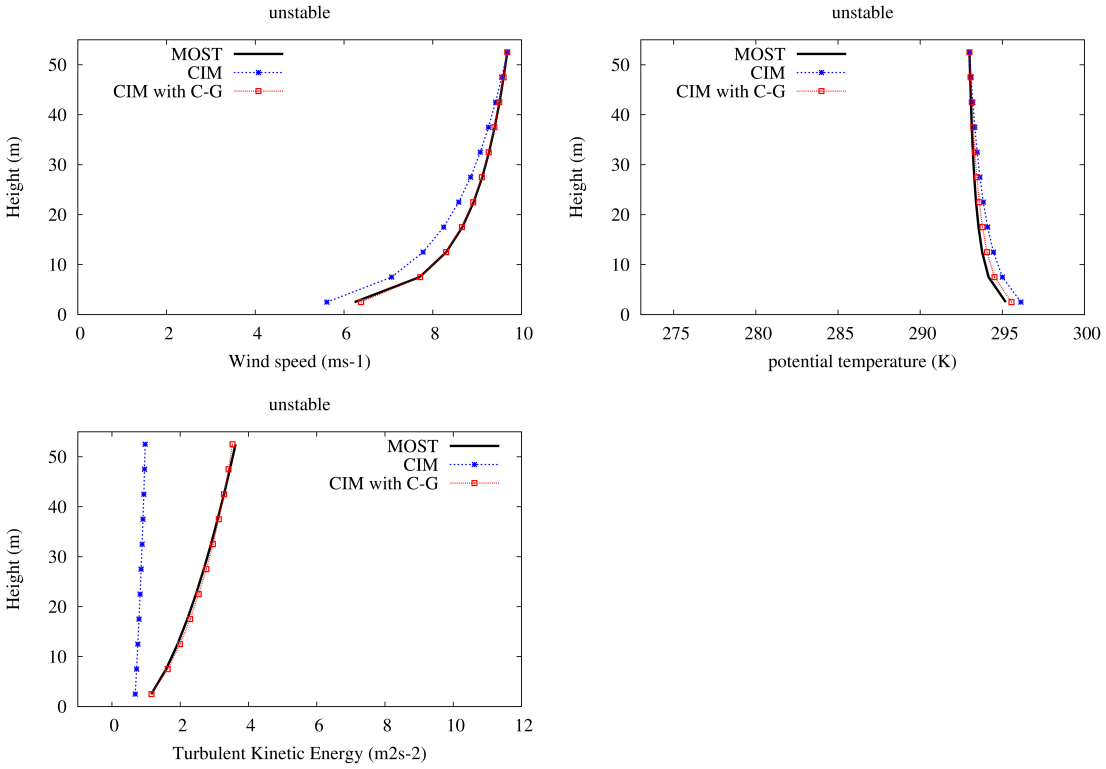

Figure 4.4: Comparison of wind (in ms^{-1}), potential temperature (in K) and T.K.E (in m^2s^{-2}) vertical profiles obtained with the MOST over a plane surface and with CIM (without and with the C_G correction in the T.K.E.) under unstable conditions. Altitude is in meter.

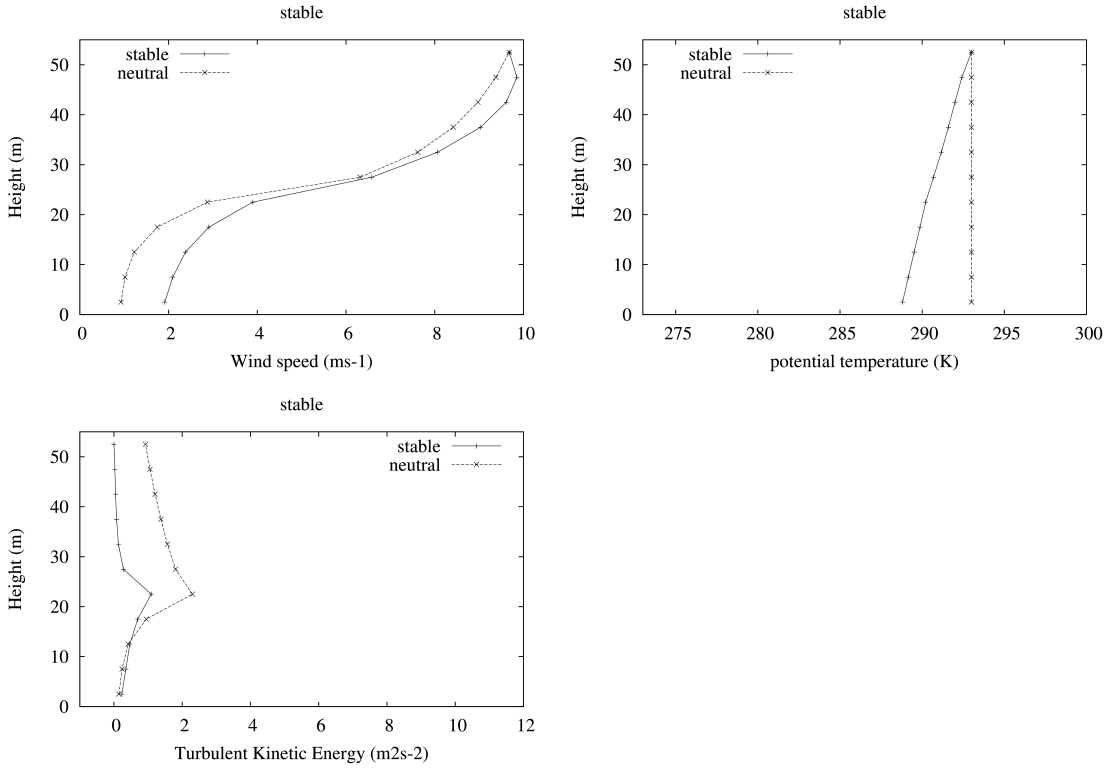

Figure 4.5: Comparison of wind (in ms^{-1}), potential temperature (in K) and T.K.E (in m^2s^{-2}) vertical profiles computed with CIM applied on a surface with obstacles under neutral and stable case atmospheric conditions

tions. Thus compared to Mauree et al. [2014b], CIM is here tested to analyze the effect of the stability of the atmosphere on the vertical profiles of wind, potential temperature and T.K.E.

Figure 4.5 shows the comparison of wind, potential temperature and T.K.E vertical profiles computed with CIM, applied on a surface with obstacles under neutral and stable atmospheric conditions. It is shown that when obstacles are present in a stable case they can further interfere with the wind profile. The potential temperature is lower close to the ground and in the canopy while the T.K.E is lower at the top and above of the canopy when comparing to the neutral case. The T.K.E are shown to decrease as compared to the neutral environment.

As for the unstable case, the profiles show slight differences when comparing to the neutral case for the temperature and the T.K.E. The change in the potential

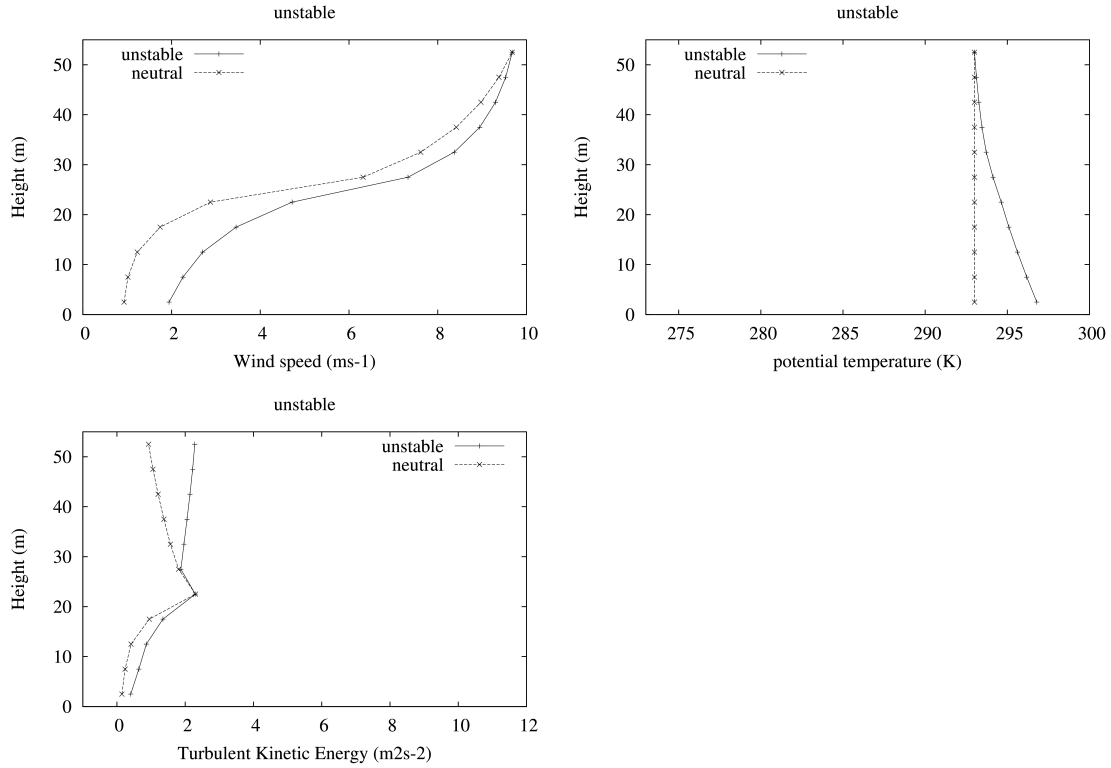

Figure 4.6: Comparison of wind (in ms^{-1}), potential temperature (in K) and T.K.E (in m^2s^{-2}) vertical profiles computed with CIM applied on a surface with obstacles under neutral and unstable case atmospheric conditions

temperature profile is expected since the surface is warmer and the lower levels of the canopy are also warmer. For the T.K.E, the profiles show that above the canopy, the buoyancy effects tend to be more important than the mechanical effect and hence affects the profile. The trend that is shown here is in good agreement with the calculations that were expected from the MOST as shown in Sect. 4.5.1. The wind speed increases in an unstable environment as does the T.K.E when compared with the neutral case.

4.7 Discussions and Conclusion

When CIM was tested over a plane surface with the MOST in stable and unstable atmospheric conditions, it was shown that there were discrepancies in the results.

For the stable case the difference for the wind speed was around 55% while for the unstable case, the differences were less than 5%. However the calculated T.K.E was quite different from the profile that was expected from the MOST.

In order to improve those results, it was proposed to modify the buoyancy term of the T.K.E. The other terms were considered to be well represented since Mauree et al. [2014b] showed good coherence between CIM and other formulations under neutral atmospheric conditions. Thus taking into account the Monin-Obhukov Similarity Theory, with the Businger formulations which are widely accepted, corrections were proposed. It was shown that a correction to this buoyancy term could be brought, if one wanted to get results which corresponded to the MOST. This was used to ascertain that the modifications we proposed to the buoyancy term in the T.K.E governing equation were good options. We showed that the correction terms, in the stable and unstable case, are indeed different if we want to be in coherence with the Businger's formulations. The correction that is proposed in the present study, improves the results significantly in both the stable and unstable case.

Finally, obstacles effects were integrated in CIM equations in the stable and unstable atmospheric conditions. The validity of the simulated profiles inside the canopy is arguable due to the lack of appropriate measurements to verify these results. However these results follow expectations. When the results from the MOST are compared to the Prandtl surface layer theory, the trends correspond to those obtained with CIM when obstacles are integrated. When compared to the profiles obtained in a neutral environment, it is expected that in an unstable case, the wind speed and the T.K.E are higher while in a stable case, the wind speed is expected to be lower. Besides above the displacement height, a surface layer is reproduced. However in the stable case, there are still some discrepancies. One of the unexpected results, in the stable case with obstacles, is that even though the T.K.E is slightly lower, we have a higher wind speed. A possible explanation for this is that as the T.K.E is lower, the diffusion of the momentum decreases. This then causes the fluxes coming from the obstacles to have a lower impact on the wind speed.

The main advantage of the development of this simple canopy model, is that not much computational time or data is needed to resolve vertical profiles of the

main meteorological variables. CIM can be used as an interface between meso-scale meteorological model and microscale models such as Building Energy Models. Further studies are however needed to complete our understanding of the impact of turbulence generation and why this correction had to be brought to the T.K.E terms. This is particularly important as it was shown that the similarity theory and the universal functions developed by the previous studies cannot be used in an urban context. Hence the modification brought here, using these universal functions are still to be improved. Data and measurements need to be collected to validate and enhance our understanding of turbulent processes in such type of canopy model.

Chapter 5

Multi-scale modeling of the urban meteorology: integration of a new canopy model in WRF model

This chapter corresponds to "Mauree, D. et al. 2014c, Integration of the Canopy Interface Model (CIM) in the Weather Research and Forecasting (WRF) model, in preparation, 2014"

Abstract

Urban parameterizations have been recently proposed and integrated in meso-scale meteorological models for a better reproduction of Urban Heat Islands and to compute building energy consumptions. These parameterizations usually improve the estimation of the surface fluxes of momentum, heat and kinetic energy, even if these surface fluxes are computed using low resolution vertical profiles of meteorological variables. The objective of the present study is to evaluate the value of the use of a module able to produce highly resolved profiles of these variables. For this purpose, the new 1D Canopy Interface Model (CIM) developed by Mauree et al. [2014a,b] has been integrated as an additional urban physics option in WRF v3.5. The coupling methodology is here detailed and its evaluation is done using a reference run based on a fine resolution WRF simulation. In order to keep both CIM and the meso-scale model in coherence, an additional term is added to CIM's calculation.

In general, this work allows the conclusions that the coupling improves the simulations of the meso-scale model and allows the WRF-CIM system to provide highly resolved vertical profiles while at the same time improving significantly computational time. The data from these preliminary results are very promising as it provides the foundations for CIM to act as an interface between meso-scale and micro-scale models.

Keywords: urban meteorology, multiscale meteorological modeling, urban canopy parameterizations, urban heat island.

5.1 Introduction

Meteorological meso-scale models were initially dedicated to weather forecast without the need to detail interactions between urban areas and the atmosphere [Salamanca et al., 2011]. For the last few years, urban parameterizations have been integrated in these meso-scale models to also simulate Urban Heat Islands (UHI) [Masson, 2000, Martilli et al., 2002], building energy consumption [Krpo et al., 2010] and improve air pollution modelling [Salamanca et al., 2011]. Table 5.1 shows the different schemes that have been developed in the recent years. The underlying purpose is thus to develop systems that could help urban planners take decisions and propose sustainable urban planning scenarios to decrease UHIs, building energy demand, or urban air pollution.

Baklanov et al. [2009] gave a guideline for the level of complexity that is needed for Urban Canopy Parameterizations based on the "fitness for purpose". For air-quality, urban climatology, strategies to mitigate heat islands and urban planning, it is necessary to have more detailed and precise meteorological profiles and fluxes (see Table 5.2).

It is now well known that urban climate depend on a series of processes taking place at different spatio-temporal scales from global to local [Oke, 1982], and that building energy demand and urban climate are closely related and interdependent [Ashie et al., 1999, Salamanca et al., 2011]. However using meso-scale meteorological models, with a high resolution, to cover a whole urban area and resolving at the same time local building effect and urban heat island is still not feasible with the actual computer performances [Martilli, 2007]. Moreover the use of available micro-scale models (such as Envimet [Bruse and Fleer, 1998] or EnergyPlus [Crawley et al., 2008]) on more than a neighborhood (few streets) is also not feasible. Thus multi-scale modeling is proposed as a solution.

Using the same methodology as Martilli et al. [2002], Muller [2007] designed experiments to show that a canopy module can be coupled with meso-scale models. He showed that the use of a canopy module in a meso-scale model with a low resolution gives the same trend as using a very high resolution in such models [Muller, 2007]. Using a canopy model is hence expected to reduce computational time while allowing at the same time a more precise integration of obstacles and

Model	Authors	Resolution of canopy	Vegetation	Primary use	Anthropogenic heat
MM5 MRF BL	Liu et al. [2006]	No canopy, roughness length modification	No	Weather Forecast	No
ARPS	Sarkar and De Ridder [2011]		Yes	UHI formation	Yes
Meso-NH-TEB	Masson [2000]	Single layer	Yes	Urban meteorology	from fixed temporal files
	Kusaka et al. [2001]		Yes		Yes
SUMM	Kanda et al. [2005]		Yes		No
FVM-BEP	Martilli et al. [2002]	Multi-layer	Yes	Air pollution modeling	No
WRF-BEP			Yes		No
NIRE-M	Kondo et al. [2005]		Yes		No
MM-CM-BEM	Kikegawa et al. [2003]	Multi-layer	Yes	Building energy use, air pollution modeling and urban planning	Yes
WRF-BEP-BEM	Salamanca et al. [2010]		Yes		Yes

Table 5.1: Urban canopy parameterization implemented in meso-scale models (adapted from Salamanca et al. [2011])

Application v/s Importance	Air quality	Urban climatology	Urban Planning	Weather forecasting
Wind speed	++	+	++	+ (above canopy)
Temperature (and Humidity)	+	+++	++	++ (2-m temperature)
Turbulent fluxes	++	++	++	++ (at the top of the canopy)
Pollutant concentration	+++		++	

Table 5.2: Variable importance versus application adapted from [Baklanov et al., 2009] (*'+' represent important, ++ 'very important' and +++ 'very very important'*)

calculation of the fluxes generated by the presence of these obstacles.

Based on the same methodology, a Canopy Interface Model (CIM) was developed and tested in an offline mode by Mauree et al. [2014a,b]. CIM is here introduced in the Weather Research and Forecasting model (WRF v3.5) community research model [Skamarock et al., 2005, 2008] in order to build a multi-scale urban meteorological system able to produce highly resolved vertical profiles of meteorological variables in low resolution meso-scale meteorological models. The idea is to use these profiles to improve the estimation of surface fluxes of momentum, heat, kinetic energy and humidity inside the meso-scale model and at the same time to allow the meso-scale model to be coupled in with a micro-scale model, if needed.

The objective of the present article is to detail the steps followed to set up and to evaluate the coupling. Indeed, a new methodology is proposed to ensure the maximum of coherence between the models and to take advantages of both models in the coupling system. When used with a low resolution, the meso-scale model cannot reproduce correctly the vertical meteorological profiles and surface fluxes in the canopy. However it still simulates the horizontal fluxes that are not considered in CIM, which is able to well reproduce the vertical transport. A correction of CIM computations is thus proposed to add horizontal fluxes effects in an effective way.

In Sect. 5.2 a brief description of the governing equations in WRF is given. In Sect. 5.3 it will be explained how CIM has been integrated in WRF in order to keep in coherence both the meso-scale model and CIM. In Sect. 5.4 a description of the experiments conducted with WRF is presented. In Sect. 5.5 the results from the series of sensitivity tests are presented to evaluate the value of the use of CIM and the proposed coupling. The last section is devoted to the discussions and the conclusions of this study.

5.2 Weather Research and Forecasting model

The Weather Research and Forecasting model [Skamarock et al., 2005, 2008] is a numerical weather prediction (NWP) and atmospheric simulation system. The Advanced Research WRF (ARW), version 3.5, developed by the National Center

for Atmospheric Research (NCAR) for research purpose, is used in the present study and will be referred to hereafter as WRF. Broad variety of physics and dynamics options has been proposed by the scientific community. In Sects. 5.2.1 and 5.2.2, only a brief description of the conservation equations and the physics options that are used to simulate the surface layer is given. The objective of this section is mainly to help understand the coupling of the Canopy Interface Model with WRF, which is fully described in Sect. 5.3.

5.2.1 Governing equations and turbulent closure

Following Ooyama [1990], variables with conservation properties (mass for example) are written with equations in their flux form and using a terrain-following mass vertical coordinate. We here present briefly these equations to prepare the presentation of the coupling with CIM. More details on the chosen formulations can be found in Skamarock et al. [2008].

Momentum and Heat

The following equation represents the conservation of momentum or heat.

$$\partial_t N + (\nabla . \vec{F_N})_\eta = F_N^s \tag{5.1}$$

where N is the momentum for the x, y or z or the heat and F_N^s is the source or sink terms from the surface. The second term on the left hand side of the equation is a flux divergence term which represents the advection, the pressure-gradient and the diffusion terms. The latter is a function of the diffusion coefficients, $K_{h,v}$ which will be described later. The $\nabla . \vec{F_N}$ term depends on η, the eta-levels given by:

$$\eta = \frac{(p_h - p_{ht})}{\mu} \tag{5.2}$$

where p_h is the hydrostatic pressure at this height, p_{ht} is the pressure at the top boundary and μ is the mass per unit area within the column in the domain, given by $\mu = p_{hs} - p_{ht}$ where p_{hs} is the pressure at the surface.

1.5 order turbulence closure

WRF provides several closure formulations for the calculation of the turbulent diffusion coefficients. A prognostic Turbulent Kinetic Energy (T.K.E) closure is chosen here. With this closure the turbulent diffusion coefficient can be computed using:

$$K_{h,v} = C_k l_{h,v} \sqrt{e} \tag{5.3}$$

where the subscript h, v represent horizontal and vertical directions respectively, C_k is a constant (ranging from 0.15 to 0.25), $l_{h,v}$ is the mixing length and e is the turbulent kinetic energy.

Turbulent Kinetic Energy

The T.K.E, E, can be calculated using a prognostic equation:

$$\partial_t(e) + (\nabla . \vec{F_e})_\eta = \mu(P + G - \varepsilon) \tag{5.4}$$

where e is μE, P is the mechanical production, G is the buoyancy and ε is the dissipation.

5.2.2 Focus on specific physics schemes

WRF provides a large variety of physics schemes to represent different processes taking place in the atmosphere. For the purpose of this study, the focus is mainly on specific schemes that are in relation with a future use of CIM.

Surface layer scheme

The surface layer schemes, proposed in WRF, calculate the friction velocities and exchange coefficients that enable the computation of surface heat and moisture fluxes by the land-surface models and surface stress in the Planetary Boundary Layer. The Monin-Obukhov Similarity Theory [Monin and Obukhov, 1954] option was chosen for this study.

Land-Surface Model

The Land-Surface Model (LSM) is a 1-D column model computing surface fluxes over land and sea-ice grid point starting from land-surface properties and outputs

of the surface layer scheme and the radiation scheme. These fluxes give a lower boundary condition for the vertical transport done in the Planetary Boundary Layer (PBL) schemes. The Noah LSM [Chen and Dudhia, 2001] was selected.

For the purpose of this study, we also chose to use the BEP-BEM [Salamanca et al., 2011] urban physics option to simulate the buildings effects on the long wave and short wave radiation (shadow effects and multi-reflexion) and the surface fluxes of momentum and heat.

The Building Effect Parameterization (BEP) module is based on Martilli et al. [2002] who proposed a multi-layer model. Obstacles effects are estimated in several layers of the meso-scale model. It takes into account the 3-D geometry of urban surfaces as well as the ability for buildings to diffuse sources and sinks of heat and momentum vertically through the whole urban canopy layer. The Building Energy Model (BEM), developed by Krpo et al. [2010], computes the building energy balance (and the associated building demand) to keep a comfort temperature inside buildings. This energy balance takes into account the effect of anthropogenic heating and heat diffusion through surfaces, radiation exchange through windows.

Planetary Boundary Layer

The PBL scheme calculates flux profiles so as to compute the temperature, moisture and horizontal momentum profiles for the atmosphere. One important aspect of this type of schemes is that they are one dimensional and assume that there is a clear separation between resolved and sub-grid eddies [Skamarock et al., 2008]. For the purpose of this study the Bougeault and Laccarère turbulence closure scheme [Bougeault and Lacarrère, 1989] developed specially for the BEP-BEM schemes will be used to compute $l_{h,v}$.

5.3 Canopy Interface Model integration in WRF

A 1-D Canopy Interface Model (CIM) was developed by Mauree et al. [2014a,b] in order to improve low resolution meso-scale meteorological models or to be used as an interface between low resolution meteorological meso-scale model and micro-scale models. After a brief description of CIM, it is explained in the present section how CIM was introduced in WRF.

5.3.1 Canopy Interface Model

CIM solves 1-D transport equations, i.e. only terms along the vertical (z-direction) are kept from Eq. (5.1).

$$\frac{\partial u}{\partial t} = \frac{\partial}{\partial z}\left(\mu_t \frac{\partial u}{\partial z}\right) + f_u^s \tag{5.5}$$

$$\frac{\partial \theta}{\partial t} = \frac{\partial}{\partial z}\left(\kappa_t \frac{\partial \theta}{\partial z}\right) + f_\theta^s \tag{5.6}$$

where u is the mean wind speed in the x or y directions, θ is the mean potential temperature, f_u^s and f_θ^s are the momentum and heat surface fluxes and μ_t and κ_t are the turbulent diffusion coefficients. κ_t is μ_t divided by the Prandtl number (0.95).

CIM solves these equations using a 1.5 order turbulence closure based the Turbulent Kinetic Energy (T.K.E).

$$\mu_t = C_k l \sqrt{e} \tag{5.7}$$

where C_k is a coefficient calculated to be equal to $k^{\frac{4}{3}}$, from Mauree et al. [2014b], where k is the von Kàrmàn constant (0.41), l is the mixing length calculated according to Santiago and Martilli [2010] and E is the T.K.E calculated independently as follows:

$$\frac{\partial E}{\partial t} = \frac{\partial}{\partial z}\left(\lambda_t \frac{\partial E}{\partial z}\right) + C_\varepsilon^* \frac{\sqrt{E}}{l}(E_{stat} - E) + f_e^s \tag{5.8}$$

where λ_t is here assumed to be equal to μ_t and E_{stat} is a stationary T.K.E value obtained in neutral condition and without obstacles as explained by Mauree et al. [2014b]. Further details about the development of CIM and the governing equations used in CIM can be found in Mauree et al. [2014a,b].

5.3.2 WRF-CIM coupling strategy

CIM computes highly resolved vertical profiles of meteorological variables, but it doesnt include horizontal fluxes like a mesoscale model such as WRF (see Eq. 5.1). In such a context, it is possible to force CIM with WRF in a one-way nesting but it will not be valuable to correct the values calculated by WRF using CIM values as it could have been proposed in a traditional two-way nesting.

Thus two methodologies are tested : the first one is based on a coupling using fixed top boundary conditions as done by Muller [2007] ; the second is a new proposition to add an additional term in CIM's calculation in order to account for the processes described by the flux divergence term in Eq. (5.1).

Coupling by fixing top boundary condition - Method FT

CIM can calculate vertical profiles using prescribed top boundary conditions and description of the surface obstacles in each grid (geometry and surface temperature). In an offline mode, the boundary conditions may be fixed at the top with a constant value, while when coupled with a meso-scale model, this value is interpolated from the meso-scale model at each time step. At the initialization time step, the meso-scale values are interpolated on each of CIM vertical level and used to initialize the computation of the surface fluxes done by the BEP-BEM system. At other time steps, CIM high resolution vertical profiles (wind speed, temperature and humidity) are given to BEP-BEM which then proceeds to a potentially more detailed estimation of compute sources/sinks. The sources and sinks are then given back to CIM to compute new vertical profiles, and to the meso-scale model (the surface fluxes are in this way aggregated at each of the meso-scale vertical levels and represent the F_N^s terms in the Eq. 5.1 from Sect. 5.2).

This coupling may be enough when the mixing boundary layer is well developed but could be limited in stable conditions when the exchanges between air layers are low. Indeed, in such cases the horizontal fluxes cannot be neglected anymore as compared to the vertical fluxes and the method will not conserve the coherence between the two models from a fluxes point of view.

Coupling by fixing fluxes - Method FF

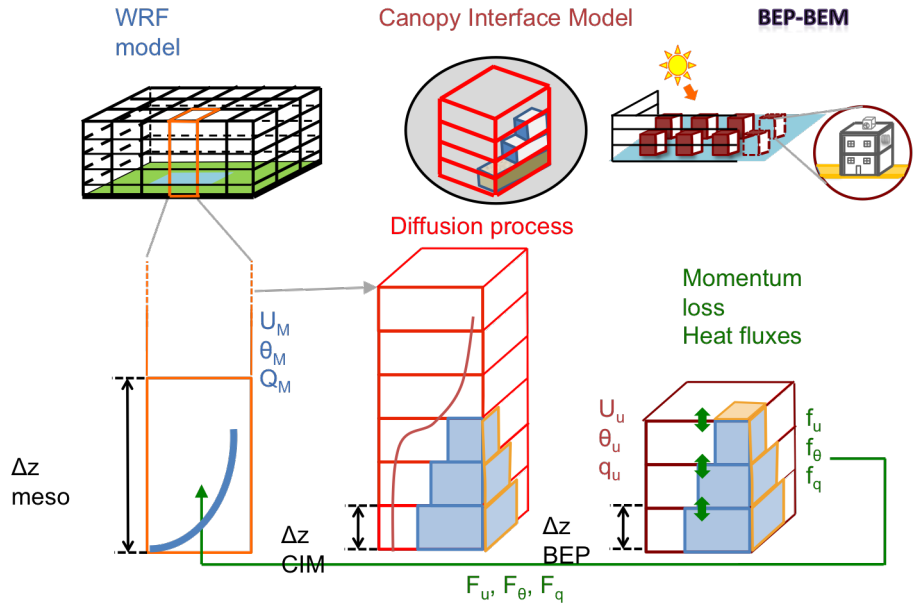

Figure 5.1: WRF scheme with the implementation of CIM *(all in blue corresponds to WRF, in red variables corresponding to CIM and the fluxes are represented in green)*

We hence propose in this section a methodology to keep the coherence between the models and take into account the horizontal transport in CIM as well as a new forcing at the top of CIM using fluxes. To develop this new methodology, an analysis of the fluxes budget is done over the vertical column of CIM and for a corresponding volume from the meso-scale model. Figure 5.2 gives a representation of the fluxes considered in both CIM and the meso-scale model. The following statements may be noted to ensure the coherence between the models and a balance of the fluxes:

- The mean value of each variables calculated on the CIM column should be the same as the one computed by the meso-scale model (both models proposing an estimation of the same real profiles);

- Bottom surface fluxes (i.e. surface fluxes calculated to take into account the effects of buildings at each level of the column) are computed once for forcing both the meso-scale model and CIM; the values should hence be equal

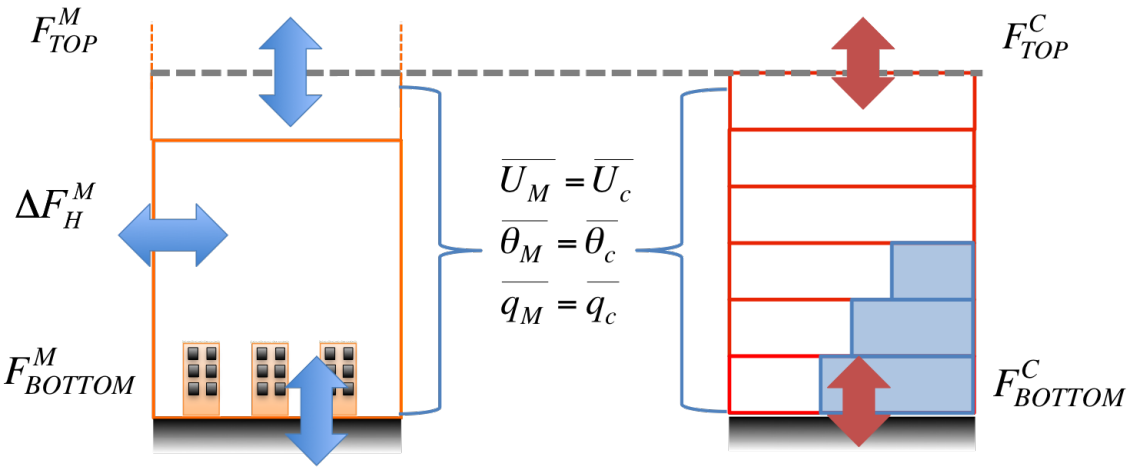

Figure 5.2: Representation of fluxes calculated on the vertical column in CIM (right) before correction and in the corresponding volume in WRF (left)

in both models (F^M_{BOTTOM}=F^C_{BOTTOM}=F_{BOTTOM});

- Far enough from the surface the flux at the top of both columns should be equal as it would be less influenced by the surface effects. In this case, a constant flux layer is considered and it is assumed that the flux at the top is equal to the bottom fluxes (F^M_{TOP}=F^C_{TOP}=F_{TOP}).

Based on the above statements, CIM's profiles may be corrected after each time step using an estimation of the horizontal fluxes. The formulation is done to allow a computation of these values that are not known *a priori* in order to ensure a coherence between the models. Equation 5.9 points out the consequences of this condition on the new CIM profiles.

$$\begin{aligned} \text{For } i < n \left\{ N_i^{Ct+1} \right. &= N_i^{C*} + \Delta F_{Hi} \\ \text{For } i = n \left\{ N_n^{Ct+1} \right. &= N_n^{C*} + \Delta F_{Hi} - F_{TOP} \end{aligned} \tag{5.9}$$

where N is one of the variables calculated by CIM (wind speed, potential temperature or humidity), t is the time step considered, i is an index corresponding to the center of a grid cell in CIM, N_i^{Ct+1} is the updated vertical value of CIM, N_i^{C*} is an "initial" value and ΔF_{Hi} the horizontal fluxes to be added. A different equation is proposed for the top most level of CIM since the objective is to not

force the model with a value of wind, temperature and humidity but with a flux value at the top, F_{TOP}, that ensures the balance of both models. For each of the other levels, this flux may be computed at the cell faces. However the flux value on the top surface of the CIM column cannot be determined and has to be fixed. Thus, N_i^{C*} represents N_i^{Ct} including all fluxes except the horizontal ones and the top one.

To ensure coherence between the models using these formulation, we can write that the mean value of the variables calculated by CIM have to be equal to the meso-scale value:

$$\overline{N_i^{Mt+1}} = \overline{N_i^{Ct+1}} = \overline{N_i^{C*}} + \overline{\Delta F_{Hi}} - \frac{F_{TOP}}{n} \tag{5.10}$$

where $\overline{N_i^{Mt+1}}$ is the mean meso-scale value interpolated from the meso-scale model over the n levels present in CIM's column and where n is the number of levels in the urban grid. As a first assumption, the horizontal fluxes, can be assumed constant over CIM's column (equal to their mean) and it can then be written using Equation 5.10 as:

$$\Delta F_{Hi} = \overline{\Delta F_{Hi}} = \overline{N_i^{Mt+1}} - \overline{N_i^{C*}} + \frac{F_{TOP}}{n} \tag{5.11}$$

This then leads with Eqs. 5.9 to the Eqs. 5.12, which give the new formulations used in CIM.

$$\begin{aligned} \text{For } i < n \left\{ N_i^{Ct+1} \right. &= N_i^{C*} + \overline{N_i^{Mt+1}} - \overline{N_i^{C*}} + \frac{F_{TOP}}{n} \\ \text{For } i = n \left\{ N_n^{Ct+1} \right. &= N_n^{C*} + \overline{N_i^{Ct+1}} - \overline{N_i^{C*}} + \frac{F_{TOP}}{n} - F_{TOP} \end{aligned} \tag{5.12}$$

When this correction is made, the results from CIM and the meso-scale models should be coherent. It is proposed here to fix F_{TOP} equal to F_{BOTTOM}, in accordance with the statement formulated earlier.

5.4 Experiments with WRF-CIM

Sensitivity tests were designed to assess the value of the use of CIM in WRF and specially to see how CIM can improve the meteorological profiles when using a coarse vertical resolution and what its impact will be on the computational time.

A theoretical domain of 20*20 cells was designed each with a horizontal resolution of $45km$*$45km$. It was centered at latitude $48.404N$ and longitude $2.248E$, situated near the "Ile-de-France" region in France, such that the topography did not interfere with the test that have been conducted. An urban area of 9 cells at the centre of the domain has been designed and the land use for the rest of the domain was taken from the MODIS database.

Several simulations were performed, with WRF all using the urban parameterization BEP-BEM, over 5 days from the 27th of January 2010 at 00h00 to the 1st of February 2010 at 00h00 (with the first day of initialization not being discussed here). Simulations were also conducted for a summer period, but since the results showed similar behavior to the results presented in this study they are not further discussed.

Reference Simulation (Ref.) : WRF is run with a fine vertical resolution of 5m (corresponding to the vertical resolution of CIM), for the first 10 levels, without CIM. This is considered to be the reference simulation and will be denoted "Fine res. (Ref)". The simulation integrates all processes needed to compute high resolved vertical profiles with BEP-BEM computing the urban effects.
C1 : WRF is run with a coarse vertical resolution of 94m, for the first level, without CIM. This simulation ("Coarse res. (C1)"), compared to the reference one, will show the impact of the vertical resolution on the surface representation and on the calculation of the meteorological variables in the WRF model.
C2 : WRF is run with the same resolution as the reference run with CIM coupled using Method FF (denoted "Fine res. with CIM - FF (C2)"). BEP-BEM has no connection to the meso-scale model but runs with CIM profiles. This test is carried out to see if the integration of CIM in WRF when using high resolution will have an effect on the meso-scale solution.
C3 : WRF is run with a coarse vertical resolution with CIM coupled using Method

FF. BEP-BEM also runs with CIM profiles issued from the coarse resolution WRF. This test, denoted "Coarse res. with CIM - FF (C3)", is performed to see how the profiles that are calculated by CIM when it is integrated in the WRF model correspond to the simulation with a fine resolution and how this will in turn influence the meso-scale processes in a low resolution simulation.
C4 : WRF is run with a fine vertical resolution with CIM coupled using Method FT. This test, denoted "Fine res. with CIM - FT (C4)"), is done to compare with the FF method.
C5 : WRF is run with a coarse vertical resolution with CIM coupled using Method FT. This test, denoted "Coarse res. with CIM - FT (C5)", is also done to compare with the FF method in a low resolution simulation.

5.5 Results

This section aims at evaluating the coupling of CIM and WRF and to justify the strategy that has been developed. As previously mentioned, the simulations presented here were performed for a period of 5 days in January 2010. We only show results for the horizontal wind speed and the temperature.

5.5.1 Global comparisons on specific vertical levels

We present here the comparisons over the four days of simulation and a series of statistical tests in order to show the general trends when CIM is integrated in WRF. Table 5.3 summarizes the comparisons in terms of biases, correlations and the root mean square errors (R.M.S.E) computed on hourly values of the simulated temperatures and wind speeds for the 4 days of simulation. Figure 5.3 present a time-evolution of the different simulations cases discussed in Sect. 5.4 over the 4 days at $5m$ and $50m$.

Effect of the WRF vertical resolution - (Ref./C1)
We focus here on the differences observed between the fine and coarse resolution WRF simulations, without CIM, as increasing the resolution can have a significant effect on the temperature and the wind speed. It can indeed be seen from Table 5.3

that on average the coarse WRF configuration (C1) tends to over-estimate the potential temperatures and to under-estimate the wind speed.

But Fig. 5.3a shows that the differences in temperature may be under-estimated by more than $1K$ for some hours. The horizontal wind speed computed at 50m is weaker for the coarse resolution than in the fine resolution simulation and these differences may reach $4ms^{-1}$. These first results justify the development of CIM model and its coupling in WRF since the vertical resolution may influence the accuracy of the temperature and wind profiles.

Effect of a coupling with CIM at high resolution - (Ref./C2)
Another experience constisted of introducing CIM in WRF and test the system with a high vertical resolution in the meso-scale model (C2). One can note from Table 5.3 that the comparison with the high resolution simulation with CIM gives satisfactory correlations. There were no biases on average for temperature and small positive bias for the wind speed. This experience showed that the meso-scale simulations were not significantly modified when CIM was used with a fine vertical grid resolution in WRF and hence that CIM is not disturbing the WRF simulations.

Effect of a coupling with CIM at low resolution - (Ref./C3)
The integration of CIM in WRF drastically reduces the under-estimations of the coarse meso-scale model from -35% to -17% at $50m$ and improves the over-estimation of the temperature from 10% to 7% (see Table 5.3). It can also be noted that in some cases the temperature is still under-estimated by about $1K$. CIM produces new high vertical resolution profiles that only slightly over-estimate the wind speed by 2% at $50m$ and respect their variability (high correlation coefficient). Although the wind speed from CIM at $50m$ is in agreement with the fine resolution simulation, there are a few hours where the difference can be up to $1ms^{-1}$. It however under-estimates the wind speed by 24% at 5m and the variability of these values is not as well represented, at the surface, as at $50m$. But as shown in Fig. 5.3d the variability amplitude is also less important at $5m$ than at $50m$. There are also some periods when CIM has a good correspondence with the fine resolution simulation.

Simulations	Resolution		Method		Bias		R.M.S.E		R
	Fine	Coarse	FF	FT	Value	%	Value	%	
For Potential Temperature									
Meso outputs at 50 m									
WRF C1		x			0.4	10	0.5	12	0.99
WRF-CIM C2	x		x		0.0	0	0.0	0	1.0
WRF-CIM C3		x	x		0.3	7	0.5	12	0.99
WRF-CIM C4	x			x	0.0	0	0.1	2	1.0
WRF-CIM C5		x		x	0.3	7	0.6	15	0.97
CIM outputs at 50 m									
WRF-CIM C3		x	x		0.2	5	0.4	10	0.99
WRF-CIM C5		x		x	0.4	10	0.5	12	0.99
CIM outputs at 5 m									
WRF-CIM C3		x	x		0.4	9	0.5	12	0.99
WRF-CIM C5		x		x	0.7	16	0.8	19	0.98
For Wind									
Meso outputs at 50 m									
WRF C1		x			-1.8	-35	1.9	37	0.97
WRF-CIM C2	x		x		0.1	2	0.2	4	1.0
WRF-CIM C3		x	x		-0.9	-17	0.9	17	0.99
WRF-CIM C4	x			x	0.4	8	0.6	12	1.0
WRF-CIM C5		x		x	-0.5	-10	0.8	15	0.96
CIM outputs at 50 m									
WRF-CIM C3		x	x		0.1	2	0.5	10	0.99
WRF-CIM C5		x		x	-0.3	-6	0.5	10	0.99
CIM outputs at 5 m									
WRF-CIM C3		x	x		-0.5	-24	0.6	28	0.90
WRF-CIM C5		x		x	-1.0	-47	1.3	61	0.39

Table 5.3: Statistical comparison between the fine resolution simulation (Fine res. (Ref.) and the WRF (C1), WRF-CIM (C2), WRF-CIM (meso and cim - C3), WRF-CIM (C4) and WRF-CIM (meso and cim - C5) simulations). The % represent the percentage difference with respect to the mean temperature in ($^{\circ}C$) and the mean horizontal wind speed values from the fine resolution simulation. R is the correlation. FF (fixed flux) and FT (fixed top) represent the two coupling methods.

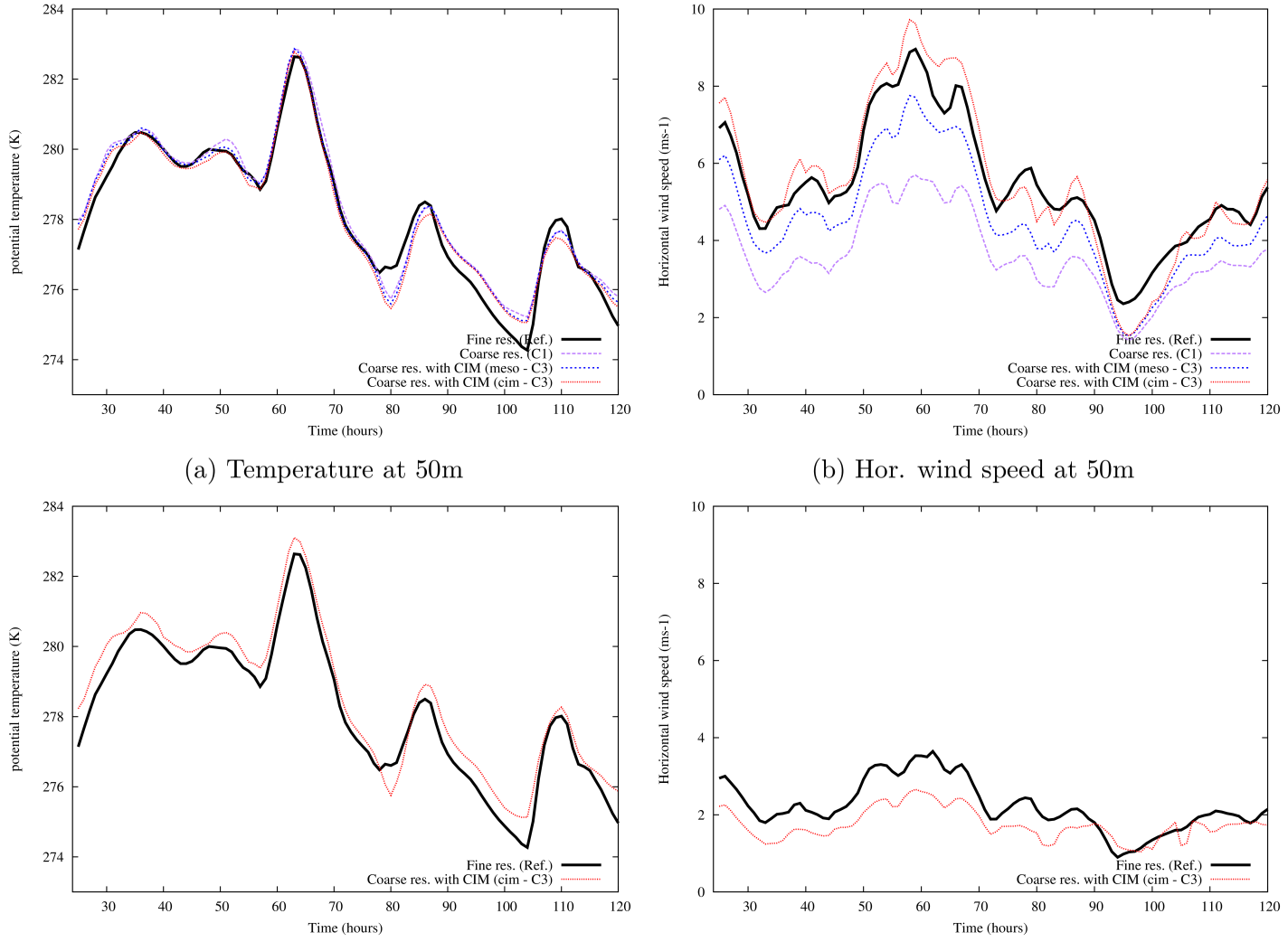

(a) Temperature at 50m

(b) Hor. wind speed at 50m

(c) Temperature at 5m

(d) Hor. wind speed at 5m

Figure 5.3: Comparison of the potential temperature (K) (left) and wind speed (ms^{-1}) (right) computed using WRF without and with the coupling of CIM at 50m (top) and at 5m (bottom). Black lines refer to reference simulation (Ref.) , purple refer to C1, blue line refer to meso-scale values from C3 (meso - C3) and red line refer to CIM values from C3 (cim - C3). Horizontal axis represents the time, in hours, after the start of the simulation

Effect of the FT coupling - (Ref./C4 and C5)

In order to show the importance of the coupling methodology proposed in Sect. 5.3, Table 5.3 also presents the results of a comparison between the WRF fine simulations and the WRF-CIM simulations without taking into account the horizontal fluxes (C4 and C5). It can be noted that when the horizontal fluxes are removed the bias and the R.M.S.E increase for both the temperature and the wind speed as compared to the simulation where the fluxes were present (except for the wind speed at 50m from the meso-scale model). The correlation coefficient for the wind speed at 5m is also drastically reduced.

Even though we know that in CIM the vertical fluxes and diffusion processes are better taken into account, we cannot conclude that the results are better in this context. The meso-scale model contains a number of processes, such as the horizontal wind advection or pressure gradient, which are not taken into account. It is thus important to take these processes into account in CIM in such a way that both calculations from CIM and WRF remain coherent.

5.5.2 Comparison on specific vertical profiles

This section aims at showing vertical profiles at specific hours to illustrate the effect of the coupling methods in different stability conditions of the atmosphere. A time-evolution of the mean wind speed and potential temperature (not shown here), over the 4 days of simulations were made and we chose some profiles based on these.

Comparison using a fine vertical grid resolution in the meso-scale model

For example, Figs. 5.4 and 5.5 show the comparison between the vertical profiles obtained by the meso-scale model when used at high resolution with or without CIM (Ref. and C2). We note that the temperature profile is not modified while the wind profile is slightly over-estimated in these cases. When CIM is used, the effect of the horizontal coupling is also tested by removing the evaluation of the horizontal fluxes of CIM's computation (C4). It turns out that CIM with the horizontal

fluxes correction is able to correctly simulate the temperature and wind profile, at both times in neutral or unstable conditions. However, when these fluxes are not taken into account, there are changes in the profiles both at the meso-scale level and in CIM. The temperature is over-estimated ($0.5K$) close to the surface while the wind speed is further under-estimated as compared to the solution with the horizontal fluxes.

The effect of the correction can be noted on the profiles at 02h00 with a disconnection at the top of the column between CIM's profile and the meso-scale profile. This is due to the fact that the correction forces CIM to give a mean value equal to the meso-scale mean value. This is not observed when the mixing is important (at 15h00).

Comparison using a coarse vertical grid resolution in the meso-scale model

As we have now ensured that CIM is not significantly changing the meso-scale model solution when using a fine resolution, we performed a series of experiments with CIM using a coarse resolution. The differences between the profiles calculated by CIM and by the meso-scale model were studied on an hourly basis and were found to be minimal during the morning when the development of the boundary layer was at a maximum. We thus chose two vertical profiles out of this zone to show that CIM can perform in near-neutral (stable) or unstable conditions. Figures 5.6 and 5.7 show the comparisons on the vertical profiles obtained by the meso-scale model when used at coarse resolution without or with CIM (Ref., C1 and C3). In the same way as previous experiences with high resolution, when CIM is used, the effect of the horizontal coupling is also tested by removing the horizontal fluxes of CIM's computation (C5).

It is shown that when CIM is used the model is able to reproduce a profile for the potential temperature, at 02h00, which is in good agreement with the profile as calculated by the fine resolution meso-scale simulation. At 15h00, with horizontal fluxes, there is a global difference of less than $0.5K$ between the profile calculated by CIM and the fine resolution. In the absence of horizontal fluxes, the temperature is over-estimated over the whole column of CIM and the difference is

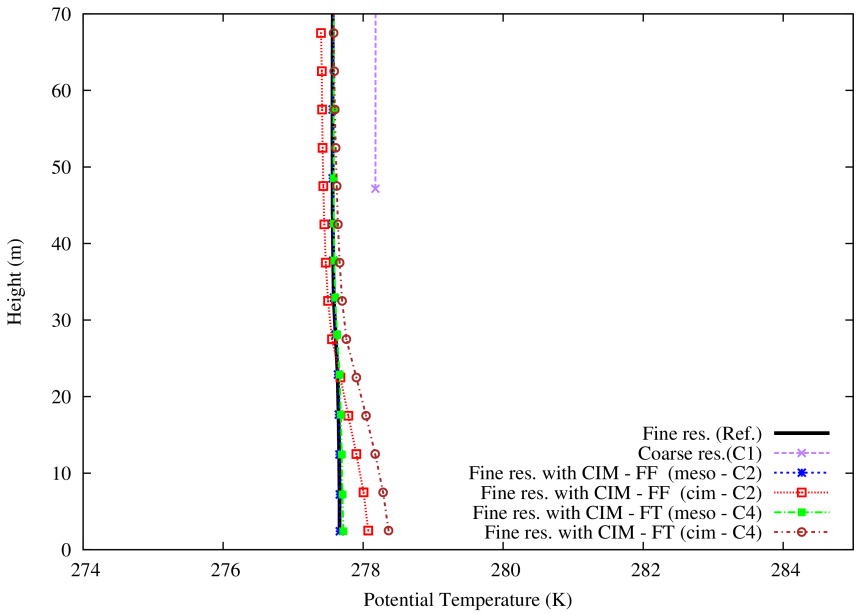

(a) Day 2 at 02h

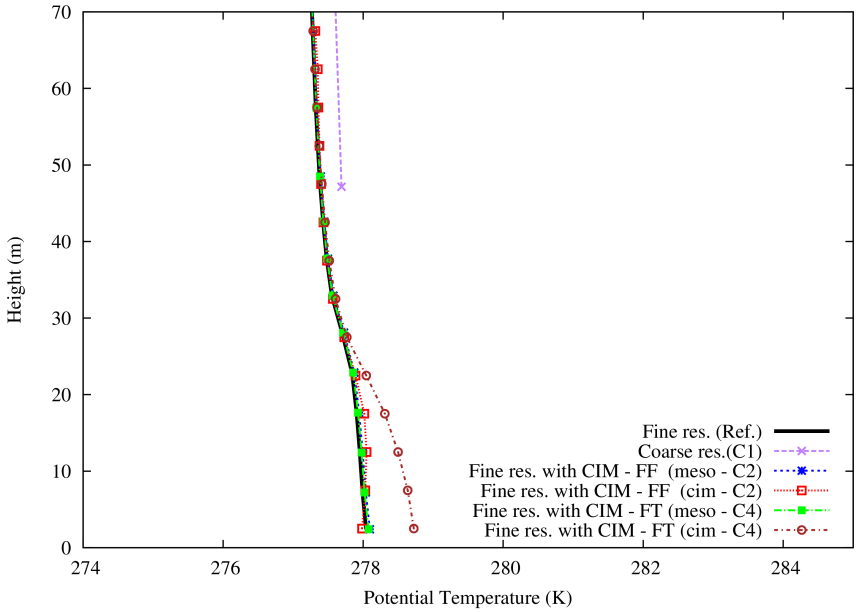

(b) Day 5 at 14h

Figure 5.4: Profile of the potential temperature (K) using a fine resolution (Ref. - bold black curve), coarse resolution (C1 - purple curve), fine resolution with CIM (meso - C2 - blue curve ; cim - C2 - red curve) and fine resolution with CIM - with no horizontal fluxes (meso - C4 - green curve ; cim - C4 - brown curve)

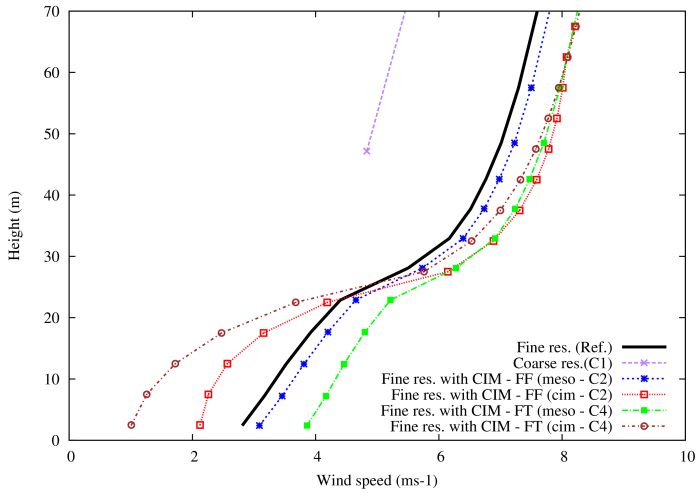

(a) Day 2 at 02h

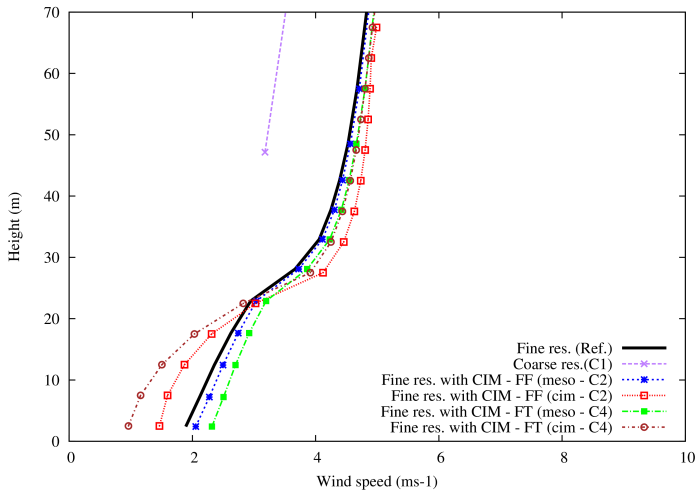

(b) Day 5 at 14h

Figure 5.5: Profile of the wind speed (ms^{-1}) using a fine resolution with WRF (Ref. - bold black curve), coarse resolution (C1 - purple curve), fine resolution with CIM (meso - C2 - blue curve ; cim - C2 - red curve) and fine resolution with CIM - with no horizontal fluxes (meso - C4 - green curve ; cim - C4 - brown curve)

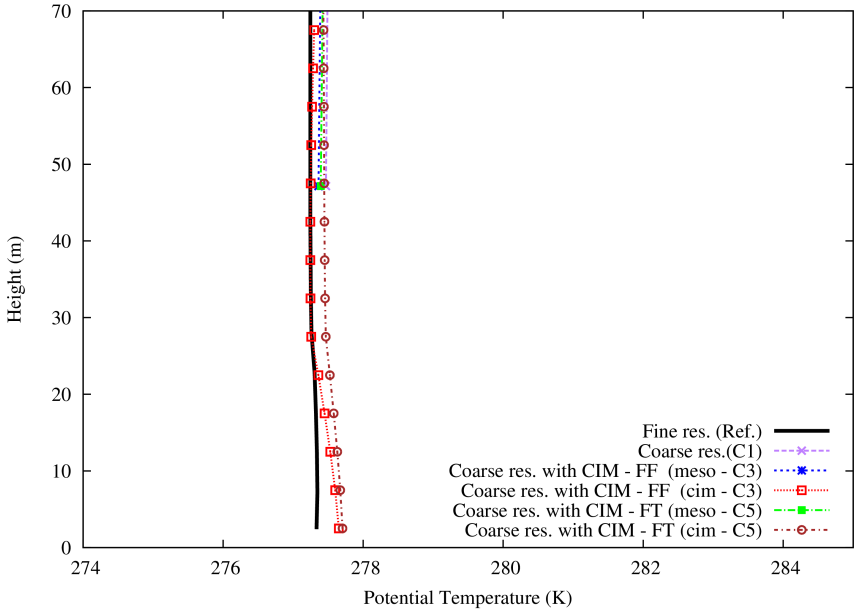

(a) Day 4 at 02h

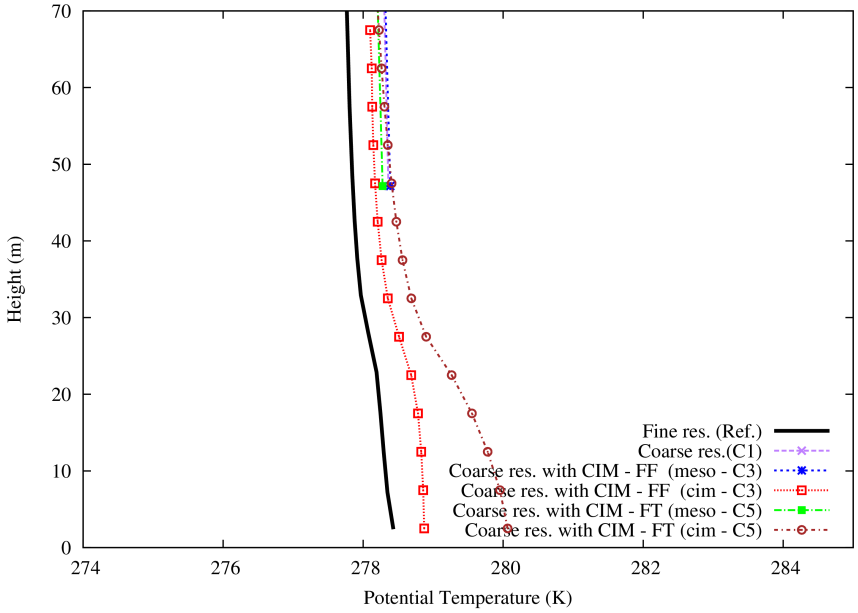

(b) Day 4 at 15h

Figure 5.6: Profile of the potential temperature (K) using a fine resolution with WRF (Ref. - bold black curve), coarse resolution (C1 - purple curve), coarse resolution with CIM (meso - C2 - blue curve ; cim - C2 - red curve) and coarse resolution with CIM - with no horizontal fluxes (meso - C4 - green curve ; cim - C4 - brown curve)

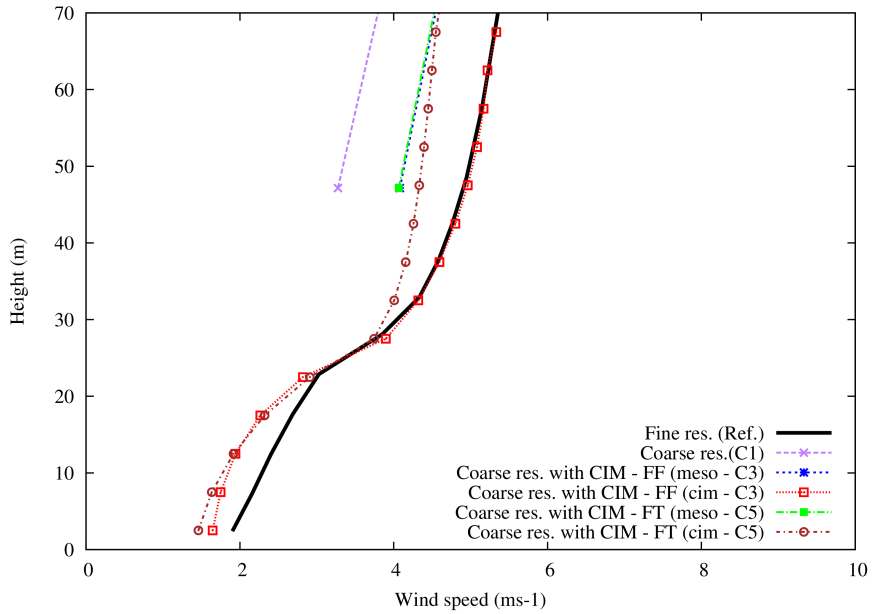

(a) Day 4 at 02h

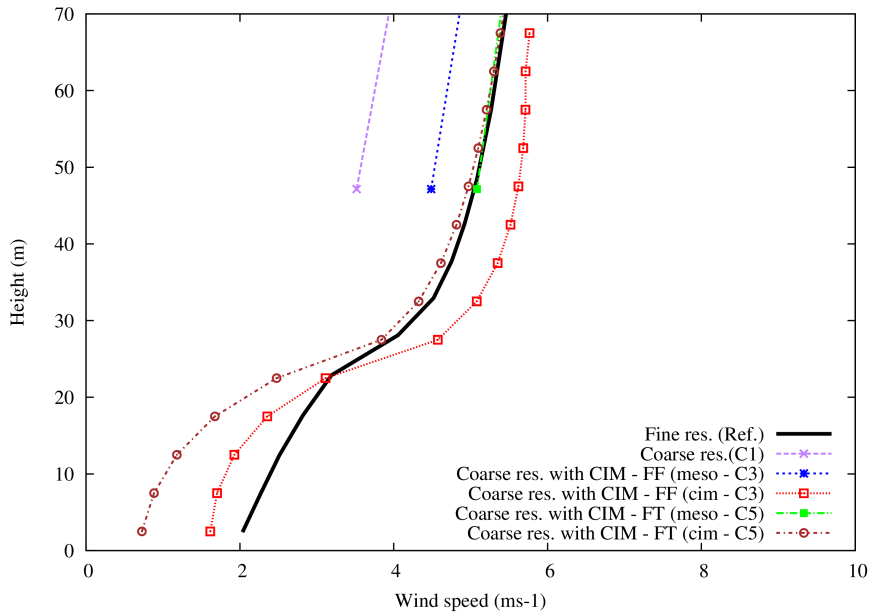

(b) Day 4 at 15h

Figure 5.7: Profile of the wind speed (ms^{-1}) using a fine resolution with WRF (Ref. - bold black curve), coarse resolution (C1 - purple curve), coarse resolution with CIM (meso - C2 - blue curve ; cim - C2 - red curve) and coarse resolution with CIM - with no horizontal fluxes (meso - C4 - green curve ; cim - C4 - brown curve)

increased to more than $1.5K$ in the first 10 meters. There are however no significant improvements of the meso-scale temperatures. It is noteworthy to mention that the correction does not change the stability regime of the atmosphere.

The horizontal wind speed in a near-neutral situation, for example at 02h00, (see Fig. 5.7a), is significantly improved for the meso-scale model. At $50m$ the wind speed is increased from $3ms^{-1}$ to over $4ms^{-1}$. The profiles which are calculated from CIM are also in very good agreement with the reference simulation. If the horizontal fluxes are removed the wind speed above the canopy is under-estimated in CIM.

The results are more contrasted in an unstable condition, such as at 15h00 (see Fig. 5.7b). The profiles calculated by CIM, with the horizontal fluxes are much closer to the reference simulation (less than $0.5ms^{-1}$ difference). However above the canopy the profile without the horizontal fluxes are closer to the reference simulation. If we look at the meso-scale profiles when using CIM with and without horizontal fluxes, we can observe that the green curve is much closer to the reference solution. This can also be explained with the methodology that we have proposed in Sect. 5.3 for the calculation of the horizontal fluxes. We worked this correction using a mean value for the canopy as well as a mean value for the meso-scale model over the corresponding volume. In order to be in agreement with this statement, if one wants to calculate a coherent profile in CIM, then there is a slight deterioration of the meso-scale value.

It is should also be noted here that in the simulation without horizontal fluxes, the value is fixed at the top boundary conditions. We evaluated in this way two possibilities for fixing the boundary condition at the top. We determined, from these experiments, that the addition of the horizontal fluxes were more important as compared to fixing the top boundary conditions, in order to keep the coherence between both models.

5.5.3 Computational time

Finally an analysis of the computational time was made. Table 5.4 gives a summary of the CPU time used for several simulations.

The data highlight the fact that when the resolution of WRF is decreased, the

Simulations	Computational Time
Ref.	14
C1	11
C2	14
C3	11

Table 5.4: Computational time (in minutes) needed to run the model for each of the simulations

computational time is decreased but when CIM is introduced the computational time is not impacted even though there is an additional calculation which is now being performed by the system to produce high resolution profiles.

5.6 Discussions and Conclusion

A Canopy Interface Model was designed by Mauree et al. [2014b,a] in such a way that it can act as an interface between meso-scale models and micro-scale models. In this study it has been coupled with the WRF model. The aim of this study was to evaluate the coupling done specially to improve surface representation in meso-scale models and to demonstrate the ability of the built system to provide valuable high resolution vertical profiles. CIM is a standalone 1-D column model that can be forced only at the top using values interpolated from the meso-scale model to calculate meteorological profiles independently of the meso-scale model. However in order to keep the coherence between both CIM and WRF models, a methodology was proposed so as to add an additional term, in CIM's calculations, to take into account the horizontal fluxes and to fix a flux at the top of the column.

Through a series of sensitivity tests, it was shown that:

- The coupling of CIM and WRF improved the meso-scale simulations specially when WRF was used with a coarse resolution (we also verified that when WRF was used with a the same vertical resolution as CIM, the simulations of both models were very similar and in this way coherent). Compared to the highly resolved simulation, it was shown that WRF, with a low resolution, tends to over-estimate the temperature and under-estimate the wind speed.

Coupled with CIM, the new system showed better performances with smaller biases and R.M.S.E. Usually the correlation was similar and very good.

- It was demonstrated that the correction brought to CIM's calculation to take into account the horizontal fluxes was very important in order for both the meso-scale model and CIM to be in coherence.

All of the experiments that were conducted were not presented here. A simulation was carried out for a summer period. The results showed similar behavior to the results presented in this study. Tests were also conducted to evaluate the influence of fixing a value at the top of the canopy or calculating a flux. There were no significant changes between the two scenarios, but it is indeed more coherent to use a flux instead of fixing a value at the top based on the methodology that we have proposed. This provides an enhanced degree of freedom for the calculation in CIM. We also analyzed the influence of having different vertical resolutions for the first meso-scale grid cell. This did not show significant impact on the results and therefore means that CIM can be used independently of the height of the first level in the meso-scale model. The assumption made, when describing the method "FF", that the flux at the top of the canopy has to be equal to the bottom flux, imposes that a constant-flux layer needs to fully develop at the top of the column. There is thus a requirement on the minimum number of levels needed in CIM to achieve the best performance. No empirical law was found to define a limit. This is something that is still to be understood.

Further investigations are needed to improve our understanding of the processes taking place at these different scales. The resolution of the turbulence closure in CIM is different from that of WRF: this would explain why close to the surface CIM has a more important impact than far enough from the surface. Moreover when a correction was brought to CIM in such a way that CIM calculations were coherent with the meso-scale calculation, this meant that the results in the meso-scale models were less affected in some cases.

In conclusion of this study, we can say that the WRF-CIM system is able to calculate coherent high resolution vertical profiles, in the canopy and these profiles were in good agreement with those calculated using WRF with a high vertical grid resolution. It was therefore demonstrated that CIM can be used with a low verti-

cal resolution meso-scale model to reduce the computational cost. In view of the above promising results, the foundation for the use of CIM as interface to improve surface representation and to couple meso-scale models to micro-scale models is established.

Chapter 6

Conclusions and Perspectives

6.1 Conclusions

The 5th report issued by the Intergovernmental Panel on Climate Change in 2013, highlighted again the role of anthropogenic greenhouse gas emissions in the current climate change we are experiencing. Non-binding and binding international agreements have encouraged countries and governments to implement new policies to reduce their greenhouse gas emissions. These emissions come typically from our energy production. Around 70% of the energy produced is used in urban areas. Since 2010, over 50% of the world's population lives in urban areas and this figure is expected to increase to 75% in 2050. Besides, buildings account for around 40% of the total final energy consumption among which 70% is dedicated to the thermal comfort of their occupants. It is thus crucial to reduce this energy use in order to decrease the building footprint in the greenhouse gas emissions.

To evaluate more precisely building energy use and urban planning scenarios, it is essential to develop models that are able to grasp all the processes taking place at various spatio-temporal scales and that influences the urban climate. To address this issue, it was proposed to develop a 1-D column model, the Canopy Interface Model (CIM). The intended objective of CIM is to provide an interface in order to couple meso-scale model and micro-scale models.

CIM is a standalone model using a 1.5 order turbulence closure. It was first tested in an offline mode, where values were prescribed at the top for the boundary conditions and in a neutral environment. Fluxes coming from the surface (horizontal and vertical) were calculated according to Martilli et al. [2002]. A new formulation for the resolution of the Turbulent Kinetic Energy (T.K.E) was derived. To be in coherence with the traditional Prandtl surface layer theory, a constant T.K.E profile is obtained. In such cases, it was then showed that the value of the T.K.E corresponds to the stationary T.K.E. Obstacles were then integrated in CIM according to Krpo [2009] and Kohler et al. [2012]. The novelty with this approach was that any kind of obstacles could be integrated in CIM as porosities. This means that CIM can be used with building energy use models or other vegetation models such as EnviMet [Bruse and Fleer, 1998] where the obstacles will

be better represented. Furthermore the mixing length was modified according to Santiago and Martilli [2010]. The results that were obtained when obstacles were integrated in CIM were in very good agreement with a C.F.D experiment from Santiago et al. [2007] and Martilli and Santiago [2007]. However, there were still some discrepancies in the magnitude of the maximum T.K.E but the horizontal wind speed was well reproduced.

In the second part of this study, the buoyancy term was included in the T.K.E equation. The fluxes were also modified with the Louis functions [**?**]. The results from CIM were then compared with the Monin-Obukhov Simularity Theory (MOST [Monin and Obukhov, 1954] in both a stable and unstable condition above a plane surface. It was shown that if the traditional formulation of the buoyancy term was used then the results from CIM when compared with the MOST were different. It was demonstrated that a coefficient, C_G, based on the Businger functions [Businger et al., 1971], has to be used to multiply the buoyancy term so that the results would be coherent with the MOST. Finally obstacles were integrated and CIM was tested in different stability conditions. The results from CIM were very promising as they provided a canopy model which was able to produce high resolution meteorological profiles which were in very good agreement with traditional theories.

In the last part of this study, CIM was integrated in the meso-scale meteorological model WRF v3.5 [Skamarock et al., 2008]. The aim of this integration was to provide high resolution data to the urban parameterization scheme (BEP-BEM [Martilli et al., 2002, Krpo, 2009, Salamanca et al., 2010]. To keep the coherence between profiles calculated by CIM and by WRF, a new methodology was proposed to also include horizontal fluxes in CIM's calculation. When CIM is running offline it can be forced only at the top. In the case where it is coupled with a meso-scale model, we derived a new formulation where a flux can be used instead as the top boundary condition. A theoretical study was designed to demonstrate the effectiveness of CIM. It was shown that CIM was able to reproduce high resolution vertical profiles of the horizontal wind and potential temperature and that they were in good agreement with a high resolution simulation of WRF. CIM brought consider-

able improvement to the wind speed of the meso-scale meteorological model when using a low resolution. This was expected with the use CIM, as the calculation of the surface fluxes in low resolution meso-scale models have been enhanced. Additionally it was seen that CIM did not have an impact on the computational time.

These results provided a solid foundation for the future coupling of meso-scale and micro-scale models. The use of CIM has insignificant impact on the computational time and can hence be used in low resolution models to provide high resolution vertical profiles.

6.2 Perspectives

Further work is needed to address some of the issues that have been encountered during our studies. Firstly, when comparing CIM with the C.F.D experiment from Santiago et al. [2007] and Martilli and Santiago [2007], it was seen that even though the horizontal wind speed was in very good agreement, there were still some differences between the T.K.E profiles. CIM seems to underestimate the T.K.E but this does not appear to have an influence on the diffusion process. One of the questions which rises is the importance of the magnitude of the T.K.E particularly in the transition zone above the obstacles and the canopy.

Secondly, when the buoyancy term is added to the T.K.E equation, we observed that to obtain results in agreement with the well-known and accepted theories, a coefficient has to be added. The fact that this coefficient is a function of the ϕ_m function from Businger et al. [1971] means that this equation cannot be used in all cases. A simple diffusion process using a 1.5 order turbulence closure was adopted for CIM. The use of the ϕ_m functions in the resolution of the T.K.E equation is not intended to be a permanent solution. These functions can only be applied over a plane surface when it can be assumed that the fluxes are constant. In the case where obstacles are constant this statement does not hold true and hence we expect the ϕ_m functions to be erroneous. In order to generalize the use of CIM and the formulations as proposed by Mauree et al. [2014b,a], it is necessary to find a new formulation for this coefficient and to understand why this correction

is needed.

Thirdly, one of the major obstacles that we came across during this study is the lack of experimental data to validate the simulations that have been made. The aim of CIM was to provide highly resolved meteorological data at the neighborhood scale. In neutral conditions results were validated with a C.F.D experiment. However in other stability conditions and in real cases, no appropriate dataset could be exploited. Various means were hence designed to justify the methodology that was chosen and to validate the results which were obtained from the experiments that were conducted.

The integration of CIM in WRF was only a preliminary step to test the validity of CIM when coupled with a meso-scale model and an urban parameterization scheme. A few questions are still to be investigated for that purpose. For the simulations that were run it was noted that BEP had higher walls and surface temperatures (up to 10K more than the air temperature). Although this might be the case during summer, it is hardly plausible that such a situation will occur when the sun is very low in winter at high latitudes. Further investigations are therefore needed to understand why the wall temperatures are so high.

Coupling CIM and WRF with another micro-scale model may bring an insight to this particular question. The coupling with another model should prove to be relatively simple. CIM can provide vertical meteorological profiles to this model and needs in return only fluxes and obstacles characteristics.

For the purpose of this study, a theoretical domain was designed and used. Although this was enough for the present context, this type of domain is not the best configuration for using meso-scale meteorological models. It is therefore strongly advised, in the future, to use CIM on a more realistic and smaller domain over a longer time period and where data is available to validate the meteorological profiles as well as the energy use. In such a configuration, it would then be judicious to analyze the influence of land use changes on urban energy consumption. Urban planning scenarios have to be evaluated to determine whether the

thermal comfort of the inhabitants as well as legislation concerning the energy use in buildings are respected in the construction of new neighborhoods in urban areas.

In view of the results obtained from the current study, CIM can be used as a tool to couple meso-scale meteorological models to micro-scale models. It can thus be fully integrated in a meso-scale model like it has been done with WRF and precise vertical meteorological profiles can be provided to building energy models. This will prove to be very useful in the design of more energy efficient buildings as well as in evaluating urban planning scenarios.

Furthermore, since CIM has been built to be a standalone column model, it can be used in various type of model to improve the representation of the surface in low resolution meteorological models, and at the same time decrease computational time. It can thus prove very useful in global climate model where it is very costly to use high vertical resolution.

Chapter 7

Résumé en français

7.1 Le changement climatique et les dépenses énergétiques des bâtiments

7.1.1 Changements climatiques globaux

Le cinquième rapport d'évaluation (AR5), du Groupe d'experts Intergouvernemental sur l'Evolution du Climat (GIEC), sur le changement climatique paru en 2013, démontre clairement que le changement climatique actuel est dû aux activités humaines. Des preuves irréfutables montrent que cela est dûe aux émissions de gaz à effet de serre (GES), comme le dioxyde de carbone (voir Figure 7.1), issues de la combustion de carburants fossiles lors de la production d'énergie[IPCC, 2013].

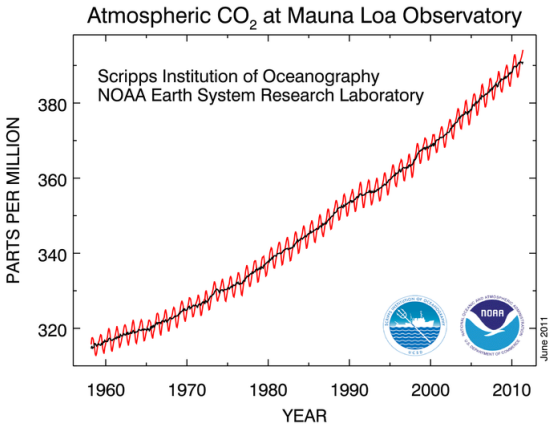

Figure 7.1: Concentration du dioxyde de carbone à l'Observatoire de Mauna Loa de 1960 à 2011

Le changement climatique anthropogénique, comme décrit par le AR5, indique que des mesures d'atténuation et adaptation doivent être prise pour s'assurer que les effets du changement climatique sur la Terre et ses écosystèmes soient le moins possible. Depuis 2007, l'Union Européenne et le gouvernement français ont demandé des actions immédiates pour réduire les émissions de GES par 4 avant 2050.

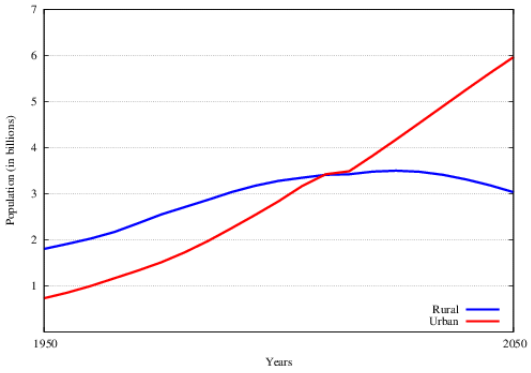

Figure 7.2: Population mondiale urbaine et rurale (en milliards) de 1950 à 2050 [UN, 2012]

Par ailleurs, après la première crise pétrolière, il y a eu des craintes quant à notre forte dépendance énergétique et cela n'a fait qu'empirer avec l'augmentation du coût du pétrole sur les marchés internationaux et par le fait que ces ressources sont non-renouvelables. Cela a donc aussi mis en évidence le besoin de réduire la consommation énergétique et d'augmenter l'efficacité énergétique des procédés (comme la consommation de combustibles dans les voitures ou les dépenses énergétiques de bâtiments). De plus, les dépenses énergétiques sont l'un des principaux moteurs de l'économie mondiale et on peut s'attendre à ce que la consommation d'énergie augmente dans le futur avec une augmentation de la population.

7.1.2 Développement urbain

Après la deuxième guerre mondiale, il y a une eu une forte augmentation de la population dans les zones urbaines (voir Figure 7.2). En 2008, plus de la moitié de la population mondiale vivait dans les villes [UN, 2012]. Ceci peut être expliqué par le fait que l'agriculture n'était plus considérée comme la source de revenue principale pour la majeur partie de la population et par les réformes du système de marché dans les années 1970 [Davis, 2006].

La migration des habitants, des campagnes vers les villes, et l'augmentation de la population, dans les zones urbaines, ont donné lieu à un manque de planification de l'aménagement territorial. Les bâtiments ont été construits sans considérer

pour leurs besoins énergétiques, ni leurs influences sur les écosystèmes naturels. Le développement urbain et l'expansion des villes, de part la modification des occupations du sol (de naturel à artificiel) ont modifié le bilan thermique local et les régimes de vent. Ces effets sont à l'origine d'un phénomène plus communément appelé Ilôt de Chaleur Urbain (ICU) [Oke, 1982]. L'industrialisation des zones urbaines a accentué, par ailleurs, la pollution sonore, de l'air et de l'eau. Depuis, des réglementations ont été mises en place pour protéger la santé et le bien-être des citadins mais aussi de la faune et de la flore existante.

UN-Habitat [2009] prévoit que d'ici 2050 environ 70% de la population mondiale habitera dans les zones urbaines et que cette augmentation aura lieu essentiellement dans les pays dit en voie de développement. Il est indéniable que ceci conduira à une expansion des zones urbaines [UN, 2012]. D'après l'Agence Internationale de l'Energie, environ 70% de l'énergie finale produite est consommée dans les villes [IEA, 2008]. Il est donc fort probable qu'une augmentation de la population accentuera la responsabilité des villes face aux changements climatiques si des villes et des bâtiments plus durables ne sont pas construits.

7.1.3 Stratégies d'adaption et d'atténuation

Deux approches sont donc nécessaires dans ce contexte: l'atténuation et l'adaptation. Les solutions d'atténuation du changement climatique sont indispensables si les villes et les collectivités veulent réduire leurs émissions de gaz à effet de serre. Pour atteindre les objectifs qui ont été fixés par les accords internationaux, des systèmes énergétiques plus efficaces doivent être construits. Cela s'applique à tous les secteurs consommateurs d'énergie tel que les transports, l'industrie mais aussi les bâtiments. Quant aux stratégies d'adaptation, elles impliquent que les villes soient repensés ou modifiés afin de permettre aux citadins, de mêmes que les autres écosystèmes, de vivre dans un monde affecté par le changement climatique.

Dans ce contexte, il est indispensable que les villes soient aménagées pour tenant en compte de ces contraintes. Les dépenses énergétiques des bâtiments (secteur résidentiel et tertiaire) représentent environ 40% de la consommation énergétique en France (voir Figure 7.3). Ces dépenses contribuent à environ 25% des émissions

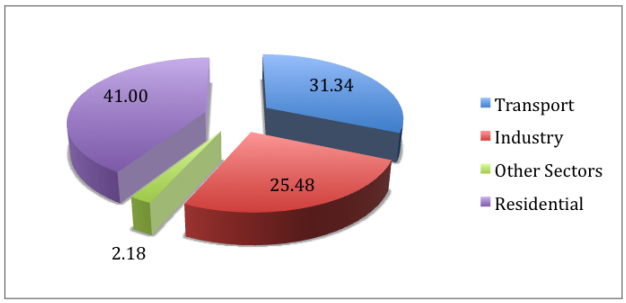

Figure 7.3: Consommation d'énergie par secteur dans les zones urbaines [ADEME, 2012]

de GES en France et sont essentiellement liées aux conforts thermiques (70%) des usagers [ADEME, 2012].

Les besoins de chauffage et de climatisation sont fortement dépendants du climat. Dans les hautes latitudes, en hiver, davantage d'énergie est nécessaire pour chauffer les bâtiments, alors qu'en été, de l'énergie est utilisée pour les refroidir. L'utilisation d'énergie dans les villes modifie aussi le bilan thermique localement et peut entrainer une hausse de la consommation d'énergie dans les bâtiments. Les techniques architecturales, de construction et d'ingénierie (isolation des murs ou des toits, fenêtres double ou triple vitrage, ...) sont maintenant utilisées pour diminuer la consommation d'énergie des bâtiments en les rendant plus efficaces. Lors de leur conception, des outils de modélisation sont souvent utilisés pour estimer leurs dépenses énergétiques.

Il est donc indispensable de disposer d'outils qui puissent évaluer avec le plus de précision possible les interactions qui existent entre les dépenses énergétiques des bâtiments et le climat local.

7.2 Modèles existants

Le climat urbain résulte d'une série de processus physiques complexes et non-linéaires. De plus,, la consommation d'énergie d'un bâtiment est fortement liée au climat local et à l'architecture et l'enveloppe du bâtiment. Le développement de nouveaux matériaux ainsi que l'aménagement de villes plus durable, est es-

sentiel pour réduire les dépenses énergétiques (et donc les émissions de GES) et les pertes à l'environnement extérieur. Cela souligne l'importance de développer de nouveaux outils pour comprendre et prendre en compte tous les processus qui régulent les dépenses énergétiques des bâtiments. Des progrès considérables ont été fait au cours de ces dernières décennies dans le domaine de la modélisation du climat urbain et des dépenses énergétiques des bâtiments.

Les modèles méso-échelles fonctionnent à l'échelle de la ville ou à l'échelle regionale. Ces modèles considèrent d'un certain nombre de processus (comme le développement de la couche limite atmosphérique) et des interactions (interactions entre zones urbaines et rurales) et ceci nécessitent que les domaines soient suffisamment grandes (de 100km à 500km). Les échelles de temps qui sont liées à ces modèles sont essentiellement régies par l'advection du vent et les changements dans la radiation solaire. La performance et la puissance des ordinateurs ont limité jusqu'à présent la résolution horizontale des modèles et ces derniers ont une résolution grossière (autour de 1km). Cela ne permet pas de définir précisément les occupations du sol et donc des interactions qui peuvent exister entre l'atmosphère et la surface de la Terre. Des paramétrisation urbaines [Kondo and Liu, 1998, Masson, 2000, Martilli et al., 2002] ont été développés et utilisés dans des modèles méso-échelles, ces dernières décennies, pour améliorer la représentation des obstacles dans les zones urbaines. Même si ces paramétrisation représentent mieux l'influence des zones urbaines sur la circulation, ils ne sont toujours pas capable de simuler correctement la température et le vent très proche de la surface [Salamanca et al., 2011] alors même que ces variables sont indispensables pour l'évaluation des dépenses énergétiques.

Contrairement aux modèles méso-échelles, les modèles micro-échelles (tels que EnergyPlus [**?**], Solene [Groleau et al., 2003], BEM [Salamanca et al., 2010]) ont une résolution très fine. Cela implique que les obstacles, tels que les bâtiments ou les plantes, peuvent être représentés explicitement. Les caractéristiques techniques et physiques, des matériaux de construction et d'isolation de bâtiments, pour les bâtiments ou classes de bâtiments, sont utilisées comme données d'entrées pour ces modèles. Ces paramètres sont utilisés pour calculer les flux (de moment, de chaleur

ou d'humidité) provenant des murs, des toits ou des fenêtres. Augmenter la taille du domaine (qui est de l'ordre du kilomètre, en général) pour la prise en compte des processus à plus grande échelle, nécessiterait des besoins considérables en temps de calcul et n'est pas réalisable à ce jour. Par ailleurs, ces modèles sont souvent forcés avec des données météorologiques annuelles moyennées pour un endroit particulier. Les données ne tiennent pas compte de l'historique des effets thermiques et mécaniques qui peuvent être transportés sur de très grandes distances. Elles ne sont donc pas aussi précises qu'elles devraient l'être pour évaluer au mieux les dépenses énergétiques. De plus, comme les modèles micro-échelles (qui calculent les flux à partir des surfaces ou de systèmes d'air conditionné) et méso-échelles ne sont pas couplés, il n'y a pas de retour d'informations. Les systèmes d'air conditionné peuvent être, par exemple, à l'origine d'une augmentation de la température en zone urbaine de 1-2°C [Ashie et al., 1999] et peuvent donc influencer en retour les dépenses énergétiques.

7.3 Objectif de la thèse

Comme démontré dans la partie précédente, des modèles distincts ont été utilisés dans le passé pour prévoir la circulation atmosphérique à l'échelle régionale et pour évaluer les dépenses énergétiques. Il y a toutefois un manque de modèles qui sont capables de passer résolument de l'échelle d'une ville à l'échelle du bâtiment pour une meilleure prise en compte de toute l'étendue des processus qui influencent l'intensité des îlôts de chaleurs urbains et pour calculer de façon plus précise les dépenses énergétiques des bâtiments. L'objectif final est de développer un modèle de canopée qui pourra être utilisé pour coupler les modèles météorologiques méso-échelles à des modèles micro-échelles. Les conditions de bord, plus précises, dans les deux types de modèles devraient améliorer les simulations aux deux échelles. De plus, l'historique des variables sera donc présente dans les deux types de modèles. Les modèles méso-echelles fournissent des variables qui incluent les interactions à plus grandes échelles alors que les modèles micro-échelles vont donner en retour des calculs de flux plus précis.

Pour cette étude, un modèle de canopée (Canopy Interface Model (CIM)) a été développé et couplé au modèle météorologique WRF [Skamarock et al., 2008]. Le

but de ce travail était d'estimer les apports d'un tel modèle de canopée dans un modèle météorologique avec une faible résolution. Une méthodologie a été mise en place afin d'évaluer si le modèle a pu améliorer les simulations dans le modèle méso-échelles et s'il a été capable de fournir des profils verticaux avec une très forte résolution. Ce travail s'est déroulé en trois parties qui seront decrites dans les sections suivantes.

7.4 Développement d'un modèle de canopée. Partie 1: cas neutre et comparaison avec un modèle C.F.D

Développement d'un modèle de canopée. Partie 1: cas neutre et comparaison avec un modèle C.F.DDéveloppement d'un modèle de canopée. Partie 1

Un modèle colonne 1-D, qui utilise un processus de diffusion basé sur une fermeture turbulente d'ordre 1.5, a été développé [Mauree et al., 2014a]. Dans un premier temps, le modèle a été testé dans un environnement neutre et sans obstacles.

Une nouvelle méthodologie a été mise en place pour le calcul de l'énergie cinétique turbulente (T.K.E). Nous avons proposé de calculer une valeur stationnaire de la T.K.E, ce qui a aussi simplifié, par ailleurs, la résolution numérique de l'énergie cinétique turbulente dans le modèle (voir Equation 7.1).

$$\frac{\partial E}{\partial t} = \frac{\partial}{\partial z}\left(\lambda_t \frac{\partial E}{\partial z}\right) + C_\varepsilon^* \frac{\sqrt{E}}{l}\left(E_{stat} - E\right) + f_e \tag{7.1}$$

où E est la T.K.E, λ_t est un coefficient de diffusion, C_ε^* est une constante, l une longueur de mélange, f_e représente les sources de T.K.E et où E_{stat} est la valeur stationnaire de la T.K.E qui peut être écrit comme suit:

$$E_{stat} = \frac{C_k}{C_\varepsilon^*} l^2 \left(\frac{\partial U}{\partial z}\right)^2 \tag{7.2}$$

où C_k est une constante et U représente le vent horizontal moyen.

Les résultats ont été comparés à la théorie de la couche limite de Prandtl

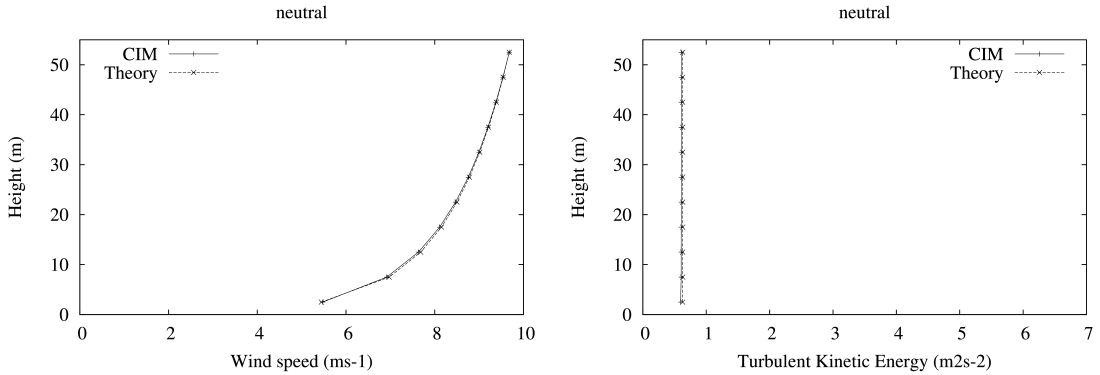

Figure 7.4: Comparaison du profil de vent (en ms^{-1}) et de l'énergie cinétique turbulente (en m^2s^{-2}) calculées à partir de la solution analytique issue de la théorie de la surface de Prandtl et de CIM. L'altitude est en mètre.

[Prandtl, 1925]. Afin de garder la cohérence entre la théorie et la formulation qui a été adoptée, il a été démontré que le profil de l'énergie cinétique turbulente doit être constant au dessus d'une surface plane dans un cas neutre (Figure 7.4).

Les obstacles ont ensuite été intégrés suivant les travaux de Krpo [2009] et de Kohler et al. [2012] et le modèle a été validé avec des résultats issues d'une expérience C.F.D de Santiago et al. [2007] et de Martilli and Santiago [2007]. Afin d'obtenir des résultats comparables à ceux du C.F.D, une formulation proposée par [Santiago and Martilli, 2010] pour la longueur de mélange a été adoptée (Figure 7.5).

7.5 Développement d'un modèle de canopée. Partie 2: cas stable et instable, modification de la l'énergie cinétique turbulente

Développement d'un modèle de canopée. Partie 2: cas stable et instable, modification de la l'énergie cinétique turbulenteDéveloppement d'un modèle de canopée. Partie 2

Dans la deuxième partie de cette étude [Mauree et al., 2014b], les équations ont

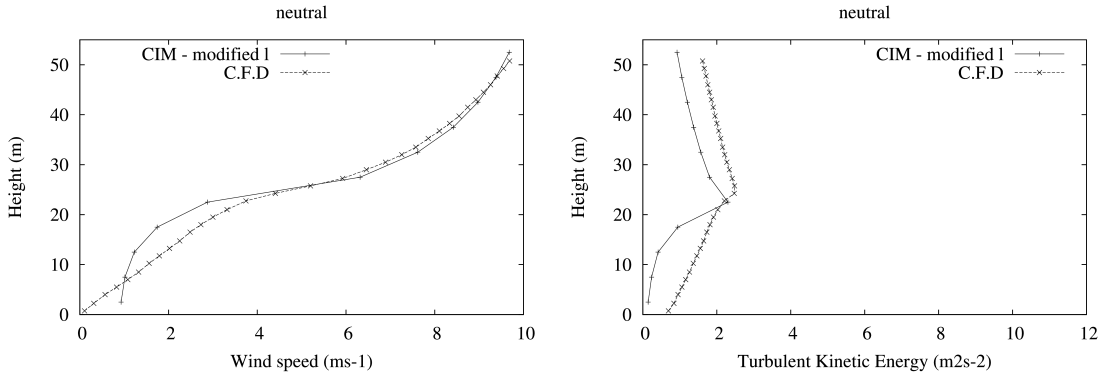

Figure 7.5: Comparaison du profil de vent (en ms^{-1}) et de l'énergie cinétique turbulente (en m^2s^{-2}) avec des obstacles à partir de CIM et du C.F.D. L'altitude est en mètre.

été modifiées pour la prise en compte de la stabilité de l'atmosphère. Le modèle a été testé au dessus d'une surface plane et les résultats ont été comparés à la théorie de similitude de Monin-Obukhov [Monin and Obukhov, 1954] et les formulations qui ont été proposées par [Businger et al., 1971].

L'étude a permis de mettre en évidence que, pour garder la cohérence avec les théories et la formulation de Businger, il fallait ajouter un coefficient au terme de flottabilité dans l'équation régissant l'énergie cinétique turbulente qui a été proposée.

$$\frac{\partial E}{\partial t} = \frac{\partial}{\partial z}\left(\lambda_t \frac{\partial E}{\partial z}\right) + C_\varepsilon^* \frac{\sqrt{E}}{l}\left(E_{stat} - E\right) + f_e \tag{7.3}$$

où E_{stat} est maintenant exprimé comme suit:

$$E_{stat} = \frac{C_k}{C_\varepsilon^*} l^2 \left(\frac{\partial U}{\partial z}\right)^2 \left(1 - C_G \cdot Ri_f\right) \tag{7.4}$$

où C_G est la correction qui est apporté et Ri_f est le nombre de Richardson.

Les Figure 7.6 et Figure 7.7 montrent les résultats qui ont été obtenus avec et sans l'ajout de cette correction. On peut voir qu'avec cette correction, les résultats sont très similaires aux courbes théoriques.

Des obstacles ont aussi été intégré pour mieux comprendre l'influence de la stabilité de l'atmosphère sur les profils de vents et de l'énergie cinétique turbulente

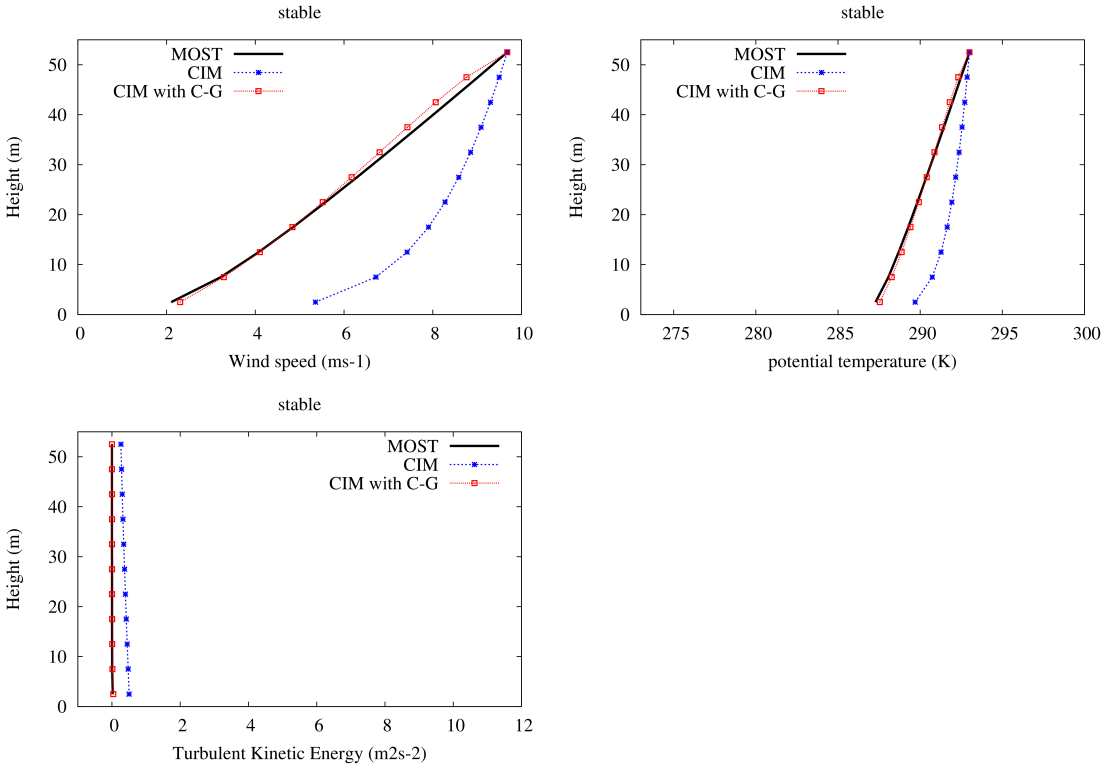

Figure 7.6: Comparaison du profil de vent (en ms^{-1}), de la température potentielle (en K) et de l'énergie cinétique turbulente (en m^2s^{-2}) obtenu avec la MOST au dessus d'une surface plane et avec CIM (avec et sans la correction C_G dans la T.K.E.) dans des conditions stable. L'altitude est en mètre.

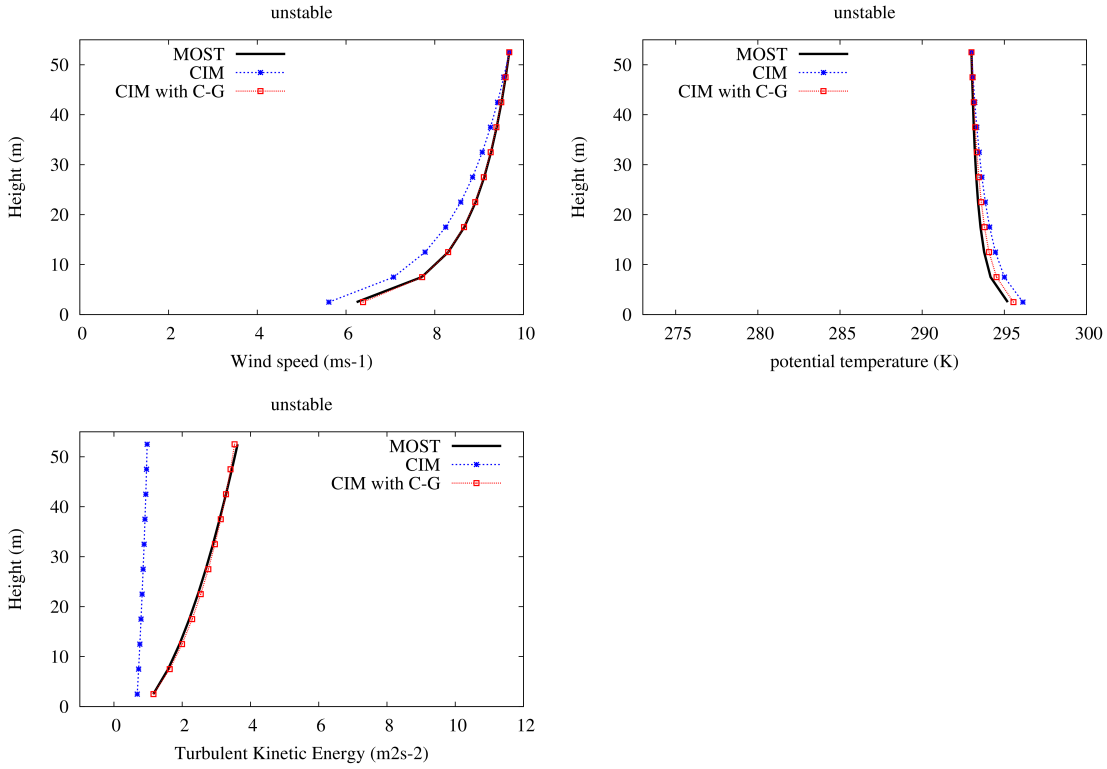

Figure 7.7: Comparaison du profil de vent (en ms^{-1}), de la température potentielle (en K) et de l'énergie cinétique turbulente (en m^2s^{-2}) obtenu avec la MOST au dessus d'une surface plane et avec CIM (avec et sans la correction C_G dans la T.K.E.) dans des conditions instable. L'altitude est en mètre.

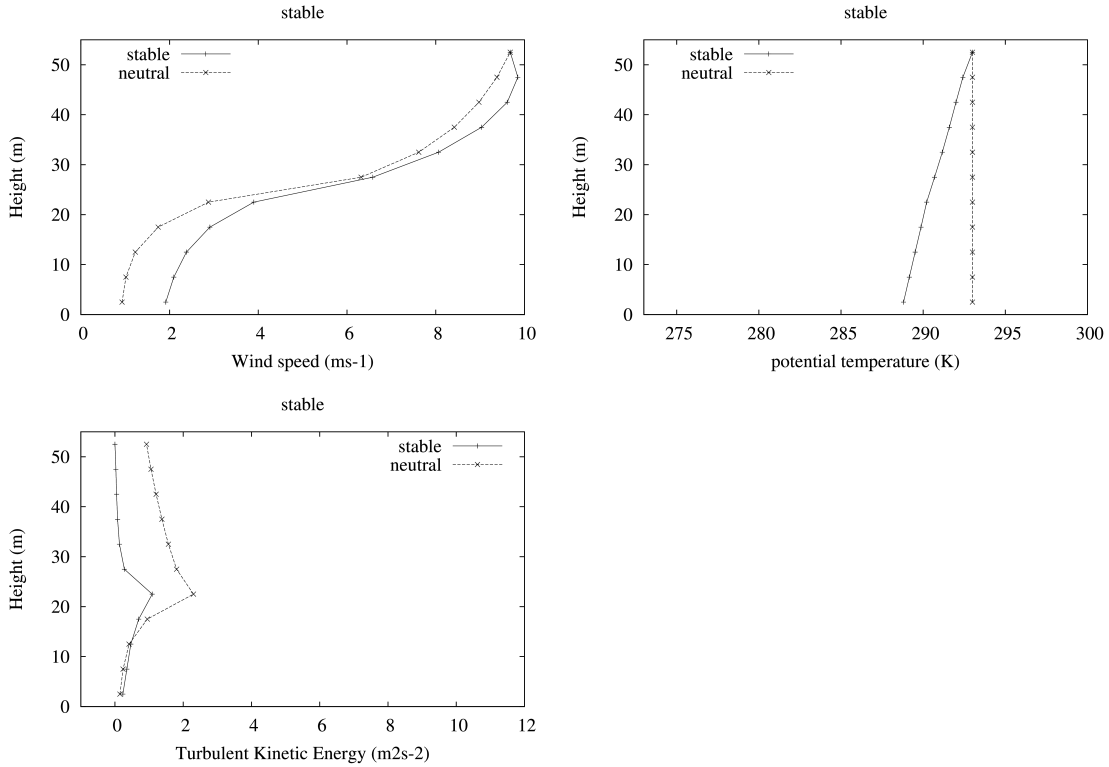

Figure 7.8: Comparaison du profil de vent (en ms^{-1}), de la température potentielle (en K) et de l'énergie cinétique turbulente (en m^2s^{-2}) issues de CIM avec des obstacles dans des conditions stable et neutre. L'altitude est en mètre.

(Figure 7.8 et Figure 7.9).

Face au manque de mesures appropriées pour valider les simulations, avec les obstacles, les résultats peuvent être discutés. Toutefois, les tendances obtenues dans les deux cas (stable et instable) sont en cohérence avec ce qu'on aurait pu avoir dans des cas sans obstacles en comparant les profiles neutre, stable et instable.

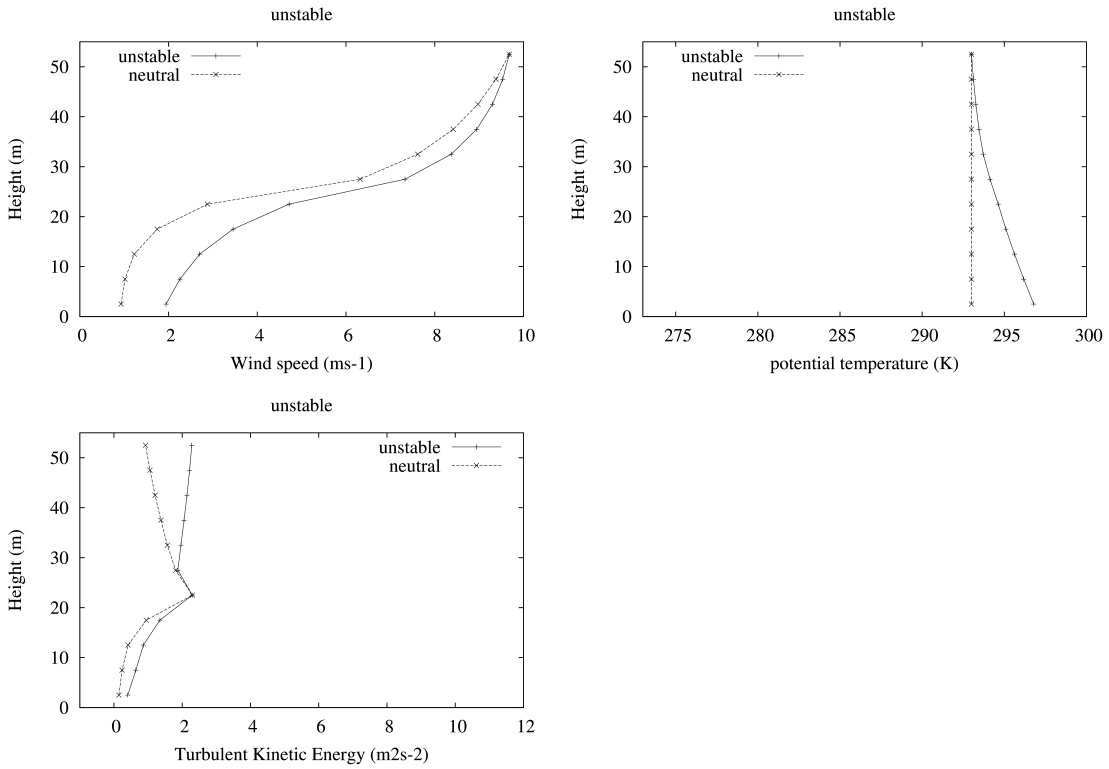

Figure 7.9: Comparaison du profil de vent (en ms^{-1}), de la température potentielle (en K) et de l'énergie cinétique turbulente (en m^2s^{-2}) issues de CIM avec des obstacles dans des conditions instable et neutre. L'altitude est en mètre.

7.6 Modélisation multi-échelle de la météorologie urbaine: intégration de CIM dans le modèle météorologique WRF

Modélisation multi-échelle de la météorologie urbaine: intégration de CIM dans le modèle météorologique WRFIntégration de CIM dans le modèle météorologique WRF

Dans la dernière partie de cette étude [Mauree et al., 2014c], le modèle CIM a été intégré au modèle météorologique WRF v3.5 [Skamarock et al., 2008]. Pour cette étude la paramétrisation urbaine BEP-BEM [Salamanca et al., 2011] a été choisi pour représenter les effets de la surface sur la circulation atmosphérique.

Afin de garder la cohérence avec le modèle méso-échelle, WRF, une méthodologie simple, a été mise en place pour rajouter un terme supplémentaire aux calculs de CIM (voir Equation 7.5). Ce terme additionnel représente tous les effets horizontaux (comme l'advection ou les différences de gradient de pression) qui sont prises en compte dans le modèle méso-échelle mais pas le modèle CIM.

$$\begin{aligned} \text{For } i < n \left\{ N_i^{Ct+1} \right. &= N_i^{C*} + \overline{N_i^{Ct+1}} - \overline{N_i^{C*}} + \frac{F_{TOP}}{n} \\ \text{For } i = n \left\{ N_n^{Ct+1} \right. &= N_n^{C*} + \overline{N_i^{Ct+1}} - \overline{N_i^{C*}} + \frac{F_{TOP}}{n} - F_{TOP} \end{aligned} \tag{7.5}$$

où N représente la variable à calculer (vent, température ou humidité), i est un indice pour les mailles du modèle, t est le pas de temps considéré, N_i^{C*} est N_i^{Ct} incluant tous les flux sauf les flux horizontaux et le flux au sommet, F_{TOP} le flux au top et n le nombre de niveau dans le modèle CIM.

Une étude théorique de sensibilité a été mise en place pour démontrer les améliorations que CIM a apportées. La Figure 7.10 donne un aperçu générale de l'évolution des profils issus des simulations qui ont été faites.

On peut constater que le couplage de CIM et de WRF a amélioré les simulations du modèle méso-échelle surtout avec une résolution grossière. Une comparaison statistique et une analyse temporelle des différentes simulation a montré

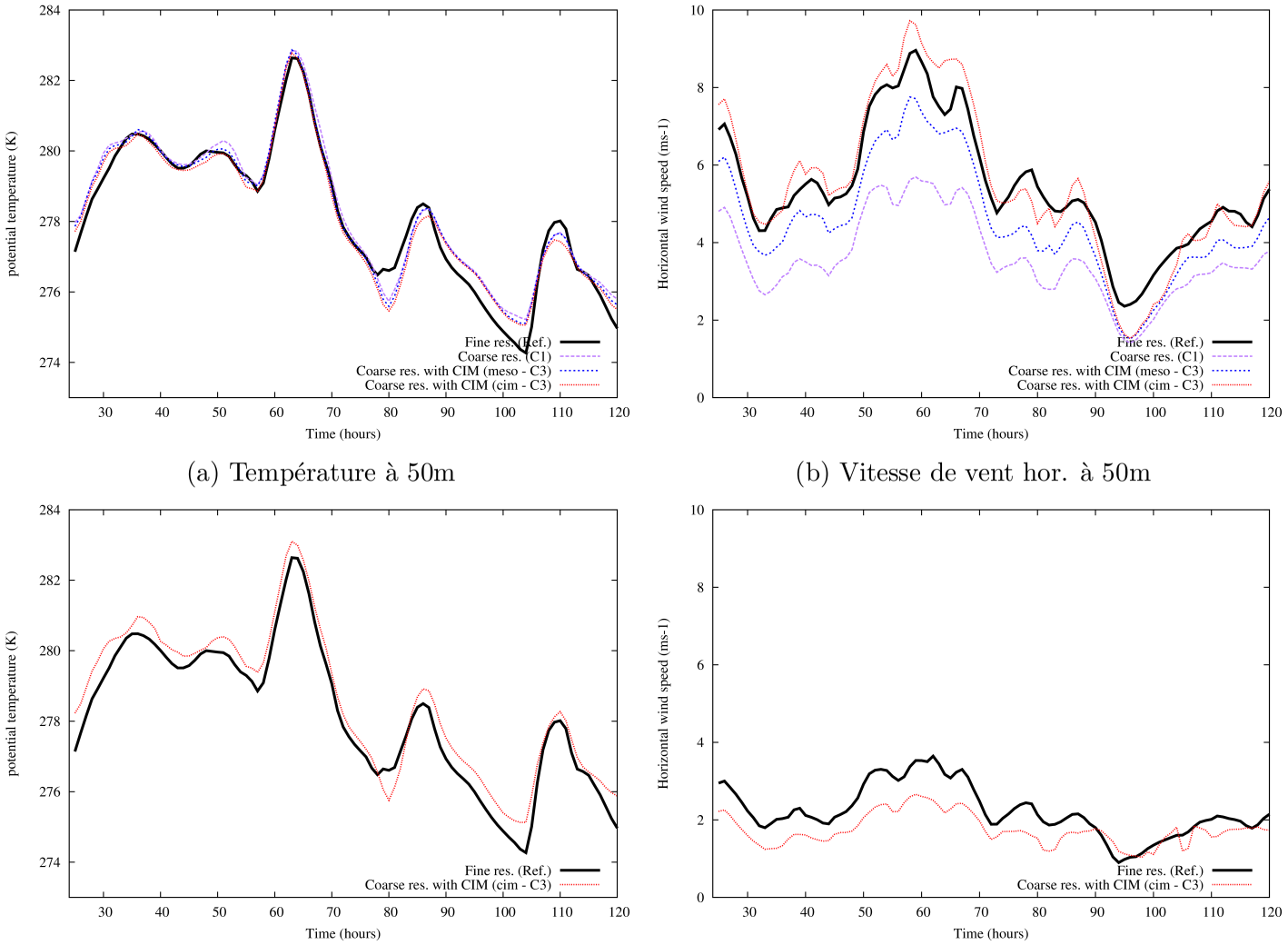

(a) Température à 50m

(b) Vitesse de vent hor. à 50m

(c) Température à 5m

(d) Vitesse de vent hor. à 5m

Figure 7.10: Comparison de la température potentiel (K) (gauche) et du vent horizontal (ms^{-1}) (droite) calculé dans WRF avec et sans le couplage de CIM à 50m (haut) et à 5m (bas). La ligne noir représente la courbe issue du modèle méso-échelle avec une résolution tr-s fine (Ref.), la courbe violette est issue du modèle méso-échelle avec une résolution grossière sans CIM (C1), la ligne blue est isue du modèle méso-échelle avec une résolution grossière avec CIM (meso - C3) et la ligne rouge est issue de CIM dans la simulation avec une résolution grossière avec CIM (cim - C3). L'abscisse représente le temps après le début de la simulation à partir de 24 heures (jour 2) jusqu'à 120 heures (jour 5).

que généralement, WRF avec une telle configuration, sur-estimait la température et sous-estimait la vitesse du vent. Le système météorologique qui a été mis en place, a montré une meilleure performance avec des biais et une erreur quadratique moyenne plus petites. Les corrélations étaient significatives par rapport à la simulation de référence. De plus, CIM a été capable de produire des profils, avec une résolution vertical très fine, qui étaient proches de la solution de la référence.

7.7 Conclusions et perspectives

Le but de ces études était d'amorcer le développement d'un outil capable d'évaluer plus précisément les dépenses énergétiques des bâtiments et de définir des stratégies de construction et d'aménagement urbains (telles que de nouvelles réglementations ou de nouveaux matériaux de construction) pour réduire l'impact des zones urbaines sur l'atmosphère. Adopter de telles stratégies devrait non seulement aider à améliorer le confort thermique des habitants (par exemple lors de vagues de chaleurs qui devraient être plus fréquentes avec le réchauffement climatique) mais pourrait aussi aider à diminuer les émissions de gaz à effet de serre et ainsi atténuer les effets du changement climatique.

Pour atteindre cet objectif, un modèle de canopée (CIM) a été développé en plusieurs étapes. Une nouvelle méthode pour la résolution de l'énergie cinétique turbulente a été mise en place. Le modèle a été testé dans un premier temps en condition neutre et sans obstacles et les résultats ont été comparés avec la théorie de Prandtl. Les obstacles ont été intégrés dans le modèle et les résultats ont été validés avec une expérience C.F.D. Les équations du modèle CIM ont ensuite été modifiées pour une prise en compte de la stabilité atmosphérique. Il a été démontré qu'un terme additionnel devait être rajouté afin d'être en cohérence avec la théorie de Monin-Obukhov. La dernière étape de ce travail a permis le couplage du modèle CIM au modèle WRF. Une méthodologie simple a été proposée pour ajouter un terme supplémentaire aux calculs de CIM. Ce terme représente les effets horizontaux qui existent dans le modèle méso-échelle WRF mais qui n'étaient pas présents dans CIM.

Au vu des résultats obtenus lors de cette étude, il a été démontré que les fondations pour l'utilisation de CIM comme une interface qui permettrait de mieux

représenter la surface et de coupler les modèles méso-échelle et les modèles micro-échelle ont bien été mises en place.

Bibliography

B. Abart. *Modelisation de la turbulence en écoulement stratifiés pour la couche limite atmosphérique*. PhD thesis, ÉCOLE CENTRALE DE NANTES, 1999.

ADEME. *Energie et Climat - Edition 2012*. Agence de l'Environnement et de la Maîtrise de l'Energie, Angers, 2012. URL http://www2.ademe.fr/servlet/getDoc?id=85364&p1=7645&ref=17597.

A. J. Arnfield. Two decades of urban climate research: a review of turbulence, exchanges of energy and water, and the urban heat island. *International Journal of Climatology*, 23(1):1–26, 2003. ISSN 1097-0088. doi: 10.1002/joc.859.

A. J. Arnfield and C. Grimmond. An urban canyon energy budget model and its application to urban storage heat flux modeling. *Energy and Buildings*, 27(1): 61 – 68, 1998. ISSN 0378-7788. doi: 10.1016/S0378-7788(97)00026-1.

P. S. Arya. *Introduction to micrometeorology*, volume 79. Access Online via Elsevier, 2001.

S. Arya. Micrometeorology and atmospheric boundary layer. *pure and applied geophysics*, 162(10):1721–1745, 2005. ISSN 0033-4553. doi: 10.1007/s00024-005-2690-y.

Y. Ashie, V. T. Ca, and T. Asaeda. Building canopy model for the analysis of urban climate. *Journal of Wind Engineering and Industrial Aerodynamics*, 81 (13):237 – 248, 1999. ISSN 0167-6105. doi: 10.1016/S0167-6105(99)00020-3.

P. Aumond, V. Masson, C. Lac, B. Gauvreau, S. Dupont, and M. Berengier. Including the drag effects of canopies: Real case large-eddy simulation studies. *Boundary-Layer Meteorology*, 146(1):65–80, 2013. ISSN 0006-8314. doi: 10.1007/s10546-012-9758-x.

A. Baklanov, A. Rasmussen, B. Fay, E. Berge, and S. Finardi. Potential and shortcomings of numerical weather prediction models in providing meteorological data for urban air pollution forecasting. *Water, Air and Soil Pollution: Focus*, 2(5-6):43–60, 2002. ISSN 1567-7230. doi: 10.1023/A:1021394126149.

A. Baklanov, P. Mestayer, A. Clappier, S. Zilitinkevich, S. Joffre, A. Mahura, and N. W. Nielsen. On the parameterisation of the urban atmospheric sublayer in meteorological models. *Atmospheric Chemistry and Physics Discussions*, 5(6): 12119–12176, 2005. doi: 10.5194/acpd-5-12119-2005.

A. Baklanov, C. Grimmond, A. Mahura, and M. Athanassiadou. *Meteorological and air quality models for urban areas*. Springer, 2009.

R. D. Bornstein. The two-dimensional urbmet urban boundary layer model. *Journal of Applied Meteorology*, 14(8):1459–1477, 1975.

P. Bougeault and P. Lacarrère. Parameterization of orography-induced turbulence in a mesobeta–scale model. *Monthly Weather Review*, 117(8):1872–1890, 1989.

R. E. Britter and S. R. Hanna. Flow and dispersion in urban areas. *Annual Review of Fluid Mechanics*, 35(1):469–496, 2003. doi: 10.1146/annurev.fluid.35.101101.161147.

J. J. H. Brouwers. Dissipation equals production in the log layer of wall-induced turbulence. *Physics of Fluids (1994-present)*, 19(10):101702, 2007. doi: http://dx.doi.org/10.1063/1.2793147.

M. Bruse and H. Fleer. Simulating surfaceplantair interactions inside urban environments with a three dimensional numerical model. *Environmental Modelling & Software*, 13(34):373 – 384, 1998. ISSN 1364-8152. doi: 10.1016/S1364-8152(98)00042-5.

J. Businger, J. Wyngaard, Y. Izumi, and E. F. Bradley. Flux-profile relationships in the atmospheric surface layer. *Journal of the Atmospheric Sciences*, 28(2): 181–189, 1971.

V. T. Ca, T. Asaeda, and Y. Ashie. Development of a numerical model for the evaluation of the urban thermal environment. *Journal of Wind Engineering and Industrial Aerodynamics*, 81(13):181 – 196, 1999. ISSN 0167-6105. doi: 10.1016/S0167-6105(99)00016-1.

D. Charuchittipan and J. Wilson. Turbulent kinetic energy dissipation in the surface layer. *Boundary-Layer Meteorology*, 132(2):193–204, 2009. ISSN 0006-8314. doi: 10.1007/s10546-009-9399-x.

F. Chen and J. Dudhia. Coupling an advanced land surface-hydrology model with the penn state-ncar mm5 modeling system. part i: Model implementation and sensitivity. *Monthly Weather Review*, 129(4):569–585, 2001.

Y.-S. Chen and S.-W. Kim. Computation of turbulent flows using an extended k-epsilon turbulence closure model. *NASA STI/Recon Technical Report N*, 88: 11969, 1987.

W. T. L. Chow and M. Roth. Temporal dynamics of the urban heat island of singapore. *International Journal of Climatology*, 26(15):2243–2260, 2006. ISSN 1097-0088. doi: 10.1002/joc.1364.

A. Christen, M. Rotach, and R. Vogt. The budget of turbulent kinetic energy in the urban roughness sublayer. *Boundary-Layer Meteorology*, 131(2):193–222, 2009. ISSN 0006-8314. doi: 10.1007/s10546-009-9359-5.

A. Clappier, P. Perrochet, A. Martilli, F. Muller, B. Krueger, et al. A new non-hydrostatic mesoscale model using a cvfe (control volume finite element) discretisation technique. In *Proceedings of EUROTRAC symposium*, volume 96, pages 527–531, 1996.

O. Coceal and S. E. Belcher. A canopy model of mean winds through urban areas. *Quarterly Journal of the Royal Meteorological Society*, 130(599):1349–1372, 2004. ISSN 1477-870X. doi: 10.1256/qj.03.40.

K. J. Craig Jr. *MM5 Simulations of urban induced convective precipitation over Atlanta, GA*. PhD thesis, San Jose State University, 2002.

D. B. Crawley, L. K. Lawrie, C. O. Pedersen, and F. C. Winkelmann. Energy plus: energy simulation program. *ASHRAE journal*, 42(4):49–56, 2000.

D. B. Crawley, J. W. Hand, M. Kummert, and B. T. Griffith. Contrasting the capabilities of building energy performance simulation programs. *Building and Environment*, 43(4):661 – 673, 2008. ISSN 0360-1323. doi: 10.1016/j.buildenv.2006.10.027. Part Special: Building Performance Simulation.

M. Davis. Planet of slums. *New Perspectives Quarterly*, 23(2):6–11, 2006. ISSN 1540-5842. doi: 10.1111/j.1540-5842.2006.00797.x.

Y. Delage. A numerical study of the nocturnal atmospheric boundary layer. *Quarterly Journal of the Royal Meteorological Society*, 100(425):351–364, 1974. ISSN 1477-870X. doi: 10.1002/qj.49710042507.

Y. Delage and P. Taylor. Numerical studies of heat island circulations. *Boundary-Layer Meteorology*, 1(2):201–226, 1970. ISSN 0006-8314. doi: 10.1007/BF00185740.

A. Dyer. A review of flux-profile relationships. *Boundary-Layer Meteorology*, 7(3): 363–372, 1974. ISSN 0006-8314. doi: 10.1007/BF00240838.

T. Foken. 50 years of the moninobukhov similarity theory. *Boundary-Layer Meteorology*, 119(3):431–447, 2006. ISSN 0006-8314. doi: 10.1007/s10546-006-9048-6.

T. Foken. *Micrometeorology*. Springer, 2008.

A. Fouillet, G. Rey, F. Laurent, G. Pavillon, S. Bellec, C. Guihenneuc-Jouyaux, J. Clavel, E. Jougla, and D. Hmon. Excess mortality related to the august 2003 heat wave in france. *International Archives of Occupational and Environmental Health*, 80(1):16–24, 2006. ISSN 0340-0131. doi: 10.1007/s00420-006-0089-4.

G. Galilei. *Dialogue sur les deux grands systmes du monde*. Seuil, France, 1632, Ed. 2000.

G. A. Grell, J. Dudhia, D. R. Stauffer, et al. A description of the fifth-generation penn state/ncar mesoscale model (mm5). 1994.

C. Grimmond and T. R. Oke. Heat storage in urban areas: Local-scale observations and evaluation of a simple model. *Journal of applied meteorology*, 38(7):922–940, 1999.

C. Grimmond, S. Potter, H. Zutter, and C. Souch. Rapid methods to estimate sky-view factors applied to urban areas. *International Journal of Climatology*, 21(7):903–913, 2001. ISSN 1097-0088. doi: 10.1002/joc.659. URL http://dx.doi.org/10.1002/joc.659.

D. Groleau, F. Fragnaud, and J.-M. Rosant. Simulation of the radiative behaviour of an urban quarter of marseille with the solene model. In *CD Proceedings, 5th International Conference on Urban Climate*, 2003.

R. Hamdi and V. Masson. Inclusion of a drag approach in the town energy balance (teb) scheme: Offline 1d evaluation in a street canyon. *Journal of Applied Meteorology and Climatology*, 47(10):2627–2644, 2008.

U. Högström. Non-dimensional wind and temperature profiles in the atmospheric surface layer: A re-evaluation. *Boundary-Layer Meteorology*, 42(1-2):55–78, 1988. ISSN 0006-8314. doi: 10.1007/BF00119875.

U. Högström. Review of some basic characteristics of the atmospheric surface layer. *Boundary-Layer Meteorology*, 78(3-4):215–246, 1996. ISSN 0006-8314. doi: 10.1007/BF00120937.

M. Idczak, D. Groleau, P. Mestayer, J.-M. Rosant, and J.-F. Sini. An application of the thermo-radiative model {SOLENE} for the evaluation of street canyon energy balance. *Building and Environment*, 45(5):1262 – 1275, 2010. ISSN 0360-1323. doi: 10.1016/j.buildenv.2009.11.011.

IEA. World energy outlook. *Organisation for Economic Co-operation and Development OECD*, 2008.

IPCC. *Fourth Assessment Report: Climate Change 2007: The Physical Science Basis. Contribution of Working Group I to the Fourth Assessment Report of the Intergovernmental Panel on Climate Change*. Geneva: Intergovernmental Panel on Climate Change, 2007. URL http://www.ipcc.ch/ipccreports/ar4-wg1.htm.

IPCC. *WORKING GROUP I CONTRIBUTION TO THE IPCC FIFTH ASSESSMENT REPORT CLIMATE CHANGE 2013: THE PHYSICAL SCIENCE BASIS*. Geneva: Intergovernmental Panel on Climate Change, 2013. URL http://www.ipcc.ch/report/ar5/wg1.

M. Z. Jacobson. *Fundamentals of atmospheric modeling*. Cambridge University Press, 1999.

J. H. Kämpf and D. Robinson. A simplified thermal model to support analysis of urban resource flows. *Energy and Buildings*, 39(4):445 – 453, 2007. ISSN 0378-7788. doi: 10.1016/j.enbuild.2006.09.002.

M. Kanda, T. Kawai, M. Kanega, R. Moriwaki, K. Narita, and A. Hagishima. A simple energy balance model for regular building arrays. *Boundary-Layer Meteorology*, 116(3):423–443, 2005. ISSN 0006-8314. doi: 10.1007/s10546-004-7956-x.

P. Kastner-Klein and M. Rotach. Mean flow and turbulence characteristics in an urban roughness sublayer. *Boundary-Layer Meteorology*, 111(1):55–84, 2004. ISSN 0006-8314. doi: 10.1023/B:BOUN.0000010994.32240.b1.

Y. Kikegawa, Y. Genchi, H. Yoshikado, and H. Kondo. Development of a numerical simulation system toward comprehensive assessments of urban warming countermeasures including their impacts upon the urban buildings' energy-demands. *Applied Energy*, 76(4):449 – 466, 2003. ISSN 0306-2619. doi: 10.1016/S0306-2619(03)00009-6.

M. Kohler, D. Mauree, N. Blond, and A. Clappier. Development of a canopy model for a multiscale urban climate system. In *Proceedings of the 8th International Conference on Urban Climate*, 2012.

H. Kondo. Description of nripr mesoscale model. *Report of the National Research Institute for Pollution and Resources*, 1989.

H. Kondo and F.-H. Liu. A study on the urban thermal environment obtained through one-dimensional urban canopy model. *J. Japan Soc. Atmos. Environ*, 33:179–192, 1998.

H. Kondo, Y. Kikegawa, Y. Genchi, and S. Yamamoto. Heating in the urban canopy by anthropogenic energy use. In *Proceedings of 15th International Congress of Biometeorology and International Conference on Urban Climatology (ICB-ICUC99)*, pages 8–12, 1999.

H. Kondo, Y. Genchi, Y. Kikegawa, Y. Ohashi, H. Yoshikado, and H. Komiyama. Development of a multi-layer urban canopy model for the analysis of energy consumption in a big city: Structure of the urban canopy model and its basic performance. *Boundary-Layer Meteorology*, 116(3):395–421, 2005. ISSN 0006-8314. doi: 10.1007/s10546-005-0905-5.

A. Krpo. *Development and application of a numerical simulation system to evaluate the impact of anthropogenic heat fluxes on urban boundary layer climate*. PhD thesis, École Polytechnique Fédérale de Lausanne, 2009.

A. Krpo, F. Salamanca, A. Martilli, and A. Clappier. On the impact of anthropogenic heat fluxes on the urban boundary layer: A two-dimensional numerical study. *Boundary-Layer Meteorology*, 136(1):105–127, 2010. ISSN 0006-8314. doi: 10.1007/s10546-010-9491-2.

F. K. H. H. Kusaka, H. and M. M. Change in the daily maximum temperature due to urbanization during an 85 year period. numerical simulation using a mesoscale model with a simple parameterization of urban canopy layer. *Proceedings of 15th International Congress of Biometeorology and International Conference on Urban Climatology (ICV-ICUC 99)*, 1999.

H. Kusaka, H. Kondo, Y. Kikegawa, and F. Kimura. A simple single-layer urban canopy model for atmospheric models: Comparison with multi-layer and slab models. *Boundary-Layer Meteorology*, 101(3):329–358, 2001. ISSN 0006-8314. doi: 10.1023/A:1019207923078.

J. Lafore, J. Stein, N. Asencio, P. Bougeault, V. Ducrocq, J. Duron, C. Fischer, P. Hreil, P. Mascart, V. Masson, J. Pinty, J. Redelsperger, E. Richard, and J.-G. Arellano. The meso-nh atmospheric simulation system. part i: adiabatic formulation and control simulations. *Annales Geophysicae*, 16(1):90–109, 1997. ISSN 0992-7689. doi: 10.1007/s00585-997-0090-6.

C.-Y. Lin, W.-C. Chen, P.-L. Chang, and Y.-F. Sheng. Impact of the urban heat island effect on precipitation over a complex geographic environment in northern taiwan. *Journal of Applied Meteorology and Climatology*, 50(2):339–353, 2011.

Y. Liu, F. Chen, T. Warner, and J. Basara. Verification of a mesoscale data-assimilation and forecasting system for the oklahoma city area during the joint

urban 2003 field project. *Journal of applied meteorology and climatology*, 45(7): 912–929, 2006.

J. Louis, A. Weill, and D. Vidal-Madjar. Dissipation length in stable layers. *Boundary-Layer Meteorology*, 25(3):229–243, 1983. ISSN 0006-8314. doi: 10.1007/BF00119538.

J.-F. Louis. A parametric model of vertical eddy fluxes in the atmosphere. *Boundary-Layer Meteorology*, 17(2):187–202, 1979. ISSN 0006-8314. doi: 10.1007/BF00117978.

R. Mahmood, R. A. Pielke, K. G. Hubbard, D. Niyogi, P. A. Dirmeyer, C. McAlpine, A. M. Carleton, R. Hale, S. Gameda, A. Beltrán-Przekurat, B. Baker, R. McNider, D. R. Legates, M. Shepherd, J. Du, P. D. Blanken, O. W. Frauenfeld, U. Nair, and S. Fall. Land cover changes and their biogeophysical effects on climate. *International Journal of Climatology*, pages n/a–n/a, 2013. ISSN 1097-0088. doi: 10.1002/joc.3736.

A. Martilli. Current research and future challenges in urban mesoscale modelling. *International Journal of Climatology*, 27(14):1909–1918, 2007. ISSN 1097-0088. doi: 10.1002/joc.1620.

A. Martilli and J. Santiago. CFD simulation of airflow over a regular array of cubes. Part II: analysis of spatial average properties. *Boundary-Layer Meteorology*, 122 (3):635–654, 2007. ISSN 0006-8314. doi: 10.1007/s10546-006-9124-y.

A. Martilli, A. Clappier, and M. W. Rotach. An urban surface exchange parameterisation for mesoscale models. *Boundary-Layer Meteorology*, 104(2):261–304, 2002. ISSN 0006-8314. doi: 10.1023/A:1016099921195.

V. Masson. A physically-based scheme for the urban energy budget in atmospheric models. *Boundary-Layer Meteorology*, 94(3):357–397, 2000. ISSN 0006-8314. doi: 10.1023/A:1002463829265.

D. Mauree, N. Blond, and A. Clappier. Development of a 1D Canopy Interface Model. Part II: Stable and Unstable case - modification brought to the T.K.E equation. *In preparation*, Chapter 4, 2014a.

D. Mauree, M. Kohler, N. Blond, and A. Clappier. Development of a 1D Canopy Interface Model. Part I: Neutral case and comparison with a C.F.D. *In preparation*, Chapter 3, 2014b.

D. Mauree, M. Kohler, N. Blond, and A. Clappier. Multi-scale modeling of the urban meteorology: integration of a new canopy model in WRF model. *In preparation*, Chapter 5, 2014c.

G. Mills. Luke howard and the climate of london. *Weather*, 63(6):153–157, 2008. ISSN 1477-8696. doi: 10.1002/wea.195.

A. S. Monin and A. M. Obukhov. Basic laws of turbulent mixing in the surface layer of the atmosphere. *Contrib. Geophys. Inst. Acad. Sci. USSR*, 151:163–187, 1954.

C. Muller. *Improvement of an urban turbulence parametrization for meteorological operational forecast and air quality modeling*. PhD thesis, École Polytechnique Fédérale de Lausanne, 2007.

A. Obukhov. Turbulence in an atmosphere with a non-uniform temperature. *Boundary-Layer Meteorology*, 2(1):7–29, 1971. ISSN 0006-8314. doi: 10.1007/BF00718085.

B. Offerle, C. S. B. Grimmond, K. Fortuniak, K. Kłysik, and T. R. Oke. Temporal variations in heat fluxes over a central european city centre. *Theoretical and Applied Climatology*, 84(1-3):103–115, 2006. ISSN 0177-798X. doi: 10.1007/s00704-005-0148-x.

Y. Ohashi, Y. Genchi, H. Kondo, Y. Kikegawa, H. Yoshikado, and Y. Hirano. Influence of air-conditioning waste heat on air temperature in tokyo during summer: numerical experiments using an urban canopy model coupled with a building energy model. *Journal of Applied Meteorology and climatology*, 46(1):66–81, 2007.

T. Oke. The distinction between canopy and boundarylayer urban heat islands. *Atmosphere*, 14(4):268–277, 1976. doi: 10.1080/00046973.1976.9648422.

T. Oke. *Boundary layer Climates*. Methuen and Co., Ltd., London, 1987.

T. Oke, G. Johnson, D. Steyn, and I. Watson. Simulation of surface urban heat islands under ideal conditions at night part 2: Diagnosis of causation. *Boundary-Layer Meteorology*, 56(4):339–358, 1991. ISSN 0006-8314. doi: 10.1007/BF00119211.

T. R. Oke. The energetic basis of the urban heat island. *Quarterly Journal of the Royal Meteorological Society*, 108(455):1–24, 1982. ISSN 1477-870X. doi: 10.1002/qj.49710845502.

K. V. Ooyama. A thermodynamic foundation for modeling the moist atmosphere. *Journal of the Atmospheric Sciences*, 47(21):2580–2593, 1990.

T. L. Otte, A. Lacser, S. Dupont, and J. K. Ching. Implementation of an urban canopy parameterization in a mesoscale meteorological model. *Journal of Applied Meteorology*, 43(11):1648–1665, 2004.

M. Park, A. Hagishima, J. Tanimoto, and K. ichi Narita. Effect of urban vegetation on outdoor thermal environment: Field measurement at a scale model site. *Building and Environment*, 56(0):38 – 46, 2012. ISSN 0360-1323. doi: 10.1016/j.buildenv.2012.02.015.

D. E. Parker. A demonstration that large-scale warming is not urban. *Journal of Climate*, 19(12):2882–2895, 2006.

R. A. Pielke. *Mesoscale meteorological modeling*. Academic press, 2002.

M. Poumadre, C. Mays, S. Le Mer, and R. Blong. The 2003 heat wave in france: Dangerous climate change here and now. *Risk Analysis*, 25(6):1483–1494, 2005. ISSN 1539-6924. doi: 10.1111/j.1539-6924.2005.00694.x.

L. Prandtl. Report on investigation of developed turbulence. *NACA Report TM-1231*, 1925.

C. H. B. Priestley and W. C. Swinbank. Vertical transport of heat by turbulence in the atmosphere. *Proceedings of the Royal Society of London. Series A. Mathematical and Physical Sciences*, 189(1019):543–561, 1947. doi: 10.1098/rspa.1947.0057.

V. Ramanathan, B. R. Barkstrom, and E. F. Harrison. Climate and the earth's radiation budget. *AIP Conference Proceedings*, 247(1):55–77, 1992. doi: 10.1063/1.41922.

A. Rasheed. *Multiscale modelling of urban climate*. PhD thesis, ÉCOLE POLYTECHNIQUE FÉDÉRALE DE LAUSANNE, 2009.

M. Raupach. Drag and drag partition on rough surfaces. *Boundary-Layer Meteorology*, 60(4):375–395, 1992. ISSN 0006-8314. doi: 10.1007/BF00155203.

M. Raupach, J. Finnigan, and Y. Brunei. Coherent eddies and turbulence in vegetation canopies: The mixing-layer analogy. *Boundary-Layer Meteorology*, 78(3-4):351–382, 1996. ISSN 0006-8314. doi: 10.1007/BF00120941.

D. Robinson, F. Haldi, J. Kämpf, P. Leroux, D. Perez, A. Rasheed, and U. Wilke. Citysim: Comprehensive micro-simulation of resource flows for sustainable urban planning. In *Proc. Building Simulation*, 2009.

M. Rotach. Turbulence close to a rough urban surface part i: Reynolds stress. *Boundary-Layer Meteorology*, 65(1-2):1–28, 1993a. ISSN 0006-8314. doi: 10.1007/BF00708816.

M. Rotach. Turbulence close to a rough urban surface part ii: Variances and gradients. *Boundary-Layer Meteorology*, 66(1-2):75–92, 1993b. ISSN 0006-8314. doi: 10.1007/BF00705460.

M. Rotach. Profiles of turbulence statistics in and above an urban street canyon. *Atmospheric Environment*, 29(13):1473 – 1486, 1995. ISSN 1352-2310. URL http://www.sciencedirect.com/science/article/pii/135223109500084C.

M. Roth. Review of atmospheric turbulence over cities. *Quarterly Journal of the Royal Meteorological Society*, 126(564):941–990, 2000. ISSN 1477-870X. doi: 10.1002/qj.49712656409.

F. Salamanca and A. Martilli. A new Building Energy Model coupled with an Urban Canopy Parameterization for urban climate simulationspart II. Validation with one dimension off-line simulations. *Theoretical and Applied Climatology*, 99(3-4):345–356, 2010. ISSN 0177-798X. doi: 10.1007/s00704-009-0143-8. URL http://dx.doi.org/10.1007/s00704-009-0143-8.

F. Salamanca, A. Krpo, A. Martilli, and A. Clappier. A new building energy model coupled with an urban canopy parameterization for urban climate simulationspart I. formulation, verification, and sensitivity analysis of the model. *Theoretical and Applied Climatology*, 99(3-4):331–344, 2010. ISSN 0177-798X. doi: 10.1007/s00704-009-0142-9. URL http://dx.doi.org/10.1007/s00704-009-0142-9.

F. Salamanca, A. Martilli, M. Tewari, and F. Chen. A study of the urban boundary layer using different urban parameterizations and high-resolution urban canopy parameters with wrf. *Journal of Applied Meteorology and Climatology*, 50(5): 1107–1128, 2011.

M. Santamouris, N. Papanikolaou, I. Livada, I. Koronakis, C. Georgakis, A. Argiriou, and D. Assimakopoulos. On the impact of urban climate on the energy consumption of buildings. *Solar Energy*, 70(3):201 – 216, 2001. ISSN 0038-092X. doi: http://dx.doi.org/10.1016/S0038-092X(00)00095-5. ¡ce:title¿Urban Environment¡/ce:title¿.

J. Santiago and A. Martilli. A dynamic urban canopy parameterization for mesoscale models based on computational fluid dynamics reynolds-averaged navierstokes microscale simulations. *Boundary-Layer Meteorology*, 137(3):417–439, 2010. ISSN 0006-8314. doi: 10.1007/s10546-010-9538-4.

J. Santiago, A. Martilli, and F. Martín. CFD simulation of airflow over a regular array of cubes. Part I: Three-dimensional simulation of the flow and validation with wind-tunnel measurements. *Boundary-Layer Meteorology*, 122(3):609–634, 2007. ISSN 0006-8314. doi: 10.1007/s10546-006-9123-z.

A. Sarkar and K. De Ridder. The urban heat island intensity of paris: A case study based on a simple urban surface parametrization. *Boundary-Layer Meteorology*, 138(3):511–520, 2011. ISSN 0006-8314. doi: 10.1007/s10546-010-9568-y. URL http://dx.doi.org/10.1007/s10546-010-9568-y.

W. C. Skamarock, J. B. Klemp, J. Dudhia, D. O. Gill, D. M. Barker, W. Wang, and J. G. Powers. A description of the advanced research wrf version 2. Technical report, DTIC Document, 2005.

W. C. Skamarock, J. B. Klemp, J. Dudhia, D. O. Gill, D. M. Barker, M. G. Duda, X.-H. Huang, W. Wang, and J. G. Powers. A description of the advanced research wrf version 2. Technical report, DTIC Document, 2008.

R. B. Stull. *An Introduction to Boundary Layer Meteorology*. Kuler Academic Publishers, 1988.

H. Taha. Urban climates and heat islands: albedo, evapotranspiration, and anthropogenic heat. *Energy and Buildings*, 25(2):99 – 103, 1997. ISSN 0378-7788. doi: 10.1016/S0378-7788(96)00999-1.

G. Therry and P. Lacarrère. Improving the eddy kinetic energy model for planetary boundary layer description. *Boundary-Layer Meteorology*, 25(1):63–88, 1983. ISSN 0006-8314. doi: 10.1007/BF00122098.

UN. World Urbanization Prospects: The 2011 Revision, CD-ROM Edition. Technical report, Department of Economic and Social Affairs, Population Division, 2012.

UN-Habitat. *Global report on human settlements 2009: Planning sustainable cities*. Earthscan: for UN-Habitat, Nairobi, 2009.

T. Watanabe and J. Kondo. The influence of canopy structure and density upon the mixing length within and above vegetation. *Journal of the Meteorological Society of Japan*, 68(2):227–235, 1990.

X. Yang, L. Zhao, M. Bruse, and Q. Meng. Evaluation of a microclimate model for predicting the thermal behavior of different ground surfaces. *Building and Environment*, 60(0):93 – 104, 2013. ISSN 0360-1323. doi: 10.1016/j.buildenv.2012.11.008.

G. J. Zhang, M. Cai, and A. Hu. Energy consumption and the unexplained winter warming over northern asia and north america. *Nature Climate Change*, 2013.

Y. Zhang, J. Ma, and Z. Cao. The von kármán constant retrieved from cases-97 dataset using a variational method. *Atmospheric Chemistry and Physics*, 8(23): 7045–7053, 2008. doi: 10.5194/acp-8-7045-2008.

S. Zilitinkevich and I. Esau. Similarity theory and calculation of turbulent fluxes at the surface for the stably stratified atmospheric boundary layer. *Boundary-Layer Meteorology*, 125(2):193–205, 2007. ISSN 0006-8314. doi: 10.1007/s10546-007-9187-4.

Dasaraden MAUREE

Development of a multi-scale meteorological system to improve urban climate modeling

Résumé

Ce travail a consisté à developper un modèle de canopée (CIM), qui pourrait servir d'interface entre des modèles méso-échelles de calcul du climat urbain et des modèles micro-échelles de besoin énergétique du bâtiment. Le développement est présenté en conditions atmosphériques variées, avec et sans obstacles, en s'appuyant sur les théories précédemment proposées. Il a été, par exemple, montré que, pour être en cohérence avec la théorie de similitude de Monin-Obukhov, un terme correctif devait être rajouté au terme de flottabilité de la T.K.E. CIM a aussi été couplé au modèle méso-échelle WRF. Une méthodologie a été proposée pour profiter de leurs avantages respectifs (un plus résolu, l'autre intégrant des termes de transports horizontaux) et pour assurer la cohérence de leurs résultats. Ces derniers ont montré que ce système, en plus d'être plus précis que le modèle WRF à la même résolution, permettait, par l'intermédiaire de CIM, de fournir des profils plus résolus près de la surface.

Mots-clés: *climat urbain, météorologie urbaine, modèle de canopée, modélisation multi-échelle, énergie cinétique turbulente, paramétrisation de la turbulence*

Résumé en anglais

This study consisted in the development of a canopy model (CIM), which could be use as an interface between meso-scale models used to simulate urban climate and micro-scale models used to evaluate building energy use. The development is based on previously proposed theories and is presented in different atmospheric conditions, with and without obstable. It has been shown, for example, that to be in coherence with the Monin-Obukhov Similarity Theory, that a correction term has to be added to the buoyancy term of the T.K.E. CIM has also been coupled with the meteorological meso-scale model WRF. A methodology was proposed to take advantage of both models (one being more resolved, the other one integrating horizontal transport terms) and to ensure a coherence of the results. Besides being more precise than the WRF model at the same resolution, this system allows, through CIM, to provide high resolved vertical profiles near the surface.

Keywords: *urban climate, urban meteorology, canopy model, multi-scale modeling, turbulent kinetic energy, turbulence parameterization*